NASA/TM—2005-213369

Investigation of Exoskeletal Engine Propulsion System Concept

Joseph M. Roche, Donald T. Palac, James E. Hunter, David E. Myers, and Christopher A. Snyder
Glenn Research Center, Cleveland, Ohio

Daniel N. Kosareo
ZIN Technologies, Inc., Brook Park, Ohio

David R. McCurdy and Kevin T. Dougherty
QSS Group, Inc., Cleveland, Ohio

August 2005

The NASA STI Program Office . . . in Profile

Since its founding, NASA has been dedicated to the advancement of aeronautics and space science. The NASA Scientific and Technical Information (STI) Program Office plays a key part in helping NASA maintain this important role.

The NASA STI Program Office is operated by Langley Research Center, the Lead Center for NASA's scientific and technical information. The NASA STI Program Office provides access to the NASA STI Database, the largest collection of aeronautical and space science STI in the world. The Program Office is also NASA's institutional mechanism for disseminating the results of its research and development activities. These results are published by NASA in the NASA STI Report Series, which includes the following report types:

- TECHNICAL PUBLICATION. Reports of completed research or a major significant phase of research that present the results of NASA programs and include extensive data or theoretical analysis. Includes compilations of significant scientific and technical data and information deemed to be of continuing reference value. NASA's counterpart of peer-reviewed formal professional papers but has less stringent limitations on manuscript length and extent of graphic presentations.

- TECHNICAL MEMORANDUM. Scientific and technical findings that are preliminary or of specialized interest, e.g., quick release reports, working papers, and bibliographies that contain minimal annotation. Does not contain extensive analysis.

- CONTRACTOR REPORT. Scientific and technical findings by NASA-sponsored contractors and grantees.

- CONFERENCE PUBLICATION. Collected papers from scientific and technical conferences, symposia, seminars, or other meetings sponsored or cosponsored by NASA.

- SPECIAL PUBLICATION. Scientific, technical, or historical information from NASA programs, projects, and missions, often concerned with subjects having substantial public interest.

- TECHNICAL TRANSLATION. English-language translations of foreign scientific and technical material pertinent to NASA's mission.

Specialized services that complement the STI Program Office's diverse offerings include creating custom thesauri, building customized databases, organizing and publishing research results . . . even providing videos.

For more information about the NASA STI Program Office, see the following:

- Access the NASA STI Program Home Page at *http://www.sti.nasa.gov*

- E-mail your question via the Internet to help@sti.nasa.gov

- Fax your question to the NASA Access Help Desk at 301–621–0134

- Telephone the NASA Access Help Desk at 301–621–0390

- Write to:
  NASA Access Help Desk
  NASA Center for AeroSpace Information
  7121 Standard Drive
  Hanover, MD 21076

Investigation of Exoskeletal Engine Propulsion System Concept

Joseph M. Roche, Donald T. Palac, James E. Hunter, David E. Myers, and Christopher A. Snyder
Glenn Research Center, Cleveland, Ohio

Daniel N. Kosareo
ZIN Technologies, Inc., Brook Park, Ohio

David R. McCurdy and Kevin T. Dougherty
QSS Group, Inc., Cleveland, Ohio

Acknowledgments

Investigation of Exoskeletal Engine Propulsion System Concept

Joseph M. Roche, Donald T. Palac, James E. Hunter, David E. Myers, and Christopher A. Snyder
National Aeronautics and Space Administration
Glenn Research Center
Cleveland, Ohio 44135

Daniel N. Kosareo
ZIN Technologies, Inc.
Brook Park, Ohio 44142

David R. McCurdy and Kevin T. Dougherty
QSS Group, Inc.
Cleveland, Ohio 44135

Summary

An innovative approach to aircraft gas turbine engine design that was disclosed in 1997 involves mounting compressor and turbine blades to an outer rotating shell. Designated the exoskeletal engine, the concept results in compression (especially preferable to tension for high-temperature ceramic materials, generally) as the dominant compressor and turbine blade force.

It was determined that the feasibility of an exoskeletal engine lay in the challenges of structural and mechanical design (as opposed to cycle or aerothermodynamic design), so the focus of this study was the development of a structural-mechanical definition of an exoskeletal concept, using the Rolls-Royce AE3007 regional airliner all-axial turbofan as a baseline. The effort was further limited to the definition of an exoskeletal high-pressure spool concept, where the major structural and thermal challenges are represented. A finite-element model of an exoskeletal engine high-pressure spool shell and bearing support structure was developed. Loads and deflections were calculated and were compared with material strengths at the temperatures expected for each portion of the shells. Magnetic and foil bearing system concepts were also defined. The mass of the high-pressure spool was calculated and compared with the mass of the comparable components of the AE3007 engine. It was found that the exoskeletal engine rotating components have the potential for significant weight savings over the rotating components of conventional engines. However, bearing technology development is required for this mass savings to emerge at an engine system level, since the mass of existing bearing systems would exceed rotating machinery mass savings. It is recommended that once bearing technology is sufficiently advanced, a "clean sheet" preliminary design of an exoskeletal system be accomplished. This design would take best advantage of exoskeletal engine features from the structural, mechanical, aerodynamic, thermal, and engine cycle perspectives. This will better quantify the potential for the exoskeletal concept to deliver benefits in mass, structural efficiency, and cycle design flexibility.

Introduction

To improve conventional turbine and compressor designs, it is hypothesized that ceramic materials would provide greater operating efficiency through higher operating temperatures and lighter engine weight. Some problems with ceramic materials are lower tensile strength and durability and damage tolerance when compared with refractory metals and nickel-based alloys, such as titanium, Hastelloy[TM] and Waspaloy[TM] that are currently used in conventional engines. Ceramics behave well in compressive loading situations where brittle fracture is minimized. A novel turbine design approach that relies on this characteristic of ceramic composites is the exoskeletal engine (Christos C. Chamis, August 9, 2002,

NASA Glenn Research Center, Cleveland, OH, personal communication), which was disclosed by Christos Chamis of NASA Glenn Research Center (GRC) in 1997. The exoskeletal concept exchanges the conventional internal rotating shaft with a stator and the stator with a rotating drum. Essentially, this concept turns a conventional gas turbine engine inside out. A cross-sectional diagram of an early conceptual exoskeletal engine configuration is shown in figure 1.

The exoskeletal engine does not in principle represent an engine cycle change, although cycle parameters could be affected somewhat in implementation. Rather, the exoskeletal concept deals primarily with engine structural and mechanical design. Some of the characteristic differences from conventional engine technology are as follows:

(1) Compressor and turbine blades are mounted to the inside of a drum rotor. Stators and combustors are mounted to a stationary hub. Blades are in compression instead of tension because of rotational inertia. Torque is transferred from turbines to compressors through the rotating drums.

(2) The drum rotor is supported by bearings between the outside of the rotor and an outer shell. In a multispool engine, the high-pressure drum rotor bearings may ride directly on the low-pressure spool drum rotor. In a partially exoskeletal engine, thrust and other forces are transferred through bearings between drum rotors and shells or hubs.

(3) For engines of sufficient size, a central core space (inside the stator rings) may be open (see fig. 2).

The motivations for considering an exoskeletal engine have included the opportunity to

(1) Reduce the part count and engine weight, achieve higher engine operating temperatures (or reduce/eliminate cooling), and increase component life through use of lightweight composite materials (particularly ceramic blades in compression and rotating wound shells under hoop stresses) in applications that are aligned with their strengths

(2) Reduce engine noise through management of the resulting inverted velocity profile (central flow velocity lower than surrounding flow velocity)

(3) Insert another engine cycle, such as a ramjet, into the open core space
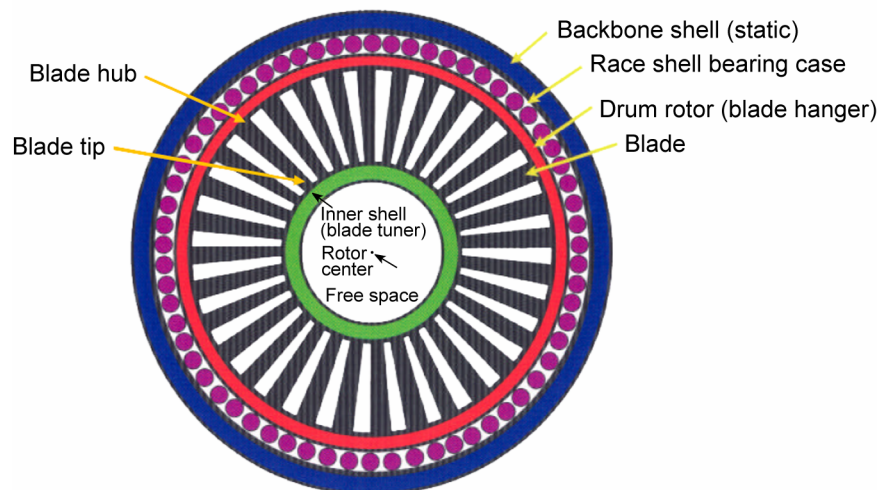
Figure 1.—Exoskeletal engine concept projected view of exoskeletal engine composite fan rotor (from Christos C. Chamis, August 9, 2002, NASA Glenn Research Center, Cleveland, OH, personal communication).
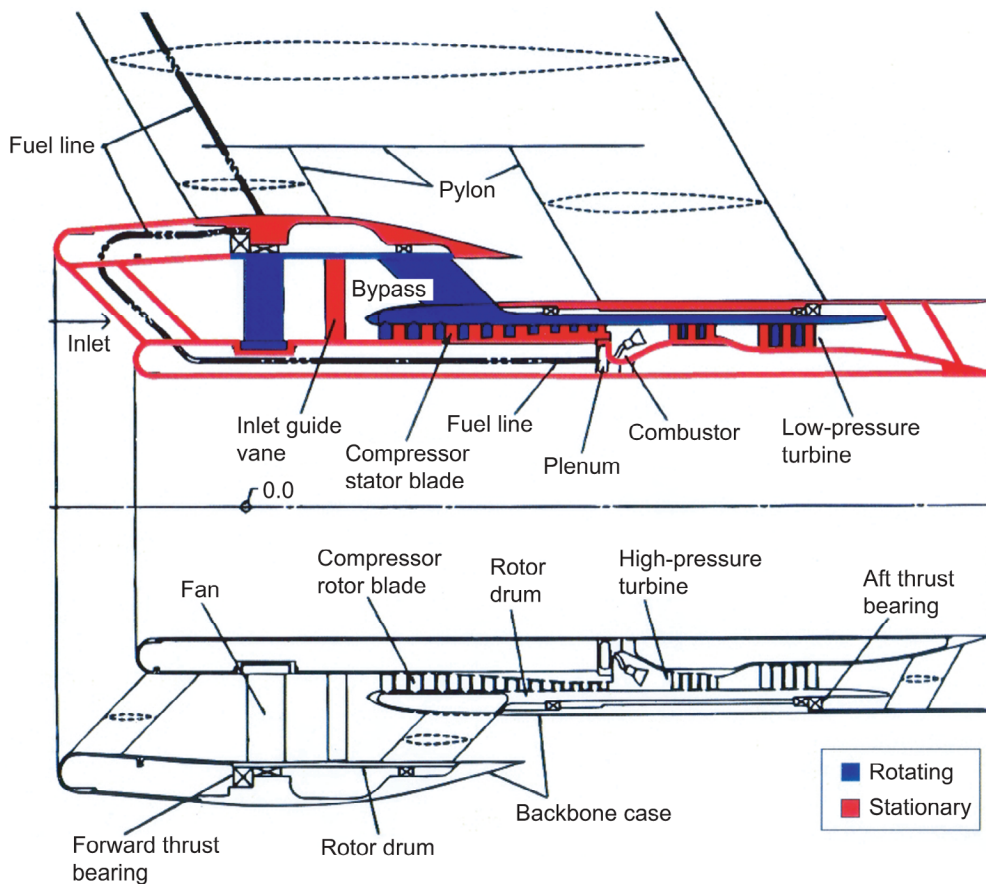
Figure 2.—Single-spool exoskeletal engine concept.

Related Prior Efforts

General Electric unducted fan.—The General Electric unducted fan (UDF), developed as part of NASA's advanced turboprop program in the 1980s, represents a successful, if not entirely similar, flight-proven predecessor to the exoskeletal engine concept as shown in figure 3. The UDF engine consisted of a standard high-pressure engine spool to which a low-pressure turbine (LPT) was added to directly drive a set of counterrotating highly swept propellers, also called unducted fan blades. The aft row of fan blades was driven by a conventional axial turbine, but the forward row of fan blades was driven by several rows of turbine blades mounted at their outer edge to a rotating drum. On the UDF, this drum was connected to and supported by a more conventional disk (ref. 1). Because the UDF low-pressure turbine drove a set of high-speed propellers (or a low-speed unducted fan), wheel speeds were low compared with turbofan engines. Centrifugal forces were not a factor in blade or drum design (David Cherry, Dec. 5, 2002, General Electric Aircraft Engines, Cincinnati, OH, private communication). In this respect, the UDF represents a significantly different set of design objectives and experience from those that would be relevant to an exoskeletal engine concept. However, the UDF does represent the successful implementation in flight of some elements of an exoskeletal engine architecture.

Modern Technologies Corporation exoskeletal engine concept studies.—NASA-sponsored studies of the exoskeletal engine concept were conducted by Modern Technologies Corporation between 1999 and 2001. These studies examined exoskeletal design concepts for 2000-, 5000-, and 25 000-lb thrust-class engines. Preliminary design concepts consisted of cycle definition and stage number and size
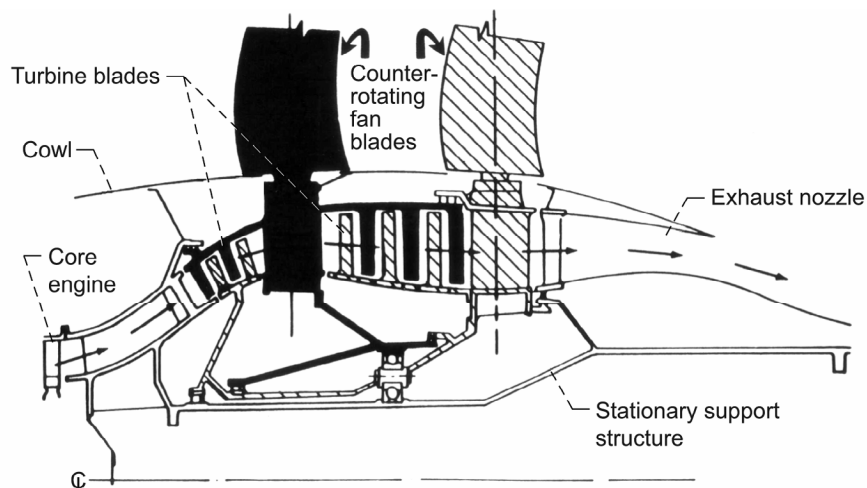
Figure 3.—General Electric unducted fan propulsor concept (from David Cherry, Dec. 5, 2002, General Electric Aircraft Engines, Cincinnati, OH, unpublished data) .

definitions (no structural analyses were performed). The studies pointed out the critical need for exoskeletal engine preliminary design guidelines and structural constraints on preliminary design because of the departure from conventional engine design practices (ref. 2).

Honeywell International, Inc., exoskeletal engine study.—In early 2000, Honeywell International, Inc., developed an exoskeletal engine concept based on an existing engine (NASA Exoskeletal Engine Study Final Report, Honeywell International, Inc., May 23, 2000). Honeywell selected the AS900 engine (approx. 6500-lb thrust at sea level static conditions) as a basis for comparison. A single-spool concept was assembled but was rejected because of performance, operability, and engine-starting limitations as compared with a two-spool configuration. A two-spool engine concept was assembled. A layout of this concept was created, and an engine cycle simulation was assembled sufficient to calculate the performance of engine components. Hoop stresses in the drum rotors were calculated and were used to identify material options and weights. High-pressure spool (HPS) rotation speeds necessary to produce performance similar to the AS900 required bearings operating at approximately 9 million mm-rpm, beyond the state of the art for bearings. The performance of a lower speed high-pressure spool was calculated for a rotation speed within state-of-the-art bearing capabilities of 6 million mm-rpm. Engine weights were calculated for rolling-element and magnetic bearing options, and weights and performance were compared with the AS900 engine. Major conclusions of this effort were

(1) An exoskeletal engine concept that delivers similar performance to an existing conventional engine is feasible but would have a radius approximately 30 percent smaller and would be approximately 50 percent longer.

(2) Exoskeletal rotating machinery is lighter (in concept) than that for conventional engines.

(3) Bearing system weight for an exoskeletal engine increases the total weight of the engine to 20 to 25 percent greater than that of a conventional engine.

It should be noted that the Honeywell AS900 engine has a centrifugal high-pressure compressor (HPC). Centrifugal compressors generally add weight and diameter but decrease the length of gas turbine engines. This creates some ambiguity about the directness of the comparison between the AS900 engine and a completely axial exoskeletal engine. However, the Honeywell study represented the first known assessment of the exoskeletal concept applied to an engine as a system. The findings of the Honeywell study indicated the importance of engine systems approach in any subsequent investigations, as well as the predominance of engine structures, materials, and bearings in the application of the exoskeletal concept.

Scope and Rationale

The present investigation focused on development and analysis of a gas turbine engine high-pressure spool of an exoskeletal engine concept. Goals of this investigation were to

(1) Determine the weight of an exoskeletal engine HPS concept. The HPS, rather than an entire engine system, was selected for study because

(a) The HPS typically represents the greatest challenges to structural, thermal, and bearing design in an engine, particularly for the exoskeletal concept characteristics of interest (e.g., high rotation speeds in compressor and turbine and high turbine temperatures). A preliminary calculation of hoop stresses in shells identified that small- to medium-size engine high-pressure spools, operating at comparable rotation speeds with existing engines, would challenge limits of existing structures and materials. A medium-class (approx. 10 000-lb thrust) engine high-pressure spool was chosen as the design example for this investigation.

(b) The analysis of an HPS is manageable in a reasonable study period, yet is enough of an engine system in itself to provide system-level answers.

(2) Perform requisite analysis to ensure that the concept is realistic yet aggressive. Analysis is needed to establish feasibility and traceability of weights of an exoskeletal HPS concept components. However, existing gas turbines benefit from 40 years of design refinement, so an aggressive approach gives the benefit of the doubt to an exoskeletal approach appropriate to making a comparison with an existing engine HPS.

(3) Compare the weight of an exoskeletal HPS concept with a representative existing gas turbine engine HPS.

(4) Identify technology challenges of the exoskeletal concept.

Several aspects of the exoskeletal engine were considered beyond the scope of this investigation. This investigation did not attempt to quantify the benefits of an exoskeletal engine for noise reduction or for compatibility with other engine cycles, such as a ramjet. It also did not include an optimization of an exoskeletal design, either structurally, aerodynamically, or thermodynamically, for a specific engine class or set of requirements. It is expected that these issues are more appropriately dealt with once an approach to exoskeletal engine structural and mechanical systems design and resolution of the inherent technology challenges have been accomplished.

Appendix A provides the output of the Weight Analysis Turbine Engine (WATE) computer program. The WATE code estimates the total engine weight by using the weights of the various components and/or subcomponents, based upon user inputs and conditions experienced. Appendix B presents the output of the NASA Engine Performance Program (NEPP), which develops a one-dimensional, steady-state thermodynamic cycle model and generates compressor and turbine maps. Appendix C presents the input data for an ANSYS structural analysis of the exoskeletal rotor when it is spinning at the over-speed condition of 16 400 rpm. This input file contains preprocessing, solution, and postprocessing commands to create the model, perform the analysis, and plot the results. Appendix D contains the input data for the Pro/Engineer® models of the compressor and turbine rotor blades. The input data for the exoskeletal compressor rotor blade shapes are based on the NACA 65A010 compressor airfoil shape.

Symbols

AR blade aspect ratio

c chord

DN diameter-number of revolutions (for bearings), millions of mm-rpm

E modulus of elasticity, lb/in.^{2}

F	force, lb_f
G	shear modulus of elasticity, lb/in.^2
g	gravitational constant
H	blade height, in.
I	area moment of inertia, in.^4
J	polar moment of inertia
K	matrix stiffness, lb/in.
k	effective stiffness, lb/in.
L	stage length, in.
M	matrix mass, lb_m
m	mass, lb_m
N	rotational speed, rpm
$\mathcal{n}_B$	number of blades
PR	pressure ratio
r	radius, in.
V	shear force, lb_f
W	weight, lb_m
W_B	blade weight (also includes fir tree), lb_m
x	axial location
α	coefficient of thermal expansion (CTE)
γ	weight density, lb/in.^3
δ	radial deflection, in.
ϑ	angular deflection, rad
θ	stagger angle, deg
μ	Poisson's ratio
ρ	material density, $\text{lb}_m/\text{in.}^3$
σ	stress, lb/in.^2
ϕ	camber line angle, deg
ω	rotational speed, rad/sec

Subscripts:

ACC	accessories weight (also includes other weights that show up but are difficult to assign to one particular part)
a	inner
B	blade
b	outer
c	corrected
cu	ultimate compressive allowable
cy	ultimate compressive yield allowable
disk	disk
e	exit
H	hub
i	inlet

lc	maximum allowable compressive stress in fiber direction
1t	maximum allowable tensile stress in fiber direction
max	maximum
min	minimum
N	nuts and bolts (also used to bolt disks together)
n	natural or local
RD	rotor drum
r	radial
row	row
stage	stage
su	ultimate shear allowable
T	tip
t	tangential
tu	ultimate tensile allowable
ty	tensile yield
vm	Von Mises
τ	shear
1	maximum principal stress, klb/in.^{2}
2	minimum principal stress, klb/in.^{2}

Assumptions, Key Challenges, and Approach

Assumptions

The first assumption was that the application of conventional aerothermodynamics design principles to an exoskeletal engine architecture was sufficient to identify the limiting structural and materials challenges. As mentioned above and in reference 2 (Halliwell), the design of exoskeletal engine blades and flow paths to deliver performance on a par with highly optimized conventional engines is likely to require significant study and development of design guidelines. For example, exoskeletal rotating blade tips are at a smaller radius than the blade root, which results in tip leakage at the engine hub increasing with rotational speed. Rotating blades supported at the outer radius and stators supported at their inner radius necessitate a structural design opposite that of conventional engines, affecting thickness, curvature, and blade dynamics. In an exoskeletal engine, the outer wall of the engine rotates with the blades, representing a large windage area (compared with a conventional shaft). The impacts on engine performance of these and other changes from conventional engine design are unknown. However, the exoskeletal engine concept proposes no intended deviations from the aerothermodynamic cycle design heritage of conventional engines. In lieu of design details, an earlier examination of the feasibility of the exoskeletal engine concept found it acceptable to transfer engine cycle parameters directly from a baseline conventional engine (Exoskeletal Technology Evaluation for Use in Aeropropulsion Applications. Presented to the Ultra-Efficient Engine Technology Program, Feb. 28, 2001). It was therefore assumed that any variations in engine aerothermodynamic cycle design are of small order compared with the issues of viability presented by structural-mechanical design and that an exoskeletal engine design can be assumed aerothermodynamically identical to a conventional engine for the purposes of this investigation.

The second assumption was that turbine engine subsystem and components currently in use can be applied to an exoskeletal engine at their existing performance levels. Typical gas turbine engine components, such as controls, actuators, and combustors, may pose significant engineering challenges in

their adaptation to an exoskeletal engine. For this investigation, however, the expectation was that no new technology would be required to apply these subsystems and components to an exoskeletal engine.

Key Challenges

Development of structural and mechanical exoskeletal HPS concept.—The central idea of an exoskeletal engine concept involves a change in the structural and mechanical design of the rotating machinery in a gas turbine engine. The concept is not proposed as a change to the engine cycle or aerodynamics, other than that necessary to accommodate changes to the structural and mechanical design. Thus, the system-level feasibility questions about the exoskeletal engine concept lie with the structural and mechanical architecture. The outer rotating shell of an exoskeletal system must withstand stresses due to the inertia of rotation, contain engine pressure loads, react to blade loads, and accommodate the engine nominal and contingency environments. It must also accommodate engine assembly and maintenance.

Development of system-integrated bearing concept for exoskeletal HPS.—The exoskeletal approach inherently involves large portions of an engine system rotating at larger radii than those in a conventional engine. The development of an appropriate bearing concept is a challenge that involves

(1) Integration with the system structural concept to minimize bearing *DN*
(2) Consideration of existing and emerging bearing technologies, including noncontact bearings
(3) Consideration of both nominal and off-nominal engine conditions, including startup, maneuvering, and landing

Approach

A conceptual analysis was deemed sufficient to determine exoskeletal structural-mechanical viability and to compare the weight of a conventional engine with its exoskeletal counterpart. This approach included both identifying the key characteristics driving the viability and weight and selecting the pertinent engine subsystems for design and analysis. A representative conventional engine was selected and the exoskeletal analogue was created. This approach minimized the design and analysis effort while still providing the understanding of the engineering issues involved with the exoskeletal architecture. In detail, the process can be described as follows:

Identification of suitable conventional gas turbine engine for comparison with exoskeletal concept.—A valid comparison of an exoskeletal approach and the conventional approach required identification of an existing gas turbine engine with the following characteristics:

(1) Representative of state-of-the-art gas turbine engine design, especially high-pressure spool rotation speeds and temperatures
(2) Availability of design information, allowing modeling and adaptation of structures and mechanisms to an exoskeletal approach
(3) Fully axial design (no centrifugal compressors or turbines)

Design of exoskeletal analogue HPS concept.—A conceptual design of an exoskeletal engine high-pressure spool was developed based on the NASA model of an existing engine. The conceptual design is described in the section Description of Exoskeletal System Concept. The approach to this design had neither a precedent nor design guidelines for exoskeletal components. Materials and structures concepts were defined consistent with the analogous environments from the conventional HPS example, consistent with an aggressive but realistic concept philosophy.

Calculation of weight of exoskeletal analogue HPS concept.—The weight of the exoskeletal HPS was calculated based on the design concept, as were the weights of shells and the stationary core. Blade weights were based on conventional engine blade weights but were modified for the exoskeletal

geometry. The weights of components, such as combustors, that were largely unaffected by the change to an exoskeletal design were adopted from existing engines.

Verification of exoskeletal HPS concept structural integrity.—Structural analyses were performed to verify the structural integrity of critical exoskeletal high-pressure spool components, such as drum rotors, bladed rings, and bearing supports. The intent was to show that the weight estimates were aggressive but reasonable. Finite-element models were not of sufficient detail to perform complete structural analyses considering the limited thermal analysis that was performed. The operating thermal environment was, however, considered in the selection of materials and in choosing an appropriate allowable stress range for applied mechanical loads. This approach was considered adequate for the purposes of this investigation. High-fidelity modeling and refinement of the environment to include all aerodynamic, inertial, and thermal loads to a greater degree of accuracy would be required prior to commitment to an exoskeletal engine development.

Identification of technology challenges.—This investigation attempted to discover not just whether an exoskeletal approach to gas turbine engine design is viable but also the critical characteristics upon which viability depends. Where new or improved technologies were important to the viability of the exoskeletal approach, they were identified. A preliminary assessment was made of the potential of new technologies to satisfy the requirements of the exoskeletal approach.

Architecture Description

Since the exoskeletal concept presents an aggressive departure from conventional turbine engines, it is imperative to look at the concept using a systems approach. A solid model of the concept was generated as the first step of the analysis and weight determination of the system. The method for developing reasonable weight comparisons consists of building component models for finite-element analyses (FEA) of the exoskeletal engine system. The intention is to look at all major components in the engine system with some consideration given to mounting and assembly procedures for all rotating parts. Hopefully, this approach will unveil any potentially significant benefits as well as any possible technical hurdles pursuant to a new direction in turbine engine technology. Finally, the comparison of engine weights as a product of the investigation will serve as the principal metric for an evaluation of exoskeletal versus conventional engine benefits.

Description of Exoskeletal System Concept

The exoskeletal engine architecture for this study is based on the Rolls-Royce (Allison) AE3007 engine. The design dimensions were scaled from a sketch of a longitudinal section through the AE3007 in Jane's Aero-Engines (ref. 3). These scaled dimensions were input to NASA's engine weight estimate computer code WATE (Weight Analysis Turbine Engine, refs. 4 and 5) to develop a government interpretation of an AE3007-like engine. Scaled dimensions and the output from the WATE code (appendix A) were used to generate a Pro/Engineer® (ref. 6) CAD model representation of the AE3007 exoskeletal engine.

The AE3007 engine shown in figure 4 is a two-shaft subsonic turbofan, and the shafts are concentric. The AE3007 engine has an axial-flow, high-pressure compressor, a combustion chamber, and a high-pressure turbine (HPT) all spinning on the outer shaft. The HPC has 14 stages, variable-inlet guide vanes, and variable-inlet stators in the first 5 rows. The overall pressure ratio of the HPC is 23. The combustion chamber is an annular design with 16 fuel nozzles. The HPT is a two-stage axial design with air-cooled blades. A three-stage, low-pressure turbine drives the inner shaft, which in turn drives a single-stage, wide-chord fan. The fan has a mass flow of 260 lb/sec and a bypass ratio of 5. The outer fan duct and jet pipe are composite designs.
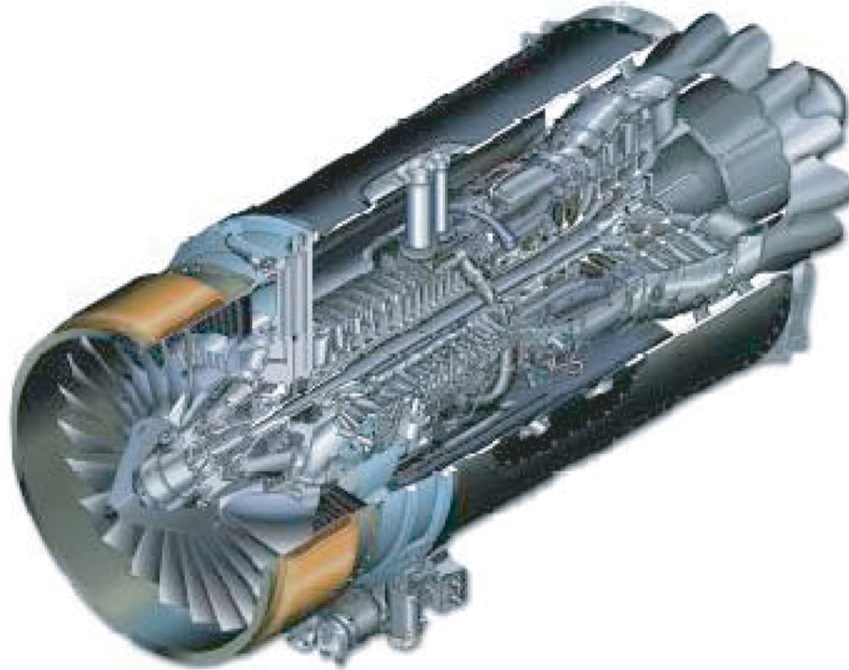
Figure 4.—Rolls-Royce AE3007 longitudinal section. Inlet diameter, 38.5 in.;
overall diameter, 43.5 in.; length, 106.5 in.; length with spinner, 115.1 in.;
dry weight with bypass duct, 1581 lb; specific fuel consumption, 0.33 lb/hr/lb st.

Heritage of Rolls-Royce (Allison) AE3007-based NASA engine cycle model.—The NASA AE3007 cycle model was developed to support NASA's goals assessment (ref. 7). Analytical models of various airframes and propulsion systems representative of the current state of the art were developed in sufficient detail to allow the inclusion of new technologies to assess the benefit of these technologies on system performance (size, cost, emissions, maintainability, etc.). To disseminate study assumptions and results, NASA developed models of these airframes and propulsions systems, based on publicly available information and good engineering judgment. Although the models developed may be similar in overall performance and capability to the actual airframes and propulsion systems in use, there could be significant differences between the NASA-developed models and the actual systems.

Development of AE3007 thermodynamic model.—As part of that activity, a model of a 50-passenger regional jet based on the EMB145 was developed, with its propulsion system based on the Rolls-Royce (Allison) AE3007. For its size and thrust class, the AE3007 is a moderately high-bypass, two-spool, mixed-flow turbofan. It uses only axial-flow components, reducing engine and core diameter. For this study, it was thought that its core diameter was within the state of the art for composite rotating materials. A one-dimensional, steady-state, thermodynamic cycle model was developed using the NASA Engine Performance Program (NEPP, ref. 8). A block model of the engine is shown in figure 5, indicating gas flow paths and mechanical connections. Table 1 shows gas conditions throughout the cycle at sea-level static conditions based on assumed component and overall engine performance (the actual NEPP output is listed in appendix B). Compressor and turbine maps were generated (refs. 9 and 10) based on component size and performance or were scaled from existing in-house maps with similar characteristics. The actual compressor and high-pressure turbine maps used are shown in figures 6 to 8. These maps are used for estimating the off-design performance of these components while the cycle model is "flown" over a range of Mach, altitude, and engine power conditions to generate performance data to be included in mission analyses. In addition, component maximum performance points are recorded (mass flow, temperature, pressure, torque, etc.) to be used to develop a flow-path weight model.
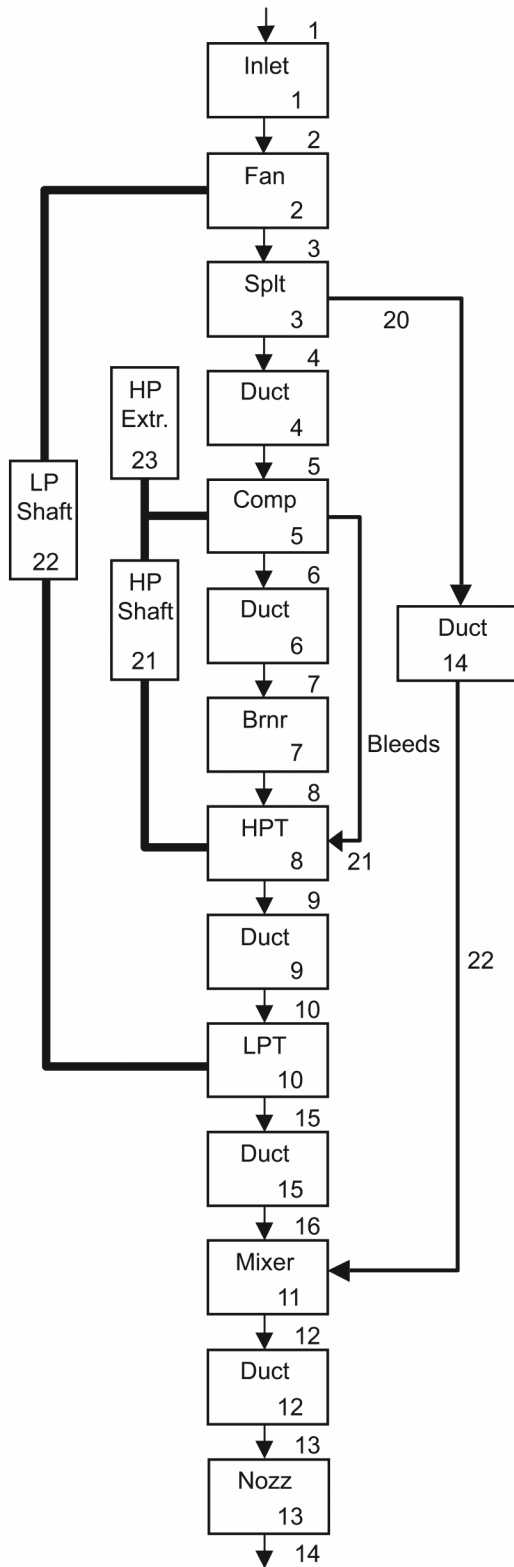
Figure 5.—NEPP model configuration for NASA AE3007.

TABLE 1.—NEPP AE3007 STATION PROPERTIES

Station number	Mass flow, lb_m/s	Pressure, psia	Temperature, °R	Fuel-to-air ratio
1	257.4	14.7	545.7	0.0000
2	257.4	14.5	545.7	
3	257.4	24.0	641.9	
4	41.7	24.0	641.9	
5	41.7	23.7	641.9	
6	36.1	353.4	1465.0	
7	36.1	348.1	1465.0	
8	36.8	332.5	2792.1	.0221
9	41.5	72.4	1942.6	.0196
10	41.5	72.0	1942.6	.0196
12	257.3	21.0	775.7	.0031
13	257.2	20.9	775.7	.0031
14	257.2	20.9	775.7	.0031
15	41.5	18.1	1426.0	.0196
16	41.5	18.0	1426.0	.0196
20	215.8	23.6	641.9	.0000
21	4.8	353.4	1465.0	.0000
22	215.8	23.6	641.9	.0000
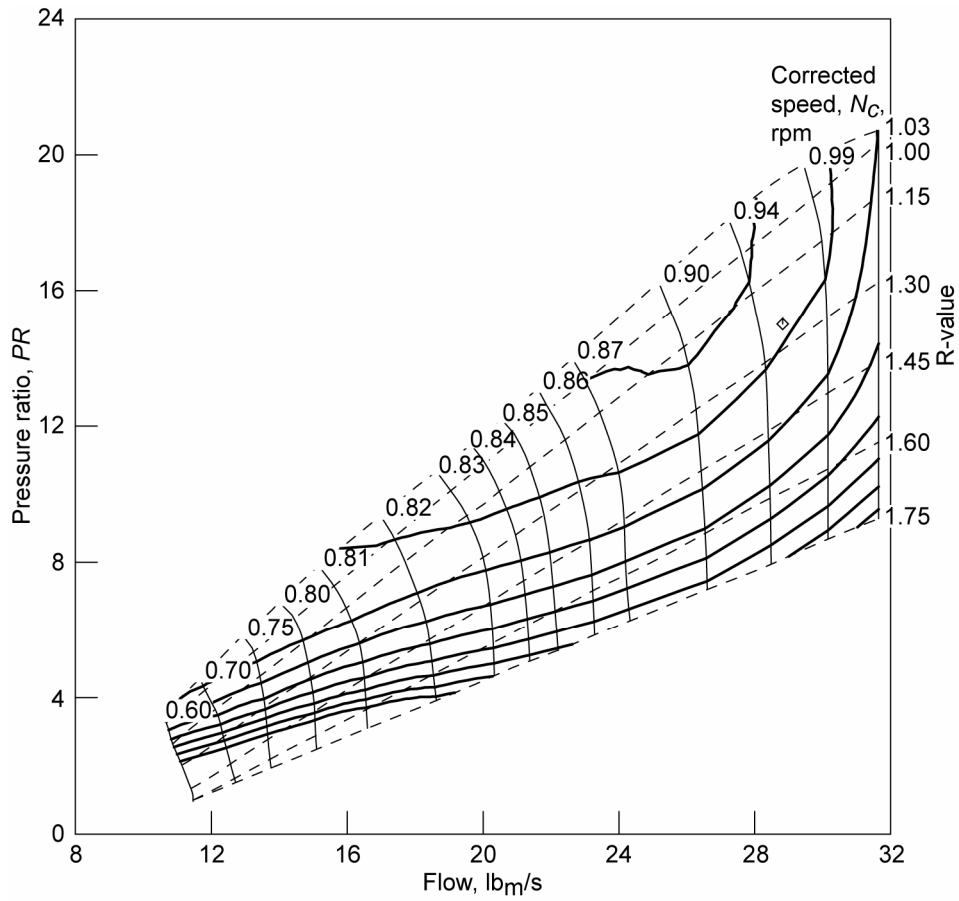
Figure 6.—Compressor map for corrected flow as function of total pressure ratio.
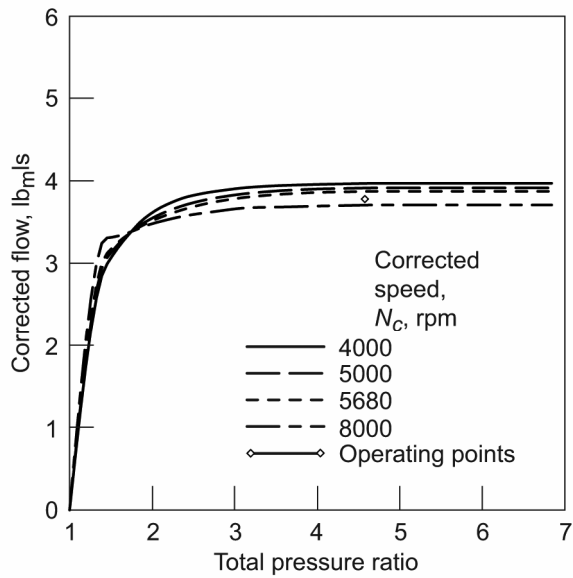
Figure 7.—Turbine map for mass flow as function of pressure ratio.
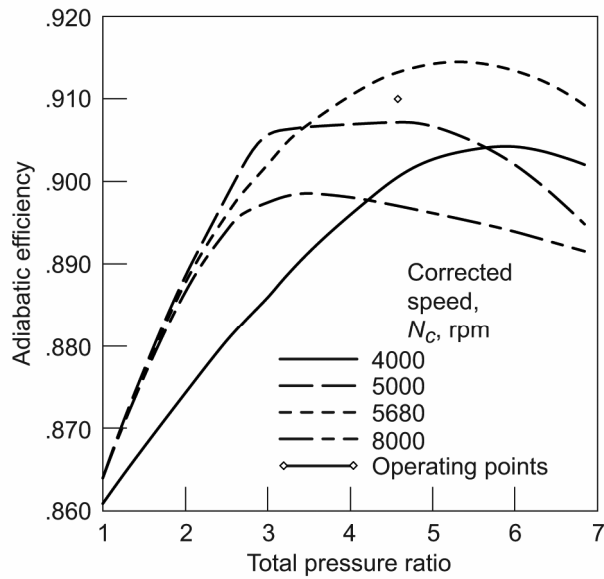
Figure 8.—Turbine map for efficiency as function of pressure ratio.

Development of the AE3007 flow-path and weight model.—An engine flow-path and weight estimation model was developed using the WATE program (refs. 11 and 12) and was based on maximum conditions determined from NEPP. A graphical output detailing the WATE analysis of the engine flow path is shown in figure 9. The WATE code estimates the total weight of various components and subcomponents based on user inputs and conditions experienced. The weight of each component is developed from its subcomponent parts. For example, the compressor weight is determined on a stage-by-stage basis, based on the flow conditions and performance of each particular stage. Input parameters include blade hub-to-tip ratio, aspect ratio, disk type, and compressor end support (e.g., frame and bearing type). Different materials may also be chosen for the various parts (disk, rotor and stator blades, surrounding case, etc.). Such detail was required for previous study efforts to assess the effect of technologies that might be applicable to only one part, such as blades, disks, and so forth. This level of detail was also helpful to start the analysis of an exoskeletal version of the AE3007. However, the WATE analysis does not go into detailed blade design, the development of which will be discussed the following section. Since the exoskeletal analysis was limited to the high-pressure spool of the engine, more detailed gas flow conditions (from NEPP/WATE) and mechanical data (from WATE) were used for subsequent analyses. Tables 2 and 3 show these data.

		COMP#	Type	NSTAGE	WT
Bare engine weight	1491	1	INLT	0	250
Accessories weight	141	2	FANH	1	294
Total engine weight	1632	3	SPLT	0	0
Inlet/nacelle weight	249	4	DUCT	0	33
Total engine pod weight	1882	5	HPC	14	262
		6	DUCT	0	2
Engine length	109.0	7	PBUR	0	130
Total engine pod length	128.2	8	HPT	2	193
Engine maximum diameter	38.5	9	DUCT	0	2
Nacelle maximum diameter	45.8	10	LPT	3	269
Engine pod center of gravity location	33.4	15	DUCT	0	0
		14	DUCT	0	117
		11	FMIX	0	47
		12	DUCT	0	0
		13	NOZ	0	67
		21	SHAF	0	15
		22	SHAF	0	60
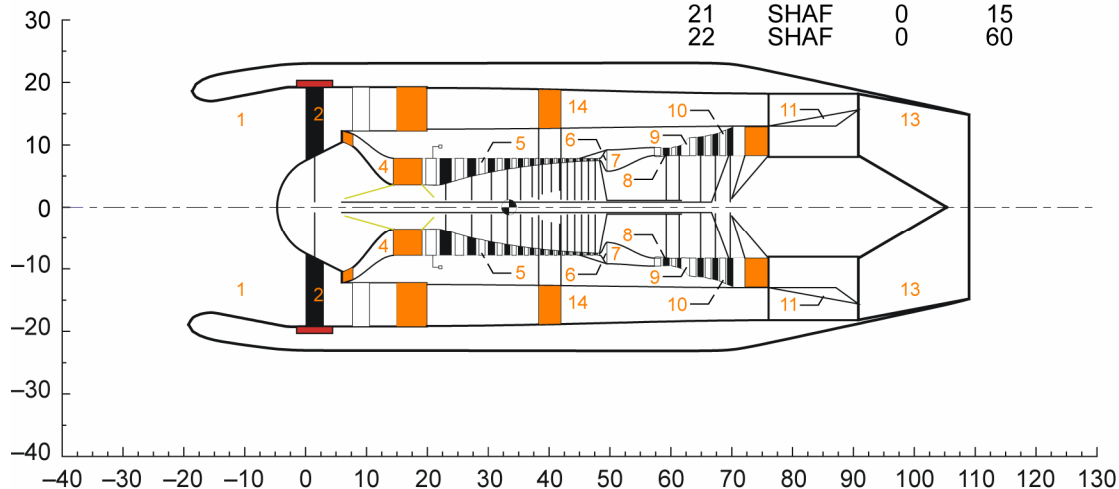
Figure 9.—WATE analysis of AE3007 flow path. (All dimensions are in inches and weight is in pounds.)

TABLE 2.—NEPP/WATE AE3007 FLOW CONDITIONS THROUGH
TURBOMACHINERY

Component	Stage	Mass flow, lb$_m$/s	Entrance temperature, °R	Entrance pressure, psia	Pressure ratio across stage
HPC	1	41.68	638	23.3	1.34
	2		699	31.2	1.30
	3		759	40.7	1.28
	4		820	52.0	1.26
	5		880	65.3	1.24
	6		940	80.7	1.22
	7		999	98.6	1.21
	8		1058	119.0	1.19
	9		1117	142.2	1.18
	10		1175	168.4	1.17
	11		1233	197.7	1.17
	12		1290	230.5	1.16
	13		1347	267.0	1.15
	14		1403	307.4	1.14
	Exit		1465	351.9	------
HPT	1	40.06	2693	329.2	2.01
	2	42.62	2319	163.5	2.27
	Exit	42.62	1944	72.1	------

TABLE 3.—WATE AE3007 STRUCTURAL WEIGHTS AND DIMENSIONS FOR
HIGH-PRESSURE COMPRESSOR (HPC) AND HIGH-PRESSURE TURBINE (HPT)

Component	Stage	Length, L_{stage}, in.	Radius, r, in. Hub, r_H	Radius, r, in. Tip, r_T	Blade Number, n_B	Blade Height, H_B, in.	Blade Aspect ratio, AR	Blade, W_B	Nuts, W_N	Weight, W, lb$_m$ Disk, W_{disk}	Rotor drum, W_{RD}	Accessories, W_{ACC}	Density, ρ, lb$_m$/in.^{3} Disk, ρ_{disk}	Density Blade, ρ_B	Pressure ratio, PR
HPC[a]	1	1.94	3.57	7.84	21	4.27	2.2	3.7	1.6	2.8			0.284	0.160	1.34
	2	1.45	4.80	7.84	28	3.04	2.1	2.0	1.2	4.3			↓	↓	1.30
	3	1.17	5.53	7.84	35	2.31	2.0	1.2	1.0	6.6					1.28
	4	.97	6.02	7.84	42	1.82	1.9	.8	.8	10.9					1.26
	5	.84	6.36	7.84	49	1.48	1.8	.6	.7	13.0					1.24
	6	.73	6.62	7.84	56	1.22	1.7	.4	.6	13.0					1.22
	7	.66	6.82	7.84	62	1.02	1.6	.3	.5	12.9					1.21
	8	.60	6.97	7.84	68	.87	1.5	.2	.5	12.6					1.19
	9	.56	7.09	7.84	74	.75	1.3	.2	.5	11.3			.297		1.18
	10	.53	7.19	7.84	78	.65	1.2	.3	.4	12.3			↓	.300	1.17
	11	.50	7.28	7.84	82	.56	1.1	.2	.4	12.7				↓	1.17
	12	.49	7.34	7.84	84	.50	1.0	.2	.4	12.7					1.16
	13	.48	7.40	7.84	85	.44	.9	.2	.4	12.9					1.15
	14	.49	7.45	7.84	84	.39	.8	.2	.4	13.3					1.14
HPT	1	1.05	8.31	9.57	40	1.26	1.2	2.5	2.4	25.2	6.2	11.7	0.298	0.281	2.01
	2	.67	8.31	9.51	63	1.20	1.8	1.5	1.5	20.5	3.9	7.4	.298	.281	2.27

[a] HPC blades have a constant taper ratio of 0.833.

Exoskeletal Engine High-Pressure Spool

Figure 10 shows the conceptual design of the exoskeletal drum rotor assembly. Inverting the AE3007 design, the HPC and HPT rotor blades are mounted to the drum rotor and the stator rows are mounted to a stationary core. The stationary core outlines the rims of the original rotor disks on the AE3007 engine. Previous exoskeletal engine studies call for the complete elimination of the shafts and disks from the engine center (ref. 13), which would provide an open channel along the centerline (ref. 14). However, a stationary core with closed ends has been designed to support the stator blades. An AE3007-like exoskeletal design provides a convenient break at the LPT since it runs at a slower speed. Conceptually, the low-pressure spool would drive the fan via a separate drum rotor. The low-pressure spool drum rotor has been neglected in this study to focus on the exoskeletal high-pressure spool, which has greater physical demands.

A hypothetical exoskeletal engine assembly is depicted by the Pro/Engineer® model in figure 11, and the overall dimensions are shown in figure 12. To minimize the complexity of the study, three sections of the high-pressure spool (the HPC, combustion chamber, and HPT) were converted to an exoskeletal drum rotor design. The Pro/Engineer® model is intended for use in the conceptual design and analysis of an exoskeletal construction, and it is not a complete representation of the propulsion system.

Figure 11 shows the high-pressure spool as four sections. The HPC drum rotor assembly is broken down into two sections to permit material choice flexibility. Figure 13 shows the HPC drum rotor design in more detail. Graphite polyimide was investigated for the first seven stages where the temperature was below 600 °F. A titanium drum rotor is used for the last seven HPC stages where temperatures could rise to 950 °F. Hastelloy™ is used in the combustion chamber and HPT drum rotors because gas temperatures could approach 2500 °F.

A bearing system is located at each end of the high-pressure spool to support the rotating drum. As shown in figure 11, the bearings transfer the loads between the drum rotor and the struts and permit relatively free rotation with minimum friction.
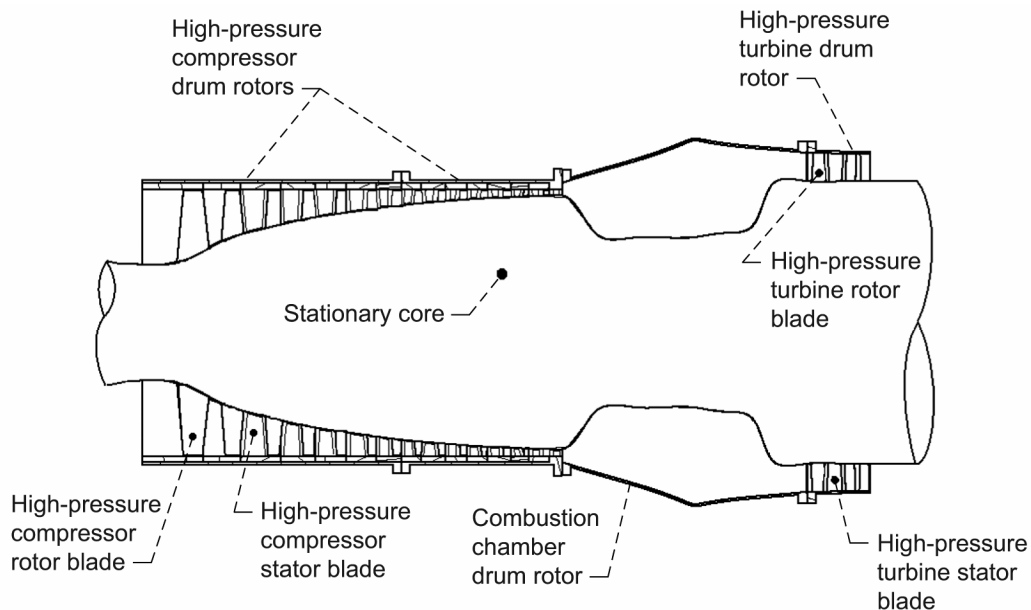
Figure 10.—Conceptual design for AE3007-like exoskeletal engine high-pressure spool.

Inlet diameter   38.5
Overall diameter   43.5
Length   110.25

High-pressure spool
rotating drum assembly

Struts

Bearing locations

First high-pressure
compressor drum rotor

Second high-pressure
compressor drum rotor

Combustion chamber drum rotor

High-pressure turbine
drum rotor

Four high-pressure spool sections of drum rotor
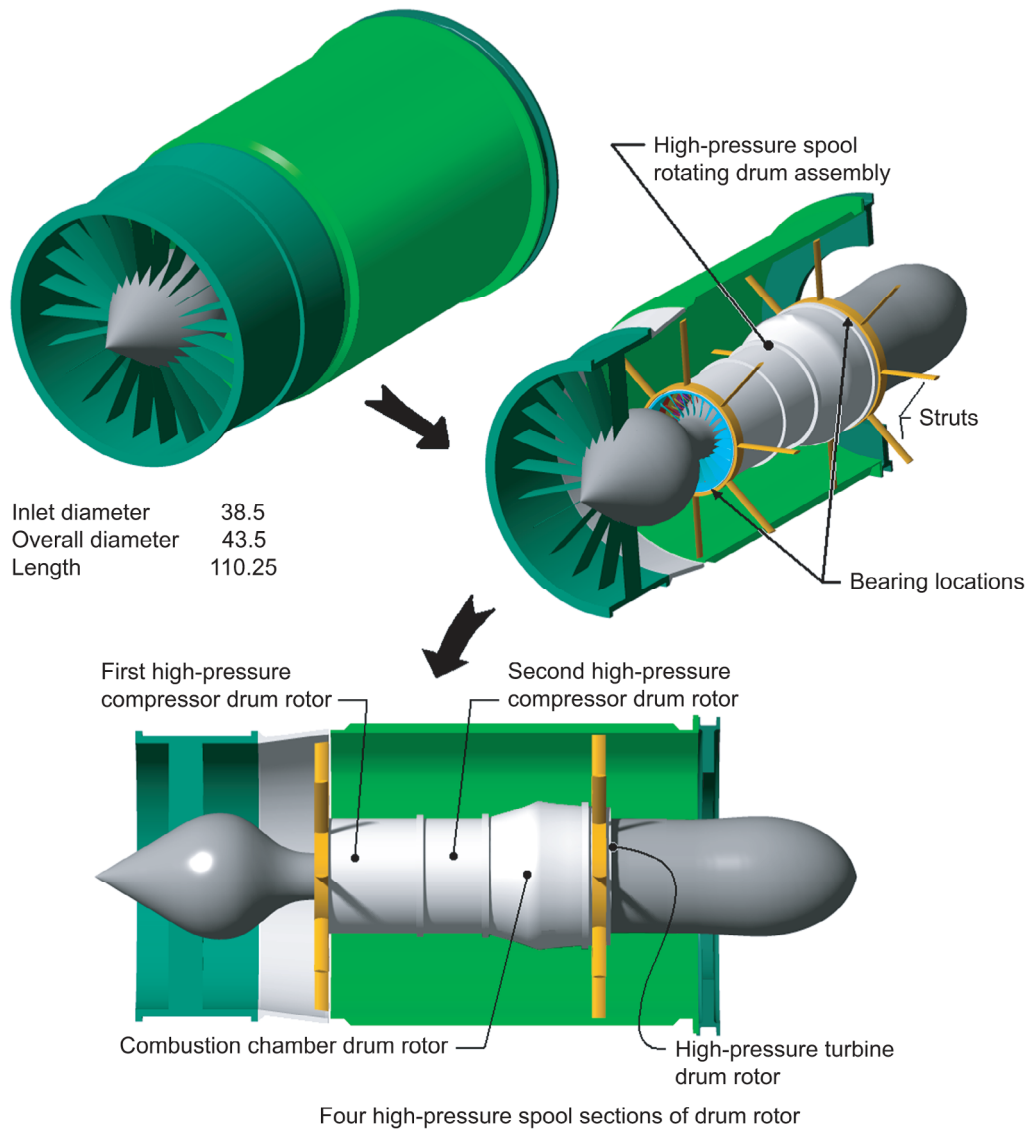
Figure 11.—Pro/Engineer® model of AE3007–like exoskeletal engine. (All dimensions are in inches.)

A

∅ 43.600
∅ 46.000

84.590

17.730

10.220

16.680

20.020

15.230

9.450

3.710

5.910

25.940

42.806

110.250

A

Section A – A
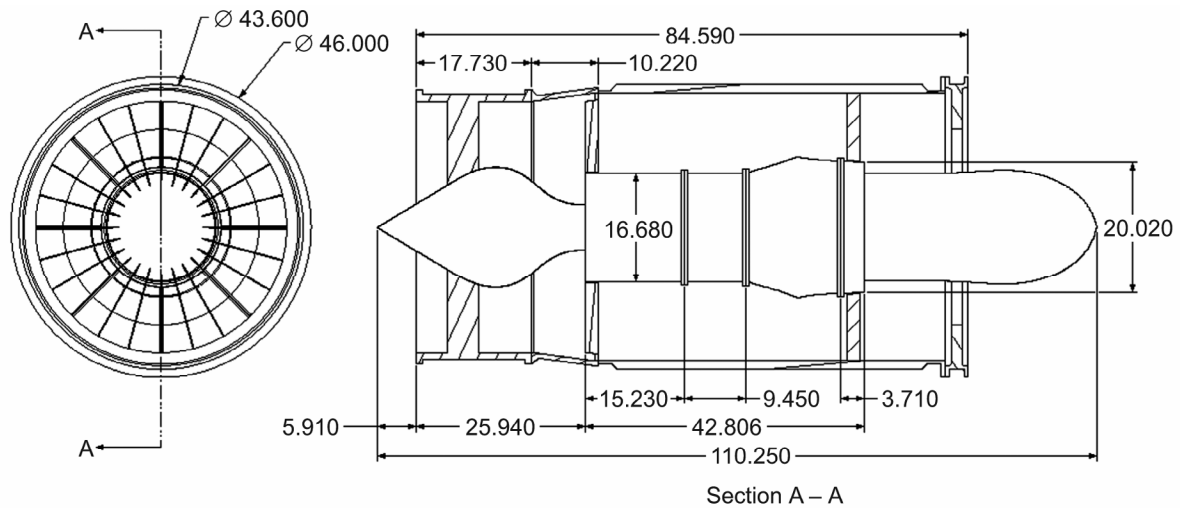
Figure 12.—Overall dimensions for AE3007–like exoskeletal engine. (All dimensions are in inches.)
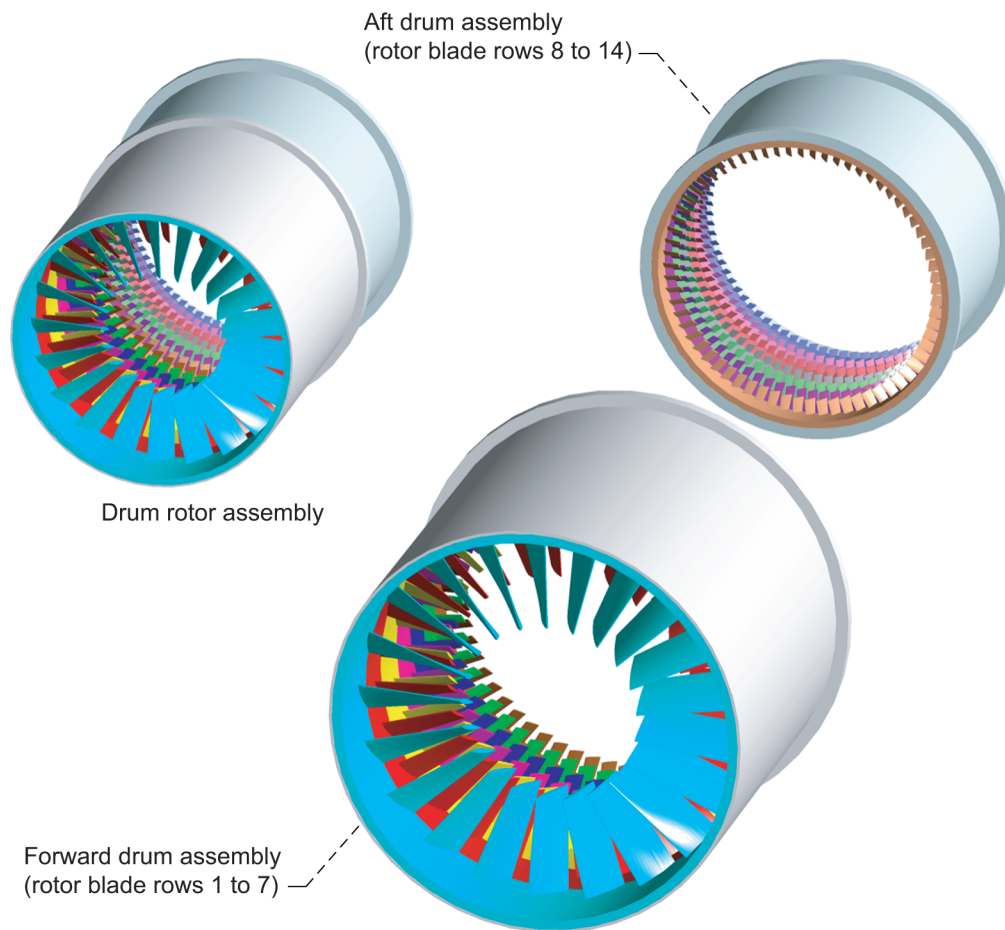
Figure 13.—Exoskeletal high-pressure compressor drum rotor assembly.

An examination of figure 13 shows that the exoskeletal engine assembly and maintenance will be more difficult than that of the conventional engine. One question is how the rotor blades will be assembled to the drum rotor using acceptable methods of construction. One answer was to divide the rotor into integral bladed rings for each stage, as shown in figure 14. Similarly, the stator would also consist of integral bladed-ring components. Since composite materials have an immense potential use in the rotor blades supported in compression, the integral bladed ring is a natural step to blend function and assembly. Manufacturing an integral bladed ring will also be a challenge, but this approach should reduce weight. To build the exoskeletal engine, each stage is installed in the rotor drum in an assembly procedure that alternates between stator bladed rings and rotor bladed rings. Each ring would provide the necessary space for the adjacent stage, or one could design a separate spacer. Although assembly and maintenance time would be increased, this concept would eliminate a longitudinal split of the drum rotor and longitudinal mounting flanges that would create rotor instability.

As stated earlier, the WATE computer code was used to generate dimensions and weights of exoskeletal components. HPC and HPT blade dimensions were also output from the WATE code. Table 4 shows the dimensions used to generate Pro/Engineer® models of each rotor stage.

A generalized NACA wing design was used to create the HPC rotor blade with stagger angles at the root and tip as shown in figure 15. The design of the HPT rotor blades is similar, but a camber angle of 15° was used to define the HPT blade curvature as shown in figure 16.
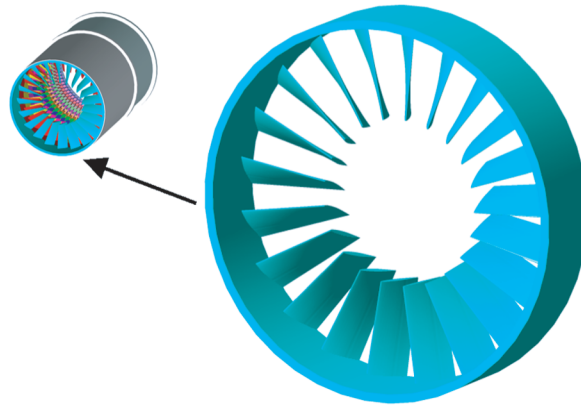
Figure 14.—Integral bladed ring for high-pressure compressor drum rotor.

TABLE 4.— BLADE DIMENSIONS FOR HPC AND HPT ROTOR STAGES

Com-ponent	Stage	Radius, r, in.		Hub			Tip			Number of blades, n_B
		Inlet, r_H	Exit, r_T	Chord length, in.	Blade width, in.	Stagger angle, θ, deg	Chord length, in.	Blade width, in.	Stagger angle, θ, deg	
HPC	1	3.57	7.84	2.117	1.970	21.47	1.765	1.107	51.14	21
	2	4.8	7.84	1.587	1.374	30.02	1.322	.830		28
	3	5.53	7.84	1.273	1.041	35.09	1.061	.665		35
	4	6.02	7.84	1.056	.827	38.49	.880	.552		42
	5	6.36	7.84	.912	.690	40.86	.760	.477		49
	6	6.62	7.84	.802	.590	42.66	.668	.419		56
	7	6.82	7.84	.718	.516	44.05	.598	.375		62
	8	6.97	7.84	.655	.462	45.09	.546	.342		68
	9	7.09	7.84	.611	.425	45.93	.509	.319		74
	10	7.19	7.84	.577	.396	46.62	.480	.301		78
	11	7.28	7.84	.546	.370	47.25	.455	.285		82
	12	7.34	7.84	.535	.360	47.67	.446	.280		84
	13	7.4	7.84	.528	.352	48.08	.440	.276		85
	14	7.45	7.84	.532	.353	48.43	.443	.278	↓	84
HPT	1	8.31	9.57	1.375	1.15	21.47	1.146	0.60	30	40
	2	8.31	9.51	.872	.73	26.54	.727	.38	30	63
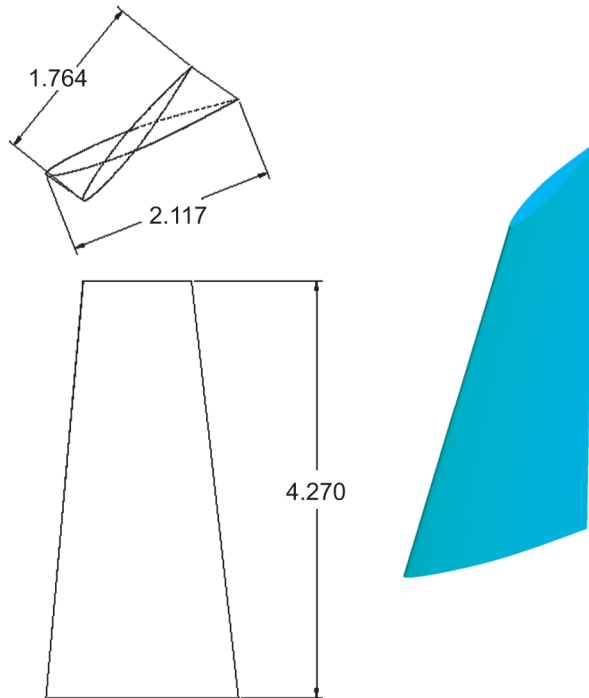
Figure 15.—Rotor blade design for first high-pressure compressor stage of exoskeletal engine concept. (All dimensions are in inches.)
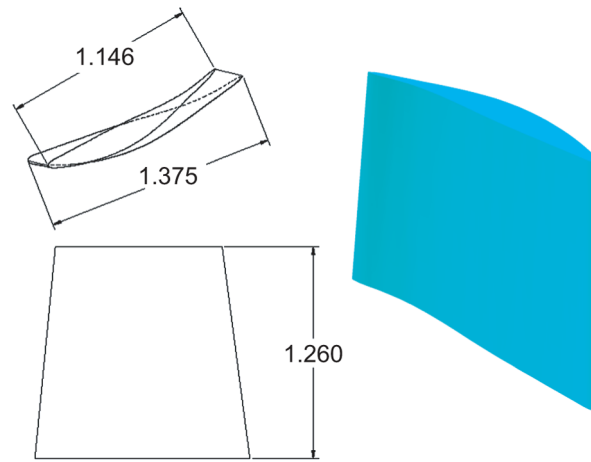
Figure 16.—Rotor blade design for first high-pressure turbine stage of exoskeletal engine concept. (All dimensions are in inches.)

Structural Analysis and Assessment

Blade Investigation

Method of analysis.—Blade geometry was generated using the WATE code as summarized in the section Development of AE3007 flow-path and weight model. The blade height varied from 4.27 to 0.39 in. between HPC stages 1 to 14, respectively. This variation in height for HPC blades is illustrated in figure 17. Parameters such as thickness, taper ratio, and chord length were varied during the investigation iteration process as required to achieve a positive margin of safety. In some cases, the camber angle was adjusted to increase compression stresses while decreasing tension stresses in the blade. A ceramic matrix composite (CMC) blade will perform better in compression than in tension. The NACA airfoil 65A010 was used as a representative blade section for the HPC and is shown in figure 18.

Using this approach, the AE3007-like blade geometries were derived and modeled using Pro/Engineer® to formulate the starting point for a finite-element analysis of each stage in the HPC and HPT. One blade was modeled for each stage in an exoskeletal design (blade in compression). The aerodynamic loads were assumed to be the same for the exoskeletal configuration as those for the conventional engine. The NEPP software code provided pressure loads for each stage, which was combined with rotational inertia for a combined static load case solved using MSC/NASTRAN™ FEA software (ref. 15). The rotational speed of the engine is 16 400 rpm (overspeed condition). For each stage, the NEPP software code also provided temperature data, which was used to select appropriate materials for the finite-element analysis. Table 5 gives the entrance temperature range for stages 1 to 14 of the HPC.
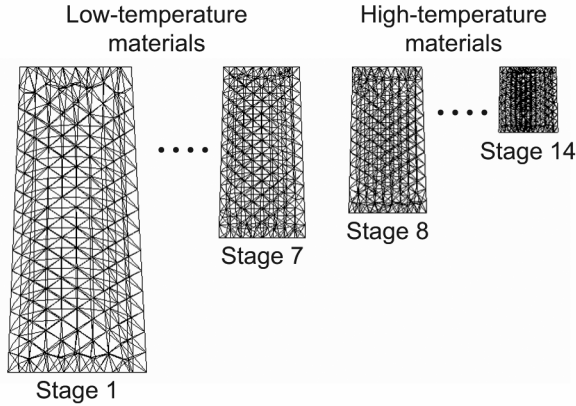
Figure 17.—High-pressure compressor blade models for finite-element solution.
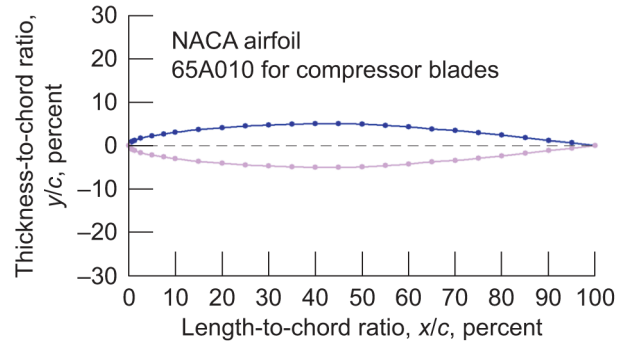
Figure 18.—Typical compressor blade-shape profile.

TABLE 5.—ENTRANCE TEMPERATURES FOR
HIGH-PRESSURE COMPRESSOR STAGES

Stage	Temperature, °F	Stage	Temperature, °F
1	178	8	598
2	239	9	657
3	299	10	715
4	360	11	773
5	420	12	830
6	480	13	887
7	539	14	943

High-pressure compressor analysis.—The first seven stages of the HPC utilize a lightweight polymer matrix composite (PMC) material. Graphite polyimide was selected as a suitable option having temperature-dependent properties up to 600 °F as shown in table 6. For stages 8 to 14, Titanium 6Al−4 Valloy, hereinafter referred to as Titanium, was selected based on temperature capabilities up to 900 °F as shown in table 7. Other candidate materials used in the investigation of HPC blades include aluminum and Waspaloy[TM] with allowable stresses as shown in tables 8 and 9, respectively. These allowable material stresses were obtained from the Metallic Materials and Elements for Aerospace Vehicle Structures (ref. 16) and include the appropriate reductions for temperature. Similarly, the composite material properties (graphite polyimide) were derived from the HyperSizer[TM] (ref. 17) data base but with a 50-percent knockdown applied to account for life and durability effects. A summary of mechanical properties for materials in this investigation is presented in table 10.

TABLE 6.—MATERIAL ALLOWABLES USED FOR GRAPHITE POLYIMIDE
[Includes 50-percent knockdown for durability.]

Temperature, °F	Allowables		
	Ultimate tensile force, F_{tu}, $klb_f/in.^2$	Ultimate compressive force, F_{cu}, $klb_f/in.^2$	Ultimate shear force, F_{su}, $klb_f/in.^2$
72	113	100	6.5
600	105	51	3.1

TABLE 7.—MATERIAL ALLOWABLES USED FOR TITANIUM 6AL–4V

Temperature, °F	Allowables		
	Ultimate tensile force, F_{tu}, klb$_f$/in.^{2}	Ultimate compressive force, F_{cu}, klb$_f$/in.^{2}	Ultimate shear force, F_{su}, klb$_f$/in.^{2}
100	134	133	85
200	126	119	80
300	114	107	75
400	103	96	70
500	94	89	67
600	92	88	65
700	90	85	58
800	86	82	52
900	77	71	46

TABLE 8.—MATERIAL ALLOWABLES USED FOR ALUMINUM

Temperature, °F	Allowables		
	Ultimate tensile force, F_{tu}, klb$_f$/in.^{2}	Ultimate compressive force, F_{cu}, klb$_f$/in.^{2}	Ultimate shear force, F_{su}, klb$_f$/in.^{2}
100	66	58	40
200	66	54	38
300	51	44	30
400	30	14	14
500	25	8	7
550	25	6	6
600	25		5
650	24		5
700	24	↓	4

TABLE 9.—MATERIAL ALLOWABLES USED FOR WASPALOY™

Temperature, °F	Allowables		
	Ultimate tensile force,[a] F_{tu}, klb$_f$/in.^{2}	Ultimate compressive force,[a] F_{cu}, klb$_f$/in.^{2}	Ultimate shear force,[b] F_{su}, klb$_f$/in.^{2}
100	138	138	83
200	136	136	82
300	132	132	79
400	129	129	77
500	127	127	76
600	125	125	75
700	123	123	74
800	121	121	73
900	120	120	72
1000	118	118	71
1100	115	115	69
1200	112	112	67
1300	104	104	62
1400	90	90	54
1500	70	70	52

[a]Applied 20-percent knockdown factor to allowable strength at ½-hr exposure.
[b]Assumed 60-percent ultimate strength as shear allowable.

TABLE 10.— SUMMARY OF MECHANICAL PROPERTIES FOR BLADE ANALYSIS

Material	Modulus of elasticity, E, lb/in.^{2}	Material density, ρ, lb$_m$/in.^{3}	Coefficient of thermal expansion, α, 1/°F	Poisson's ratio, μ	Allowables	
					Ultimate tensile force, F_{tu}, klb$_f$/in.^{2}	Ultimate compressive force, F_{cu}, klb$_f$/in.^{2}
Graphite polyimide	2.4×10^7	0.056	2×10^{-5}	0.33	See table 6	See table 6
Titanium	1.48×10^7	.160	5.2×10^{-6}	.3	See table 7	See table 7
Aluminum	1×10^7	.097	1.3×10^{-6}	.33	See table 8	See table 8
Waspaloy^{TM}	30.6×10^6	.298	7.6 to 7.9×10^{-6}	.3	See table 9	See table 9

The solid model blade geometry for each stage of the HPC was imported in the MSC/PATRAN^{TM} preprocessing software code (ref. 18) to create a finite-element model (FEM) for analysis. The initial blade models used a straight taper (ratio of tip chord to root chord is 1.0). Boundary conditions for conventional engine blades were fixed at the root or inside radius of the blade whereas the exoskeletal blade fixity is inverted as illustrated in figure 19.

Loads were applied to the exoskeletal blade FEM, including aerodynamic pressure acting on the blade combined with the rotating inertia. A static solution was then performed using MSC/NASTRAN^{TM} for each stage of the HPC. The maximum radial displacement was 0.006 in. at the stage 1 blade tip. The maximum Von Mises stress in the first seven stages using graphite polyimide was 26.2 klb/in.^{2} and occurred at the stage 5 blade root, resulting in a margin of safety of +0.95. The maximum buckling margin for the stage 1 PMC blades in compression is +2.24. It is interesting to note that both titanium and aluminum materials were investigated for the HPC stage 1 blades, and these selections fail in buckling for an exoskeletal design. Shear stress at the root of the stage 1 blade results in a negative margin of 0.60. Incorporating a taper in the blade design may reduce the negative margin, although a blade redesign such as this was not pursued in this investigation.

Stages 8 to 14 were investigated in a similar way, but the taper ratio of 1.0 was kept for each stage in this section of the HPC. Although Titanium 6Al−4V was the material of choice, a second material, Waspaloy^{TM}, was also investigated for these stages. The applied loads were combined aerodynamic pressure and rotational inertia for the static solutions using MSC/NASTRAN^{TM}. The peak stress and deflection results for this section of the HPC blade investigation are given in table 11 along with buckling margins of safety.
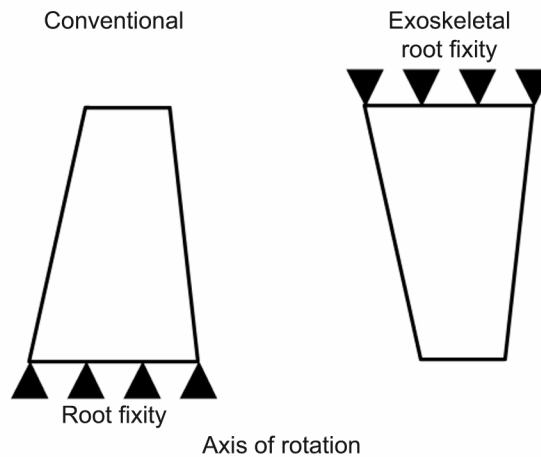
Figure 19.—Boundary conditions for exoskeletal versus conventional engine.

TABLE 11.—BLADE INVESTIGATION RESULTS FOR STAGES 1 To 14

Stage	Material	Maximum stress, σ_{max}, klb/in.^{2}	Radial displacement, in.	Margin of safety, M.S. (buckling)
1	Graphite polyimide	25.3	0.006	+2.24
5	Graphite polyimide	26.2	.0009	+9.18
8	Ti6Al–4V	28.0	.0008	+4.22
8	Waspaloy^{TM}	34.4	.0005	+4.80
9	Ti6Al–4V	28.3	.0006	+6.02

In summary, the lighter weight PMC works acceptably well in compression for the first seven stages of the HPC. Thus, graphite polyimide was used in tabulating the weights of the first seven stages of the compressor. Stages 8 to 14 of the HPC operate at temperatures above the practical range for PMC. Titanium was the selected material for blades in these stages and was used for weight calculation purposes.

High-pressure turbine analysis.—The HPT two-stage turbine is part of the high-pressure spool located aft of the combustion chamber and is subjected to higher temperatures than the HPC. Similar to the HPC, the blade geometry for the HPT was conceptually designed by first scaling the AE3007 drawing with output from the conventional design and WATE code for specific dimensions, as shown in table 4. Thermal analysis was then used to establish a thermal distribution across the blade as shown in figure 20. The intent of the investigation was to select a material that would not require cooling of the HPT blades and thereby achieve greater weight efficiency in an exoskeletal design. Based on the service temperature regime, a silicon-carbide-fiber matrix composite (SiC/SiC) was the preferred material for strength-to-weight properties. This CMC has the high-temperature capability and low-oxidation characteristics required for a combustion engine environment.

The assumed SiC/SiC properties used for this investigation are shown in table 12. The properties shown are estimated for a 1500 °F temperature under life-cycle service conditions. Although strength and durability in life-cycle applications are not readily available for SiC/SiC materials, the assumption was that these would be attainable values for current technology in CMC material systems.
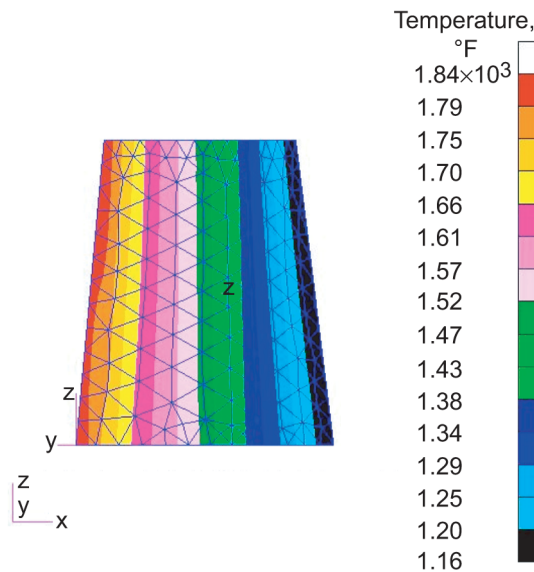
Figure 20.—Thermal distribution for high-pressure turbine blade.

TABLE 12.—PROJECTED CMC PROPERTIES AND ALLOWABLES
FOR EXOSKELETAL ENGINE ENVIRONMENT

Modulus of elasticity, Mlb/in.^{2}		Shear modulus, G_{12}, Mlb/in.^{2}	Poisson's ratio, μ_{12}	Coefficient of thermal expansion, α, 1/°F	Allowables		
$E_{1,2}$	E_3				Compressive stress, F_{lc}, klb/in.^{2}	Tensile stress, F_{lt}, klb/in.^{2}	Shear, F_{12}, klb/in.^{2}
30.4	21.3	11.4	0.18	2.42×10^{-6}	22.5	15.5	6.2

At the start of the HPT investigation, the first-stage blades had a height of 1.26 in. and a root chord length of 1.146 in. The applied loads consisted of aerodynamic pressure (165.7 psi) combined with a 16 400-rpm inertial load. The blade model was rigidly supported at the root to simulate the integral blade ring held by the rotor drum for the inverted exoskeletal design. The second-stage HPT blades were 1.20 in. in height and had a root chord length of 0.727 in. Similarly, the inertial loading plus pressure (91.5 psi) were applied as a static load on the blade. A camber angle for the HPT blades was set at 15° and the taper ratio at 0.80. The analysis results for the first attempt of these HPT blade configurations show high negative margins for compression, tensile, and shear stresses in the exoskeletal design.

Two steps were taken to alleviate the high negative margins for stress:

1. The root chord length was increased in half-inch increments.
2. The blade thickness was increased by 25 percent over the derived AE3007 values.

These changes were effective in bringing the exoskeletal tensile and compressive stresses to a positive margin, but not until the chord length reached approximately 2.75 in. The practicality of this structural-driven parameter on engine performance is not part of the investigation. The results of this parametric study of varying the chord length are shown for the exoskeletal design in table 13. As in the case of the compressor, shear margins were negative and will require further design improvement. It was observed that the material allowable reductions at the service temperature were affecting the margins of safety. Based on the findings of this investigation, the elimination of cooling in the HPT will not be as readily achieved as it was originally believed. If cooling can be done in an exoskeletal design, the allowable stresses would increase, which helps to achieve positive margins of safety. The addition of cooling in the blades is complex and may bring weight penalties into the design.

TABLE 13.—EXOSKELETAL HIGH-PRESSURE TURBINE BLADE
MARGINS OF SAFETY FOR VARIED CHORD LENGTH

Chord length, in.	Von Mises stress, σ_{vm}, klb/in.^{2}	Maximum principal stress (M.S. [a]), σ_1, klb/in.^{2}	Minimum principal stress (M.S. [a]), σ_2, klb/in.^{2}	Shear stress, σ_τ, klb/in.^{2}
1.146	167.0	62.7 (–0.75)	–182 (–0.88)	90.8 (–0.93)
1.719	37.5	33 (–0.53)	–44.4 (–0.49)	20.2 (–0.69)
2.0	29.1	29.2 (–0.47)	–36.1 (–0.38)	15.4 (–0.60)
2.5	19.9	20.8 (–0.25)	–24.6 (–0.09)	10.5 (–0.41)
3.0	15.9	12.4 (+0.25)	–19.7 (+0.14)	8.2 (–0.24)

[a]M.S., margin of safety.

Using the temperature distribution shown in figure 20, a thermal case was added to the FEA in an attempt to understand the full environmental effects on turbine blades. Difficulties were encountered, however, in the region of the blade root where rigid fixity was assumed. This fixity produced very high stress at the blade root for the static thermal solution. This result is very conservative since rigid fixity at the interface of the blade and integral blade ring (not modeled) is not entirely true. There will be some

distortion of the ring due to expansion that may relieve the high stress at the root. When the root constraints are removed, the thermal stress is no longer an issue. The real answer lies somewhere in between and would require a fully modeled blade-ring component to gain an understanding of the thermally induced stresses. This component would require a higher fidelity thermal analysis and perhaps an engine cycle analysis, which was beyond the scope of this investigation. Thus, thermal loads were not included in the analysis and margin calculations for this investigation.

Some benefits were observed for CMC material in an exoskeletal arrangement for the HPT blades. There is insufficient data, however, to conclude that negative margins in the exoskeletal design can be eliminated. Increasing the chord length lowers bending stresses at the root but may not be feasible for aerodynamic and flow-rate considerations. Similar to the HPC blades, shear margins are negative in the CMC turbine blades, which would require a design fix. Unresolved negative margins may be an issue in the use of SiC/SiC blade material for the HPT stages. The addition of cooling would increase the allowable stresses while adding complexity to the design, and this would not necessarily remove the negative margins for CMC material. Nonetheless, the CMC material was used for the tabulation of weight. It remains to be proven that CMC blades can be used in a high-pressure turbine stage meeting all strength and durability requirements. The purpose of this investigation, as stated before, was to take an aggressive approach for the potential exoskeletal engine design.

Drum Rotor Investigation

This section summarizes the stress analysis and sizing of the drum rotor in the exoskeletal engine design concept. This work is part of an overall effort to determine a feasible size and weight for the exoskeletal drum rotor. The objective of this stress analysis is to determine the adequacy of the drum rotor concept when it rotates at 16 400 rpm, the engine overspeed condition.

This stress analysis is performed using the ANSYS® finite-element analysis software (ref. 19). A longitudinal section through the drum can be modeled as a two-dimensional axisymmetric model as shown in figure 21. The final stress state for this section as a body of revolution is then determined using ANSYS for analyzing an axisymmetric solid. In a rotating body, the two components of displacement (radial and axial) in any plane section of the body along its axis of symmetry completely define its state of stress. Thus, the use of an axisymmetric model greatly reduces the modeling and analysis time compared with that of an equivalent three-dimensional model.

The exoskeletal drum rotor is modeled on a 360° basis as shown in figure 13. Since ANSYS requires the model to be defined in the plane $Z = 0.0$, the global Cartesian Y-axis is assumed to be the axis of symmetry. Furthermore, the model is developed only in the $+X$-quadrants, which defines the radial direction.

To minimize the complexity of the study, this analysis focuses only on three sections of the high-pressure spool of the exoskeletal rotor. The geometry is scaled from the AE3007 drawing, and the dimensions are shown in figure 22. The drum rotor is separated into four sections to permit material choice flexibility. The material choices are shown in figure 23.
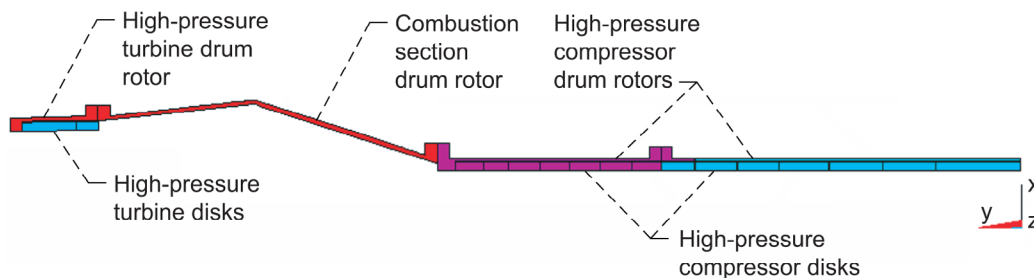
Figure 21.—Axisymmetric model of exoskeletal drum rotor.
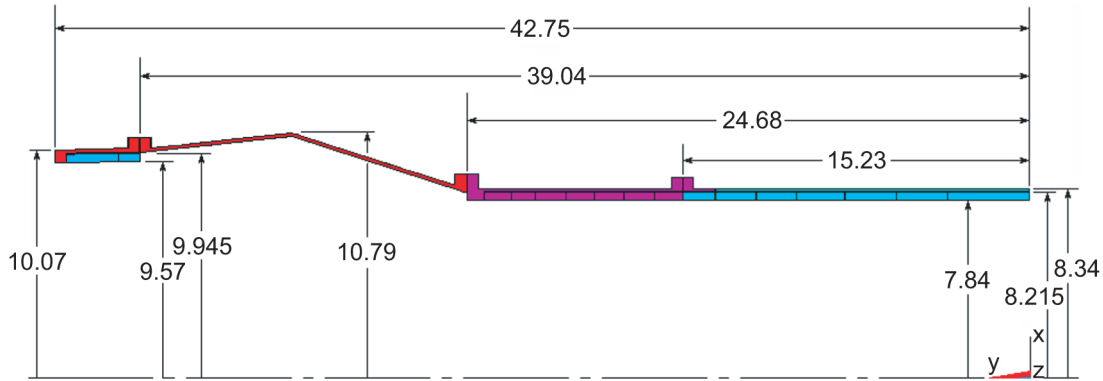
Figure 22.—Exoskeletal drum rotor. (All dimensions are in inches.)
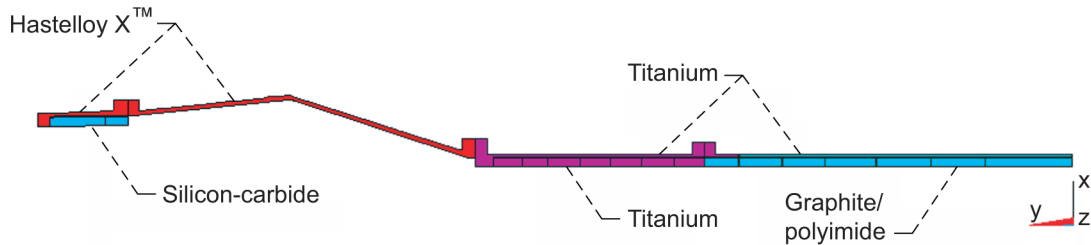
Figure 23.—Materials used in axisymmetric finite-element model of exoskeletal drum rotor.

Figure 24 shows the boundary conditions and loads applied to the exoskeletal drum rotor model. Since the rotor blades are discontinuous about the axis, an equivalent centrifugal force for each row of blades is applied to the inner radius of the disks. The weight of each rotor blade is obtained from the Pro/Engineer® model of the exoskeletal rotor. The total centrifugal force is calculated as a lumped mass at the disk inner radius spinning at 16 400 rpm:

$$F = mr_a\omega^2 = \frac{W_{\text{row}}}{g} r_a \left[\frac{2\pi(N)}{60} \right]^2 \tag{1}$$

where F is the total centrifugal force, m is lumped mass, r_a is the disk inner radius, ω is the rotational speed (radians per second), W_{row} is the total weight of all of the blades in that row, g is the gravitational constant, and N is the rotational speed (revolutions per minute). These centrifugal forces are applied to the FEM on a 360° basis, which evenly distributes the blade load on each disk.

Boundary conditions are applied to the drum rotor model at the bearing locations. There are two radial bearings (one at each end), and one thrust bearing at the inlet to the high-pressure spool. Referring to figure 24, an axial constraint is applied at the thrust bearing location. This axial constraint prevents free body motion along the spin axis.

The radial bearings are neither infinitely compliant nor rigid. Without accurate stiffness values, the actual bearing stiffness falls between no constraint and a rigid constraint. To bound the problem, two model cases are defined in the initial investigation: (1) rigid constraints are applied at the two radial bearing locations (as shown in fig. 24) and (2) no radial constraints are applied at the ends of the drum rotor model (as shown in fig. 25).
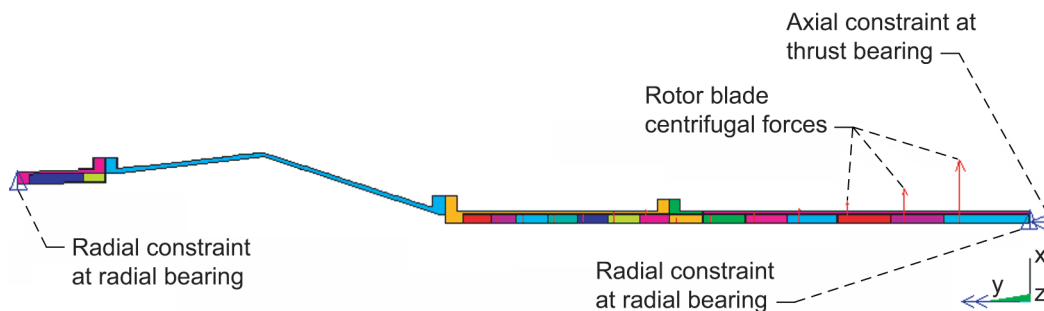
Figure 24.—Exoskeletal rotor blade centrifugal loads and bearing boundary constraints. Speed, 16 400 rpm.
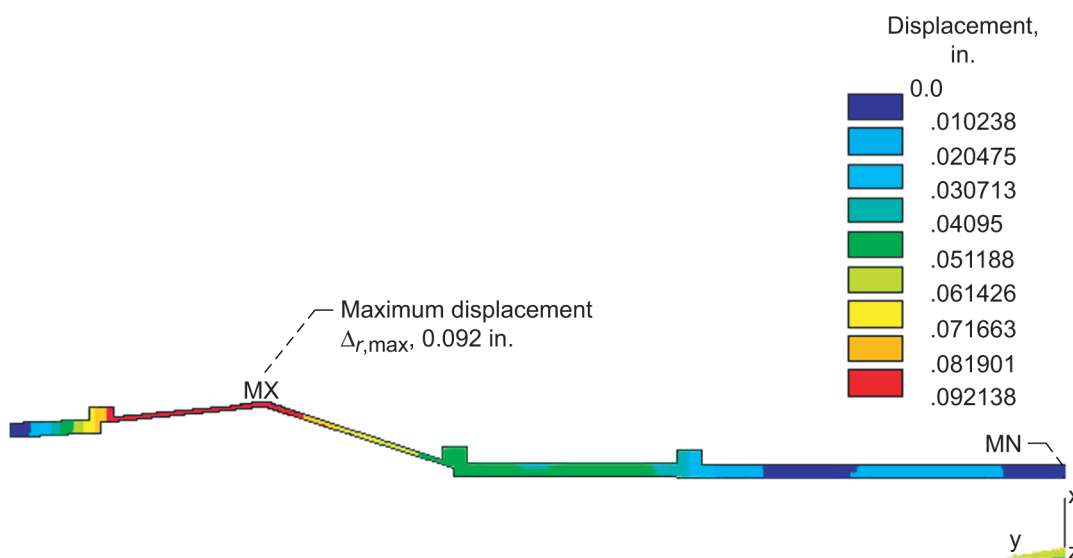
Figure 25.—Radial displacements for drum rotor with radial constraints. Speed, 16 400 rpm.

Case 1.—Figure 25 shows a radial displacement contour plot for the exoskeletal drum rotor with radial constraints. The displacement plot shows zero radial growth at the rotor ends and a maximum radial displacement of 0.092 in. at the peak of the combustion section shell. The radial stress contours for case 1 are shown in figure 26. The magnitude of the peak radial stresses indicates that the model is likely to be overconstrained at the aft radial bearing location.

The tangential stress contours for case 1 are shown in figure 27. The maximum tangential stress value of 314 720 psi at the end of the combustor section may be too great because the drum rotor is overconstrained. If the drum rotor is not free to grow in the radial direction at the ends, the heavy combustor section increases the stress near the joint flange at the high-pressure turbine.

The minimum and maximum axial stresses shown in figure 28 also indicate that the model is overconstrained at the aft radial bearing location.

Case 2.—Figure 29 shows the radial displacement contour plot for the drum rotor without radial constraints. The displacement plot shows radial growth at the rotor ends and a maximum radial displacement of 0.092 in. at the peak of the combustion section shell. The maximum radial displacement in case 2 is similar to case 1. However, each end of the drum rotor assembly is free to grow in the radial direction.

Stress, σ, psi
−645 997
−558 555
−471 112
−383 669
−296 227
−208 784
−121 341
−33 899
53 544
140 987

MN

Minimum and maximum radial stress at radial bearing locations: $\sigma_{r,min}$, −645 997 psi; $\sigma_{r,max}$, 140 987 psi

Hastelloy™ strengths at 70 °F, ultimate, F_{tu}, 100 000 psi; yield, F_{ty}, 40 000 psi
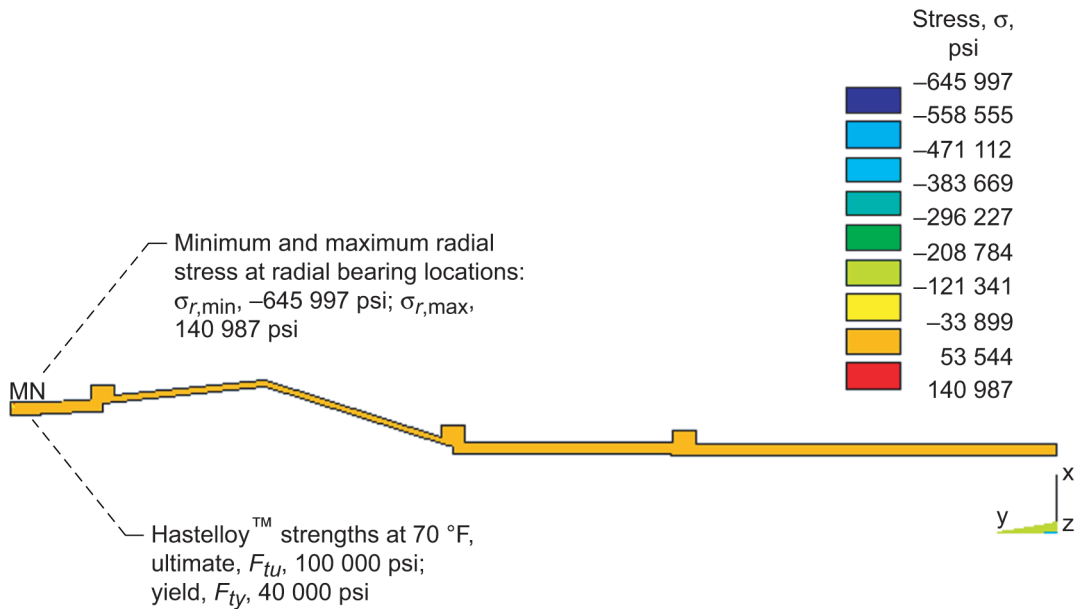
Figure 26.—Radial stresses for drum rotor with radial constraints. Speed, 16 400 rpm.

Stress, σ, psi
−375 643
−298 936
−222 229
−145 523
−68 816
7 891
84 598
161 304
238 011
314 718

MN MX

Minimum hoop stress at radial bearing location, $\sigma_{t,min}$, −375 643 psi

Maximum hoop stress at mounting flange, $\sigma_{t,max}$, −314 720 psi

Hastelloy™ strengths at 70 °F: ultimate, F_{tu}, 100 000 psi; yield, F_{ty}, 40 000 psi
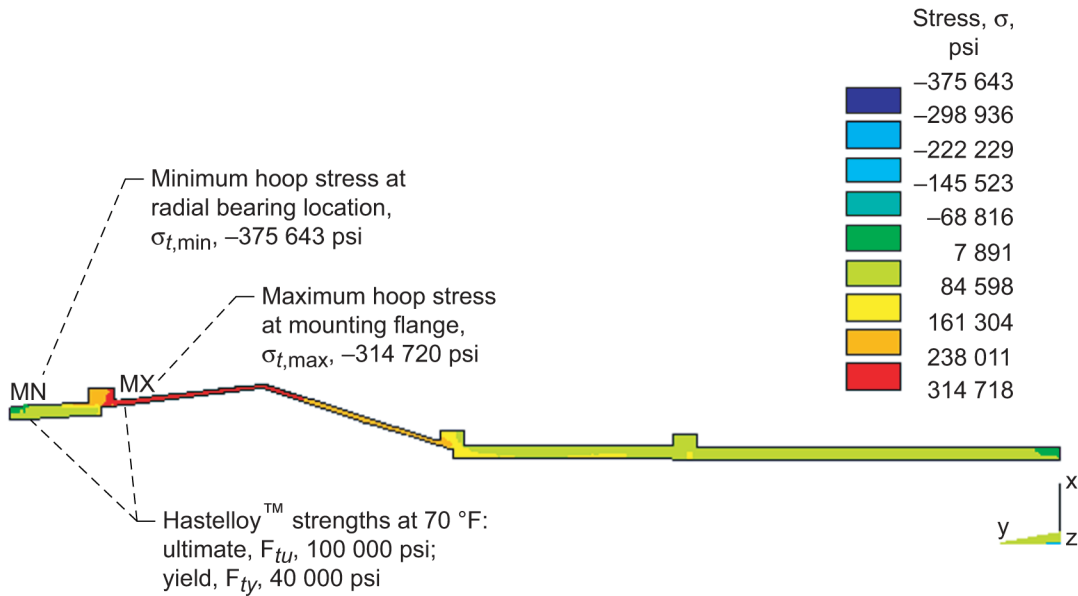
Figure 27.—Tangential stresses for drum rotor with radial constraints. Speed, 16 400 rpm.
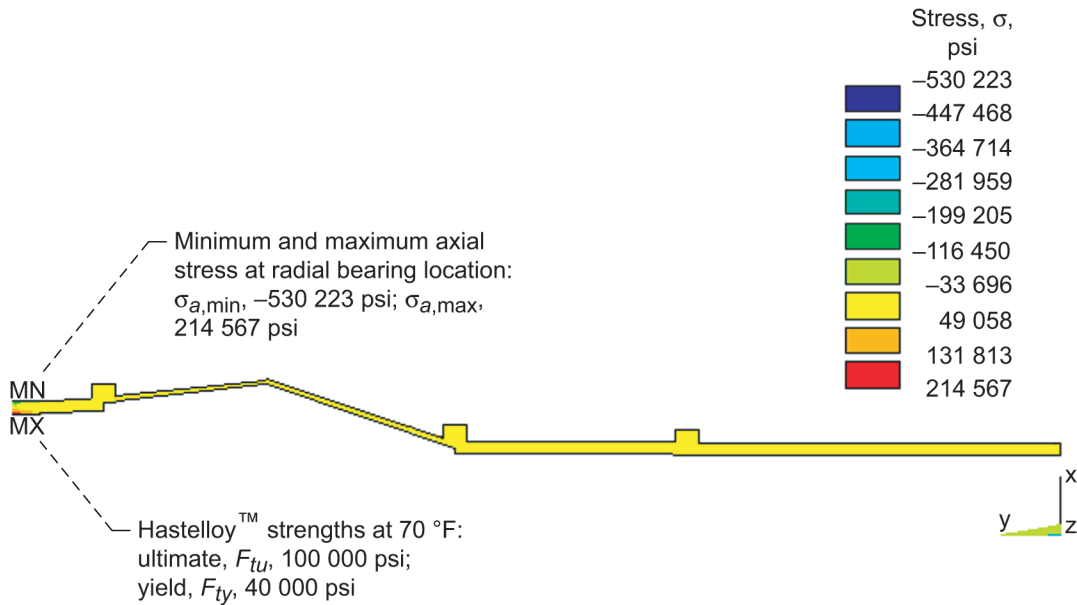
Figure 28.—Axial stresses for drum rotor with radial constraints. Speed, 16 400 rpm.
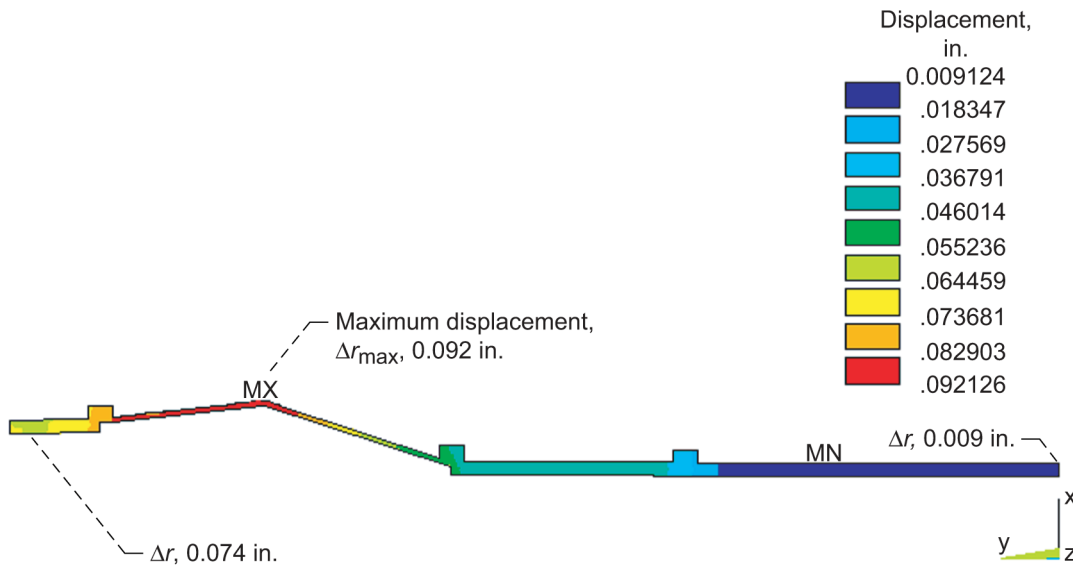
Figure 29.—Radial displacements for drum rotor without radial constraints. Speed, 16 400 rpm.

The radial stresses for case 2 are shown in figure 30. The radial stresses in case 2 are lower because the drum rotor is free to grow in the radial direction at the ends.

The tangential stress contours for case 2 are shown in figure 31. Now, the maximum tangential stress has dropped to a value of 263 610 psi. The maximum tangential stress in the combustor section near the joint flange is lower because the drum rotor is free to grow in the radial direction at the ends.

The minimum and maximum axial stresses, as shown in figure 32, also occur in the combustor section near the joint flange with the HPT. These axial stresses appear to be bending stresses because the heavy combustor section hinges at that joint flange.

As a check to the validity of peak stresses observed in the drum rotor, a simplified hand calculation of a rotating disk as shown in figure 33 was used to determine the stresses due to rotation. Additional forces operate on the disks because the rotor blades are also pushing out on the inner radius of the disks, which cause additional stresses at that interface. There are no additional forces on the combustion section, which makes it easier to compare the finite-element results with fundamental theory.

Stress, σ, psi
−41 852
−34 737
−27 623
−20 509
−13 395
−6 280
834.1
7 948
15 063
22 177

Maximum radial stress at mounting flange, $\sigma_{r,max}$, 22 177 psi

Minimum radial stress for compression at first blade row, $\sigma_{r,min}$, −41 852 psi

MX

MN

Hastelloy™ strengths at 70 °F: ultimate, F_{tu}, 100 000 psi; yield, F_{ty}, 40 000 psi

Graphite/polyimide strengths at 70 °F: tension, F_{tu}, 225 klb/in.^{2} compression, F_{cu}, 210 klb/in.^{2}
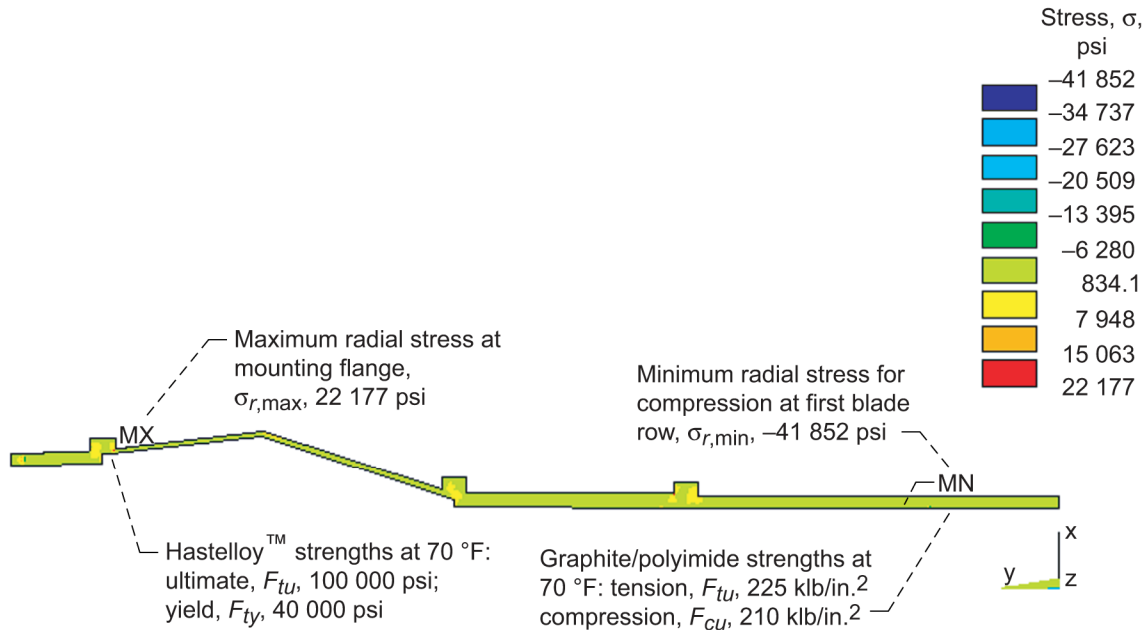
Figure 30.—Radial stresses for drum rotor without radial constraints. Speed, 16 400 rpm.

Stress, σ, psi
14 068
41 795
69 522
97 248
124 975
152 702
180 429
208 155
235 882
263 609

Maximum hoop stress at mounting flange, $\sigma_{t,max}$, 263 610 psi

Minimum hoop stress, $\sigma_{t,min}$, 14 058 psi

MX

MN

Hastelloy™ strengths at 70 °F: ultimate, F_{tu}, 100 000 psi; yield, F_{ty}, 40 000 psi

Graphite/polyimide strengths at 70 °F: tension, F_{tu}, 225 klb/in.^{2} compression, F_{cu}, 210 klb/in.^{2}
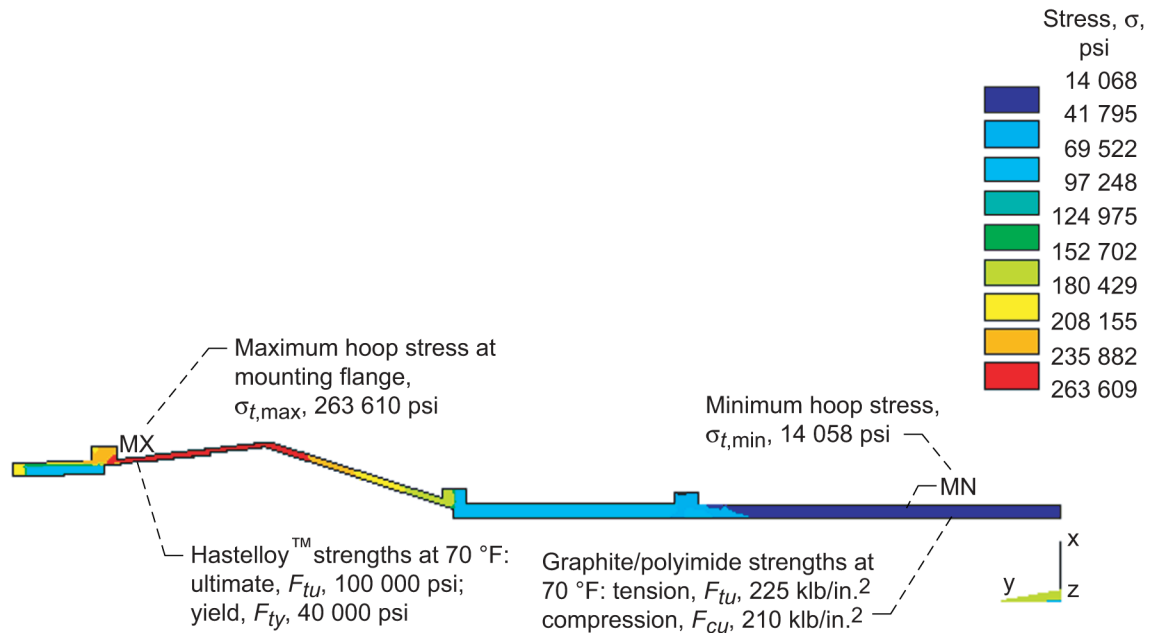
Figure 31.—Tangential stresses for drum rotor without radial constraints. Speed, 16 400 rpm.

Stress, σ, psi
- −47 337
- −37 187
- −27 036
- −16 886
- −6 736
- 3 414
- 13 564
- 23 714
- 33 865
- 44 015

Minimum and maximum axial stress at mounting flange: $\sigma_{a,min}$, −47 337 psi; $\sigma_{a,max}$, 44 015 psi

MX
MN

Hastelloy™ strengths at 70 °F: ultimate, F_{tu}, 100 000 psi; yield, F_{ty}, 40 000 psi
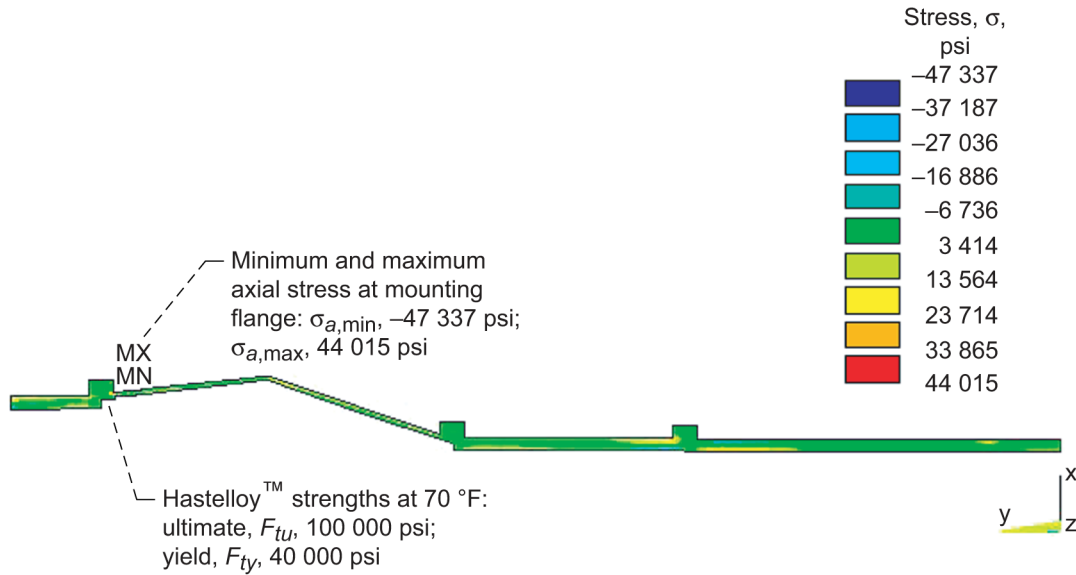
Figure 32.—Axial stresses for drum rotor without radial constraints. Speed, 16 400 rpm.
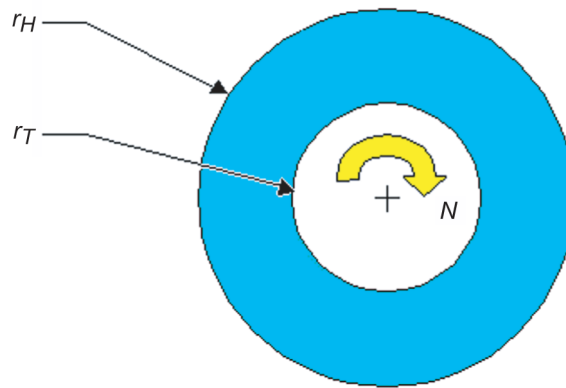
Figure 33.—Simple rotating disk. Material, Hastelloy™; weight density, γ, 0.298 lb/in.[3]; Poisson's ratio, μ, 0.33; engine rotational speed, N, 16 400 rpm.

In a spinning disk, the inertia forces create tangential and radial stresses due to the tangential elongation of the disk. In other words, both the circumference and the radius of the disk grow due to the centrifugal forces acting on material within the spinning disk.

From Shigley (ref. 20), the maximum radial stress for the simplified rotating disk occurs at the radius location $r = (r_a r_b)^{1/2}$:

$$\sigma_{r,max} = \frac{3+\mu}{8} \frac{\gamma \omega^2}{g} (r_b - r_a)^2$$

$$= \frac{(3+0.33)}{8} \frac{0.298}{386.4} \left[\frac{16\,400(2\pi)}{60} \right]^2 (10.375 - 9.75)^2 \qquad (2)$$

$$= 370 \text{ psi}$$

where $\sigma_{r,\max}$ is maximum radial stress, μ is Poisson's ratio, γ is weight density, ω is rotational speed, g is the gravitational constant, and r_b and r_a are the outer and inner disk radii, respectively,

Referring to figures 26 and 30, this stress value certainly falls within the stress contours shown in each plot. This radial stress calculation cannot validate either case 1 or case 2.

From Shigley (ref. 20), the maximum tangential stress $\sigma_{t,\max}$ occurs at the inner boundary of the disk where $r = r_a$. For the combustion section this value is calculated as follows:

$$
\begin{aligned}
\sigma_{t,\max} &= \frac{3+\mu}{4}\frac{\gamma\omega^2}{g}\left(r_b^2 + \frac{1-\mu}{3+\mu}r_a^2 \right) \\
&= \frac{(3+0.33)}{4}\frac{0.298}{386.4}\left[\frac{16\,400(2\pi)}{60} \right]^2\left(10.375^2 + \frac{1-0.33}{3+0.33}9.75^2 \right) \\
&= 240\,057 \text{ psi}
\end{aligned}
\tag{3}
$$

This stress calculation is in close agreement with the finite-element results for the exoskeletal drum rotor without radial constraints at the bearings.

Encouraged by these calculations, another study is performed using the model from case 2 (no rigid constraints at the radial bearing locations). Although the stresses were significantly reduced, the maximum tangential stress in the exoskeletal drum rotor exceeds the ultimate strength of the material, Hastelloy X™, selected for the shell over the combustion section. An adequate design is needed before the weight of the exoskeletal rotor concept is tallied.

Trade study.—The normal procedure for performing a finite-element analysis involves (1) defining the model, its boundary conditions, and loads, (2) obtaining a solution, and (3) interpreting the results. If the results indicate a design change is necessary, the whole process must be repeated. The model definition alone may be time consuming. The ANSYS Parametric Design Language (APDL, ref. 21) gives the user the ability to automate this process with user-defined variables (parameters) and programming input. The exoskeletal drum rotor model was generated using design parameters that could be easily changed. The ANSYS input data file for the exoskeletal drum rotor is found in appendix C.

The exoskeletal drum rotor model is generated using design parameters to vary the thickness of the drum rotors and rotor disks (i.e., bladed rings). A trade study is performed with this model to track the impact on rotor stresses as these thicknesses are varied. The objective of this study is to find a design in which the stresses are below the material limits while minimizing the rotor weight. A range of plausible drum rotor and bladed-ring thicknesses are used in this study to minimize stresses and weight.

Figure 34 shows the result of this trade study in a carpet plot. Unfortunately, this study shows that no combination of drum rotor and bladed-ring (disks) thicknesses can overcome the inertia forces in this design concept. Referring to the stress equations for a rotating disk, the maximum tangential stress (eq. (3)) is proportional to the square of the radius. The stress in the exoskeletal rotor increases rapidly as the rotor diameter and thicknesses increase. By moving the rotating body out to a larger diameter, the exoskeletal rotor concept increases the mass moment of inertia and weight beyond the capability of current materials. The maximum tangential stress is also proportional to the square of the rotational speed. Reducing the engine speed would significantly reduce stresses in the rotor. Furthermore, since the maximum tangential stress is directly proportional to weight density, the use of high-strength-to-weight composite materials would help to reduce stresses. However, these composite materials may not be suitable for high-temperature combustion environments where the strength is needed.

The weight estimates in this study will use a bladed-ring (disk) thickness of 0.375 in. and a drum rotor thickness of 0.125 in. The resulting weights generated in tables 14 to 16 are considered a lower bound for the structural weight of a drum rotor assembly in this size class.
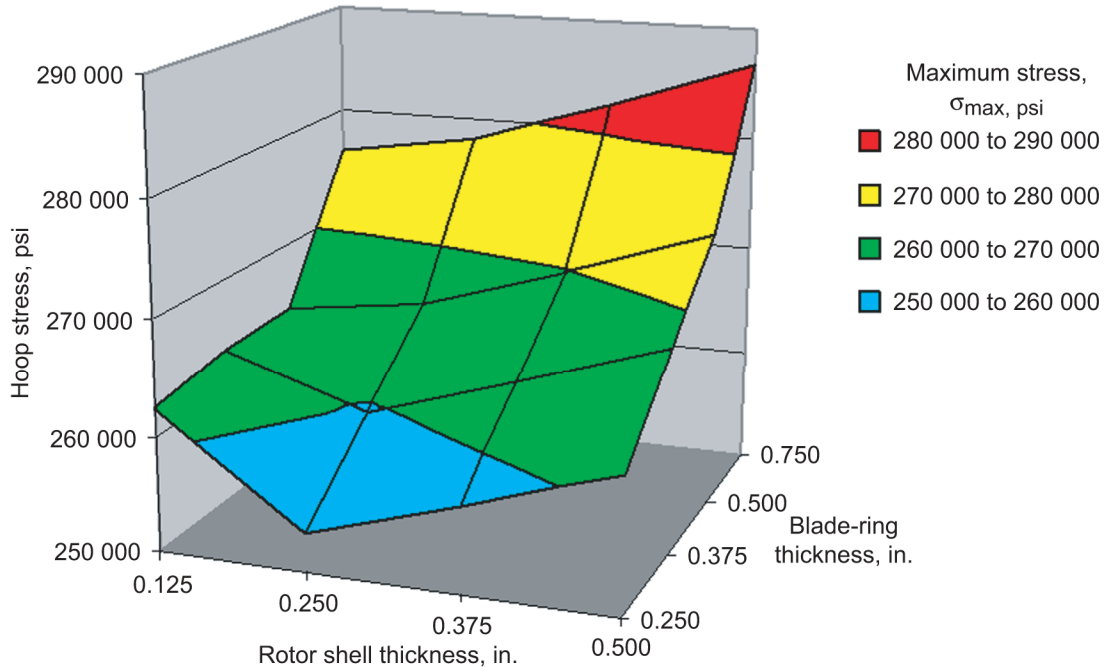
Figure 34.—Trade study for exoskeletal rotor design.

TABLE 14.—HIGH-PRESSURE COMPRESSOR DRUM ROTOR WEIGHT ESTIMATE

(a) Blade ring assembly

Rotor stage	Ring		Single airfoil weight, lb	Number of blades	Total blade airfoil weight, lb	Total blade-ring assembly weight, lb
	Mass, lb-sec²/in.	Weight, lb				
1	9.841×10^{-3}	3.8025	5.83×10^{-2}	21	1.223	5.03
2	6.031×10^{-3}	2.3302	2.38×10^{-2}	28	.667	3.00
3	6.469×10^{-3}	2.4997	1.18×10^{-2}	35	.412	2.91
4	5.592×10^{-3}	2.1608	6.41×10^{-3}	42	.269	2.43
5	4.962×10^{-3}	1.9172	3.90×10^{-3}	49	.191	2.11
6	4.879×10^{-3}	1.8854	2.49×10^{-3}	56	.139	2.02
7	3.975×10^{-3}	1.5358	1.67×10^{-3}	62	.103	1.64
8	9.242×10^{-3}	3.5710	3.38×10^{-3}	68	.230	3.80
9	1.089×10^{-2}	4.2065	2.54×10^{-3}	74	.188	4.39
10	1.010×10^{-2}	3.9039	1.96×10^{-3}	78	.153	4.06
11	9.633×10^{-3}	3.7223	1.51×10^{-3}	82	.124	3.85
12	1.049×10^{-2}	4.0552	1.30×10^{-3}	84	.109	4.16
13	8.459×10^{-3}	3.2684	1.11×10^{-3}	85	.095	3.36
14	9.242×10^{-3}	3.5710	1.00×10^{-3}	84	.084	3.66

(b) Drum rotor

Drum rotor			Flange			Total drum rotor weight, lb
Stage	Mass, lb-sec²/in.	Weight, lb	Number	Mass, lb-sec²/in.	Weight, lb	
1	2.247×10^{-2}	8.6840	1	1.298×10^{-2}	5.0168	13.70
2	4.441×10^{-2}	17.1589	--	--------------	---------	17.16
Total drum rotor weight, lb						77.28

TABLE 15.—COMBUSTOR DRUM ROTOR WEIGHT ESTIMATE

Combustor drum rotor			Flange			Total drum
Stage	Mass, lb-sec^2/in.	Weight, lb	Number	Mass, lb-sec^2/in.	Weight, lb	rotor weight, lb
3	1.112×10^{-1}	42.9719	---	--------------	---------	42.97
Total combustor drum rotor weight, lb						42.97

TABLE 16.—HIGH-PRESSURE TURBINE DRUM ROTOR WEIGHT ESTIMATE

(a) Blade ring assembly

Rotor stage	Ring		Single airfoil weight, lb	Number of blades n_B	Total blade airfoil weight, lb	Total blade-ring assembly weight, lb
	Mass, lb-sec^2/in.	Weight, lb				
1	4.332×10^{-3}	1.6737	------	-----	2.5	4.17
2	1.123×10^{-2}	4.3394	------	-----	1.5	5.84

(b) Drum rotor

Drum rotor			Flange			Drum rotor
Stage	Mass, lb-sec^2/in.	Weight, lb	Number	Mass, lb-sec^2/in.	Weight, lb	weight, lb
4	4.498×10^{-2}	17.3812	-----	--------------	---------	17.38
Total drum rotor weight, lb						27.39

Rotor Dynamics Assessment

This section covers a preliminary lateral vibration analysis of a flexible beam designed to simulate the exoskeletal rotor design. The purpose of the analysis is to determine if this structure has natural vibration modes within the operating speed range of the AE3007 turbine engine.

In this analysis, the drum assembly is mounted to two flexible bearings, which in turn are rigidly fixed. Dynamic coupling with other systems in the engine through the bearings is neglected. Since bearings play a vital role in the dynamic behavior of a rotor, one must select the appropriate bearing stiffness to ensure against potentially destructive vibrations. Thus, another purpose of this analysis is to evaluate the bearing stiffness for the exoskeletal drum rotor design.

A computer code, CRTSPD (ref. 22), has been developed especially for determining the critical speeds and mode shapes of shaft systems. This program uses a lumped-parameter rotor representation to determine all critical speeds of the exoskeletal drum rotor design. A critical speed is defined as the condition where the rotating speed of the rotor coincides with the natural frequency (ref. 23).

Prudent design practice should prevent any coincidence of critical speeds and the rated speed. As a result, the following criterion has been adopted. For a single-span rotor, the critical speeds must be outside a range of 15 percent below to 25 percent above the running speed to provide an adequate margin of safety. The high-pressure compressor and turbine in the AE3007 engine have an operating speed of 14 600 rpm, and a maximum overspeed condition of 16 400 rpm. Therefore, based on these running speeds, any critical speed must be below 12 410 rpm and above 20 500 rpm.

Lumped-parameter vibration model.—Rotating motion requires a distinctive rotor structural-dynamic model and an eigenvalue analysis. Eigenvalue analysis refers to the mathematical calculation of undamped natural frequencies (critical speeds) and mode shapes. The distribution of the mass and stiffness along the rotor and the bearing support stiffness determine the mode shapes (ref. 23).

Structural-dynamic models for flexible rotors are derived by using Timoshenko's beam models for bending and shear deflection (ref. 24), transverse and rotary inertia, and gyroscopic effects. The lumped-parameter vibration model is traditionally used to account for the distributed elastic and inertial properties of a rotor. The rotor is modeled as a collection of several rigid bodies connected by massless elastic beam elements. Assuming the rotor is axisymmetric, the general equation of motion for a lumped-parameter model, shown in figure 35, is defined by the following set of transfer matrix equations (ref. 2):

$$\begin{Bmatrix} \delta'_n \\ \vartheta'_n \\ V'_n \\ M'_n \end{Bmatrix} = \begin{bmatrix} 1 & 0 & 0 & 0 \\ 0 & 1 & 0 & 0 \\ \left(m_n \omega^2 - K_n \right) & 0 & 1 & 0 \\ 0 & \left(I_n - J_n \right) \omega^2 & 0 & 1 \end{bmatrix} \begin{Bmatrix} \delta_n \\ \vartheta_n \\ V_n \\ M_n \end{Bmatrix} \tag{4a}$$

$$\begin{Bmatrix} \delta_{n+1} \\ \vartheta_{n+1} \\ V_{n+1} \\ M_{n+1} \end{Bmatrix} = \begin{bmatrix} 1 & L_n & L_n^3/6EI_n & L_n^2/2EI_n \\ 0 & 1 & L_n^2/2EI_n & L_n/EI_n \\ 0 & 0 & 1 & 0 \\ 0 & 0 & L_n & 1 \end{bmatrix} \begin{Bmatrix} \delta'_n \\ \vartheta'_n \\ V'_n \\ M'_n \end{Bmatrix} \tag{4b}$$

Where δ is radial deflection (inches), ϑ is angular deflection (radians), V is shear force (pounds), M is bending moment (pounds-inches), K is matrix stiffness (pounds per inches), I is area moment of inertia (inches[4]), J is polar moment of inertia (inches[4]), L is shaft section length (inches), E is modulus of elasticity (pounds per square inch), and ω is shaft speed (radians per second).

Historically, two approaches have been developed to derive and solve the governing matrix equations for a lumped-parameter flexible rotor model (ref. 25). M.A. Prohl (ref. 26) and N.O. Myklestad (ref. 27) independently developed the transfer-matrix formulation method, which is now known as the Myklestad-Prohl method. Myklestad and Prohl both developed a tabular method to find the modes and frequencies of structures, such as airplane wings and turbine blades. C. Biezeno and R. Grammel developed (1959) the general mass-stiffness-matrix approach (ref. 25). Both these methods have been used to develop computer programs that define flexible-rotor matrix models from rigid-body equations and to perform the eigenvalue analysis.
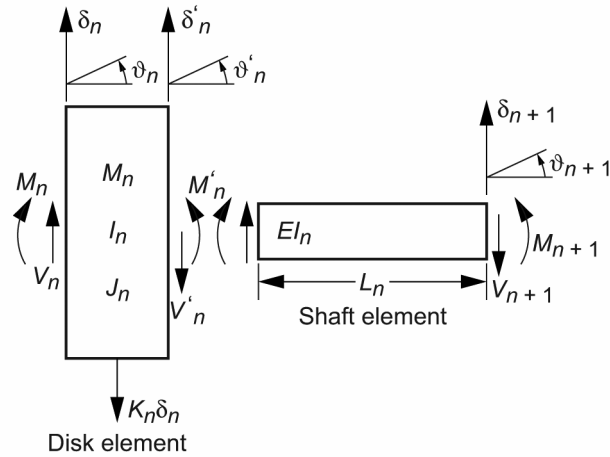
Figure 35.—Free body of elements in nth rotor station.
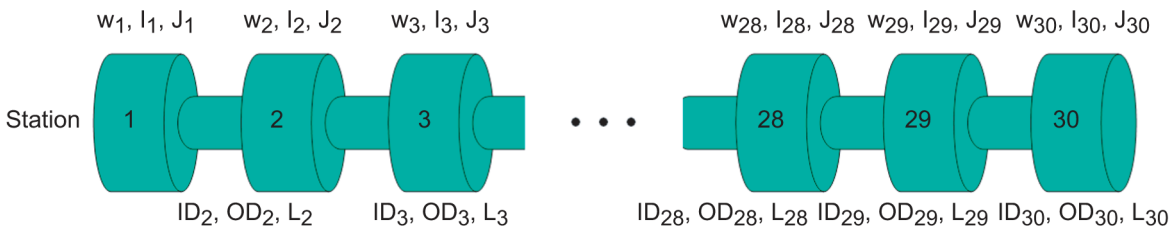
Figure 36.—Lumped-parameter critical speed model.

Calculations of rotor critical speeds and the corresponding amplitudes of vibration require the use of a computer program such as CRTSPD. To analyze the complex geometry of the exoskeletal design, the rotor was divided into a suitable number of sections defining a series of interconnected uniform beams.

Figure 36 shows a schematic of the CRTSPD model, which can contain up to 30 sections. The computer input data for each section consist of an external weight, section length, shaft outer and inner diameters, transverse moment of inertia, and rotational (polar) moment of inertia.

The generic representation of the exoskeletal rotor is a single-span, two-bearing system. In this system, the rotor, bladed disks, and bearings are assumed to be axisymmetric. In addition, all materials are assumed to be quasi-isotropic.

The computer program CRTSPD allows the user to (1) model the disk as an integral part of the shaft or (2) model only the shaft and add the disk mass properties externally. The advantage to modeling the disks as integral members of the shaft is that the program automatically calculates the cross-sectional properties. The disadvantage is that the section stiffness may be more than twice that of the shaft under the disk. However, when the disk mass properties are put separately, one loses the additional stiffness that the disks add to the shaft. In the exoskeletal case, only the drum rotor is modeled with the disk mass properties applied externally. Since critical speeds (or natural frequencies) in a flexible system are proportional to stiffness (i.e., $\omega_n \approx (k/m)^{1/2}$, this approach is more conservative. The exoskeletal rotor should be considerably stiffer than the original AE3007 because of its larger diameter. For this investigation, it is assumed that the exoskeletal rotor will behave as a rigid body on two soft bearings. If any critical speeds occur in the range of 12 410 to 20 500 rpm, the model must be modified to include the disk.

Table 17 shows the CRTSPD input data file for the exoskeletal rotor, and table 18 shows the bearing stiffness for each bearing used in this analysis. A bearing stiffness of 20 000 lb/in. is selected for this rotor (Andrew J. Provenza, March 19, 2003, NASA Glenn Research Center, Cleveland, OH, personal communication), which is a typical stiffness value for magnetic bearings.

TABLE 17.—CRTSPD LUMPED-PARAMETER MODEL FOR EXOSKELETAL ROTOR

CRTSPDM – MODAL ANALYSIS VERSION 2/2/77

N = 30 STA.   NB = 2 BRG.   NSK = STIFFNESSES   G = 0.0   NGYR = 1   MASS = 0   NPLOT = 2

STATION	WEIGHT LB	LENGTH IN.	SHAFT DIAMETER OUTSIDE	INSIDE	POLAR MOM. LB-IN.**2	TRANS. MOM. LB-IN.**2	$Ex10^{-6}$ LB/IN.**2	DENSITY LB/IN.**3
1	34.792	2.920	16.680	16.430	0.133E+05	5637.	24.00	0.056
2	5.987	2.340	16.680	16.430	0.129E+04	643.1	24.00	0.056
3	3.870	2.440	16.680	16.430	0.128E+04	640.0	24.00	0.056
4	3.726	2.040	16.680	16.430	0.128E+04	638.0	24.00	0.056
5	3.153	1.930	16.680	16.430	0.127E+04	634.8	24.00	0.056
6	2.793	1.820	16.680	16.430	0.127E+04	633.3	24.00	0.056
7	3.090	1.420	16.680	16.430	0.129E+04	646.6	16.00	0.160
8	3.060	1.310	16.680	16.430	0.132E+04	658.6	16.00	0.160
9	9.514	1.370	16.680	16.430	0.132E+04	657.7	16.00	0.160
10	5.758	1.260	16.680	16.430	0.131E+04	656.8	16.00	0.160
11	5.365	1.250	16.680	16.430	0.131E+04	654.7	16.00	0.160
12	5.171	1.290	16.680	16.430	0.131E+04	655.2	16.00	0.160
13	5.445	1.180	16.680	16.430	0.131E+04	653.9	16.00	0.160
14	4.587	1.180	16.680	16.430	0.130E+04	652.0	16.00	0.160
15	4.757	0.930	16.680	16.430	0.129E+04	647.5	16.00	0.160
16	5.454	0.000	16.680	16.430	0.125E+04	626.4	16.00	0.160
17	3.144	1.000	17.000	16.750	70.1	35.11	29.80	0.297
18	3.063	2.000	17.950	17.700	235.	118.4	29.80	0.297
19	4.306	2.000	19.220	19.970	368.	185.5	29.80	0.297
20	4.261	1.720	20.400	20.150	412.	207.3	29.80	0.297
21	3.266	1.000	21.260	21.010	347.	173.9	29.80	0.297
22	1.233	0.000	21.580	21.340	138.	68.92	29.80	0.297
23	2.477	2.000	21.360	21.110	279.	140.4	29.80	0.297
24	4.903	2.000	20.930	20.680	542.	272.5	29.80	0.297
25	5.553	2.640	20.430	20.180	585.	295.0	29.80	0.297
26	7.936	0.000	20.140	19.900	322.	162.9	29.80	0.297
27	5.912	0.950	20.020	19.770	0.226E+04	1129.	29.80	0.297
28	6.954	1.450	20.020	19.770	0.243E+04	1213.	29.80	0.297
29	9.042	1.310	20.020	19.770	0.247E+04	1234.	29.80	0.297
30	28.350	0.000	20.020	19.770	0.720E+04	3598.	29.80	0.297
	-------	-------			---------			
	196.920	42.750			48308.500			

TABLE 18.—CRTSPD BEARING STIFFNESSES

```
BEARING STATIONS    1         30


                SPEED DEPENDENT BEARING CHARACTERISTICS
```

BEARING NUMBER	BEARING LOCATION	K1 LB/IN	K2 LB-SEC/IN	K3 LB-SEC2/IN	C1 LB/IN	C2 LB-SEC/IN	C3 LB-SEC/IN
			STIFFNESS CASE NO. 1				
1	1	20000.0	0.0000E+00	0.0000E+00	0.0000E+00	28.50	0.0000E+00
2	30	20000.0	0.0000E+00	0.0000E+00	0.0000E+00	28.50	0.0000E+00

Results of eigenvalue analysis.—The modes of vibration (critical speeds) of the rotor system may be divided into two categories: (1) modes where the rotor behaves essentially as a rigid body and (2) flexural modes where the rotor whirls with a characteristic deflection curve.

Figure 37 shows the two rigid-body modes for the exoskeletal rotor. In the first critical speed at 2467 rpm, the bearing support points at each end of the rotor move in phase with one another. The locus of the rotor's whirling motion traces a cylindrical path.

At the second rigid-body mode, at a critical speed of 5776 rpm, the bearing support points move out of phase with one another. As seen in figure 37, there is a node point near or at the midspan where the deflection crosses the spin axis. The locus of the rotor's whirling motion traces two cones, point to point.

Figure 38 shows the third mode of the exoskeletal rotor, which occurs at 261 570 rpm. The third critical speed is the first flexural mode of the exoskeletal rotor, and it is due to the bearing flexibility. Using differential equations, F.C. Linn and M.A. Prohl (ref. 28) showed that the rigid-body critical speeds both approach zero as the bearing flexibility approaches infinity, as shown in figure 39. In this case, the third critical speed at 261 570 rpm is the first "free-free" mode of the rotor system because there is no apparent restraint at either support point (ref. 29).
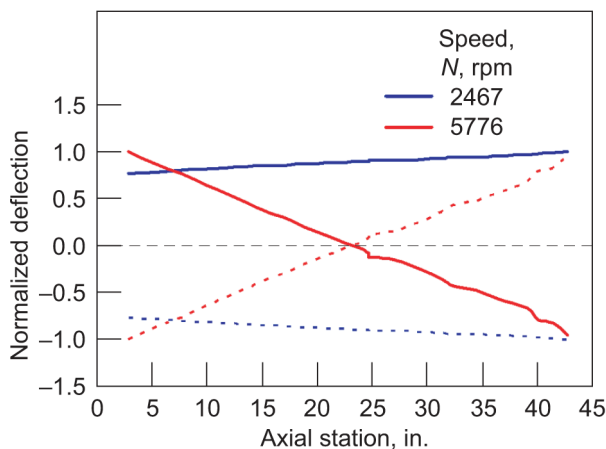
Figure 37.—Exoskeletal rotor rigid body critical speed and mode shape.
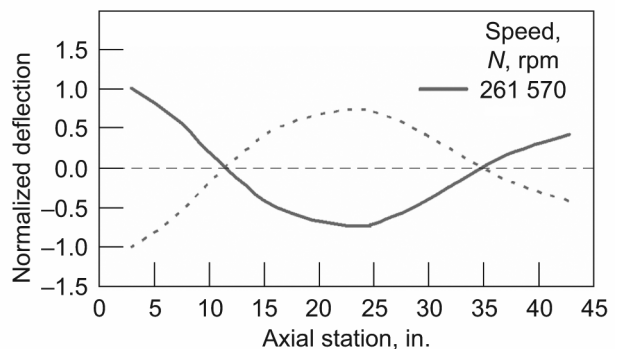
Figure 38.—Exoskeletal rotor third critical speed and mode shape.
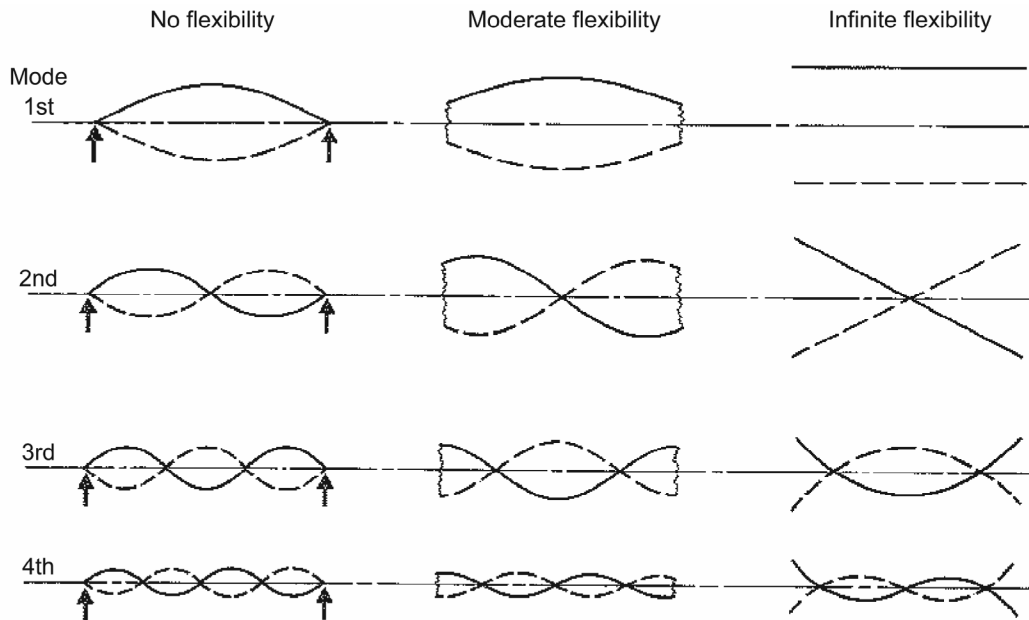
Figure 39.—Mode shapes of uniform rotor with bearing flexibility.

Rotor dynamics summary.—Assuming the bearing stiffness for this rotor design is 20 000 lb/in. for the entire speed range, the first and second undamped critical speeds or rigid-body modes occur at 2467 and 5776 rpm, respectively. These speeds are well below the operating speed of 14 600 rpm for the exoskeletal rotor design concept. Usually, the rotor flexural modes require more design consideration because the rotor and stator can vibrate out of phase with one another, which may cause rubbing of seals or internal damage. However, the third critical speed (or first flexural mode) occurs at 261 570 rpm, and this speed is well above the 16 400 rpm overspeed condition. Further study is recommended to analyze the response to imbalance, bearing location, bearing damping, and damping in the supporting structure. In this preliminary analysis, the limits placed on the critical speeds ensure satisfactory operation at the design speeds of the exoskeletal engine.

Stationary Core Investigation

Description.—The stationary core at the center of the exoskeletal engine forms the inner flow-path surface of the inlet, compressor, combustion chamber, turbine, and nozzle exit, whereas the drum rotor forms the outer flow-path surface. Additionally, the core functions as a backup structure for the stator guide vanes. The guide vanes are nonrotating, fixed-position blades integrally machined as a bladed-ring assembly. There is one guide vane ring assembly for each stage of the compressor and turbine. The ring assembly slides onto the stationary core with interlocking spacers between each stage row to accommodate the respective rotating stages of the drum.

The stationary core consists of four distinct sections along its length with each section made from a different material. The use of multiple materials gave the lightest weight design possible while providing adequate structural strength and thermal management. The first section enveloped the inlet and first seven stages of the compressor and was made of graphite polyimide to handle operating temperatures up to 600 °F. Titanium was used for the second section, which included the final seven stages of the compressor and just up to the combustion chamber. Combined pressure and temperature were the design drivers for the material selection in the combustion chamber. For this section, Hastelloy X™ was chosen for its high-strength and extreme-temperature properties. A CMC of SiC/SiC was selected for the last section, which consisted of the turbine and exit region assumed to be operating at 2200 °F or higher. This CMC does not have a particularly favorable strength-to-weight ratio but was selected to eliminate the

need for cooling and thereby realize a net weight savings. Specific details of attaching the various shells to one another were not addressed in this study, but additional weight to account for attachments was added to the weight summary prediction.

Analysis.—A finite-element shell model of the core structure was developed with appropriate material properties assigned at each section of the core. The model was constrained axially at the forward thrust ring station near the inlet. A second constraint was added at the aft ring location of the core to allow for lateral support of the structure and thermal growth along the axis. The applied boundary conditions provided an effective relief of any thermal expansion in the core structure. The primary load comes from the combustion pressure and resulting thrust of the engine. The load path for this pressure is in the compression of the core shell, and the thrust is transferred through attachment vanes between the stationary core and the nacelle at the thrust ring location. The net thrust causes an overall compression load in the core structure that could result in buckling of the shell.

Strength and linear buckling loads were determined for the stationary core. Adjustments to shell thickness were made to ensure positive margins of safety for strength and stability. A hand calculation was performed using the line loads to compute shell buckling. Results of this preliminary assessment yielded a thickness requirement of 0.05 in. for the graphite polyimide, 0.09 in. for the titanium, 0.12 in. for the Hastelloy™, and 0.12 in. for the SiC/SiC. These thicknesses were used in determining weight estimates for the stationary core assembly and guide vanes; the subtotal is 100.5 lb as listed in table 19. Figure 40 shows the stationary core Von Mises stress results for the core segments. Figure 41 illustrates the deformed shape of the first buckling mode. As shown, the critical section of the core has a 17-percent margin of safety against buckling for the shell thickness provided.

TABLE 19.—EXOSKELETAL CONCEPT STATIONARY CORE
[Ring thickness, 0.10 in.]

(a) Weight summary

Rotor stage	Single airfoil weight, lb	Number of blades, n_B	Total blade airfoil weight, lb	Radius, r, in.	Weight density, γ, $lb_m/in.^3$	Axial location		Ring weight, lb
						x_0, in.	x_1, in.	
HPC								
1	0.0583	21	1.22	3.57	0.056	2.25	3.59	0.17
2	.0238	28	.67	4.80	.056	4.72	5.79	.18
3	.0118	35	.41	5.53	.056	7.24	8.15	.18
4	.0064	42	.27	6.02	.056	9.28	10.19	.19
5	.0039	49	.19	6.36	.056	11.31	12.01	.16
6	.0025	56	.14	6.62	.056	13.19	13.78	.14
7	.0017	62	.10	6.82	.056	14.59	15.23	.15
8	.0034	68	.23	6.97	.160	16.02	16.41	.27
9	.0025	74	.19	7.09	.160	17.37	17.80	.31
10	.0020	78	.15	7.19	.160	18.60	19.09	.35
11	.0015	82	.12	7.28	.160	19.86	20.32	.34
12	.0013	84	.11	7.34	.160	21.10	21.66	.41
13	.0011	85	.09	7.40	.160	22.38	22.74	.27
14	.0010	84	.08	7.45	.160	23.55	23.92	.28
HPT								
1	0.0080	40	0.32	8.31	0.076	39.04	39.95	0.36
2	.0037	63	.23	8.31	.076	41.40	42.25	.34

(b) Weight totals

Blade airfoil, lb	Ring, lb	Blade and rings, lb	Stator shell, lb	Attachments, lb	Total weight of blade and rings, stator shell, and attachments, lb
4.54	4.09	8.6	88.9	3.0	100.5

Tip to tail	
Material	Thickness, in.
Graphite	0.05
Titanium	0.09
Hastelloy	0.12
SiC/SiC	0.12

Combustor housing —

Stress, $klb_f/in.^2$

82676.27
78543.93
74411.59
70279.27
66146.93
62014.59
57882.27
53749.93
49617.60
45485.27
41352.93
37220.60
33088.27
28955.93
24823.60
20691.27
16558.93
12426.60
8294.26
4161.93
29.60

Housing removed

Deformation, in.

1.0535
1.0009
.9482
.8955
.8428
.7901
.7375
.6848
.6321
.5794
.5268
.4741
.4214
.3687
.3161
.2634
.2107
.1580
.1054
.0527
.0000
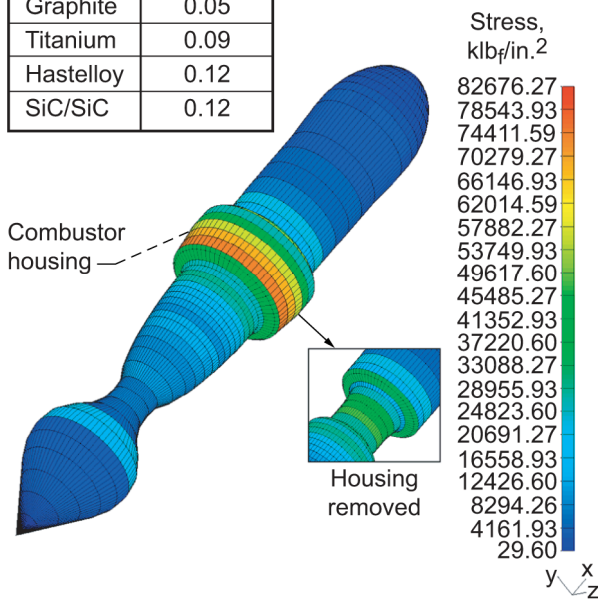
Figure 40.—Stationary core Von Mises stress with steady-state pressure and temperature. Maximum Von Mises stress, 83 $klb_f/in.^2$.
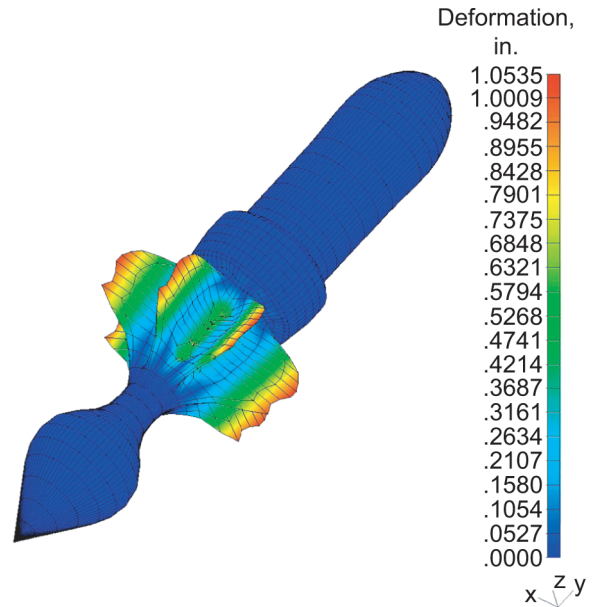
Figure 41.—Stationary core first buckling mode. Buckling load factor, 1.1748.

Bearing Subsystem

The exoskeletal engine concept requires large-diameter radial bearings on the outside diameter of the rotating drum located at both ends of the spool (as shown in fig. 42). A thrust bearing is located near the outside diameter at the inlet side of the compressor spool. The large diameter coupled with the high rotational speed poses significant challenges for bearing technology. State-of-the-art bearings for conventional engines with lubricating systems can operate at very high revolutions per minute and not exceed state-of-the-art rotational speed, which is approximately 4 M *DN* (ref. 30). For the case of the exoskeletal high-pressure spool, the bearings operate at 7 M *DN*, well beyond the state of the art. Recent work of Sullivan at the NASA Glenn Research Center has shown thermal problems with carbon-carbon (C-C) bearings for the exoskeletal application (ref. 31). There are no known lubricated systems that can handle this magnitude of velocity; consequently, noncontact bearing systems are needed to accommodate the demands of the exoskeletal high-pressure spool heat loads. Among the candidates for investigation would be (1) foil bearings and (2) magnetic bearings.

Foil bearings.—The foil bearings shown in figure 43 are noncontacting and ride on a thin film of air, which is generated hydrodynamically (ref. 32) by the rotational speed. Lightweight foils are used to suspend and center the shaft. The current state-of-the art size for this type bearing is about 4 in. in diameter (ref. 31). Typical foil bearing applications use a single foil rolled around the shaft as seen in the figure.

Competing foil bearing design technology employs a bumped foil to suspend the shaft (fig. 44). For the large-diameter application on the exoskeletal engine architecture, a hybrid system is envisioned as one in which the bumped foil provides stiffness and multiple foils are used to keep the large-diameter shaft centered (as shown in fig. 45). The complexity of the design and the significant increase in diameter

both lead to a significant and long-duration technical effort. Some of the drawbacks for the foil system include the high startup torque, the need for set-down/lift-off mechanical bearings and associated positioning hardware to accommodate anticipated duty cycle requirements. Unfortunately, no current bearing system can handle the heat generated by this system; consequently, an alternative system must be considered. For the purpose of this study, high-pressure air generated with an auxiliary power unit (APU) was selected to provide stiffness. With the help of a fast-acting control system, the bearing could be stiffened to handle extreme loads experienced in flight. The use of localized stiffening creates a viable backup bearing option, without relying on high-temperature material technology that may not be available in the near future. The weight estimation for this type of bearing system in the exoskeletal concept for this investigation was extrapolated since no data exist at the large diameter required. A concern about bearing stability is addressed by extending the width of the bearing to 4 in.
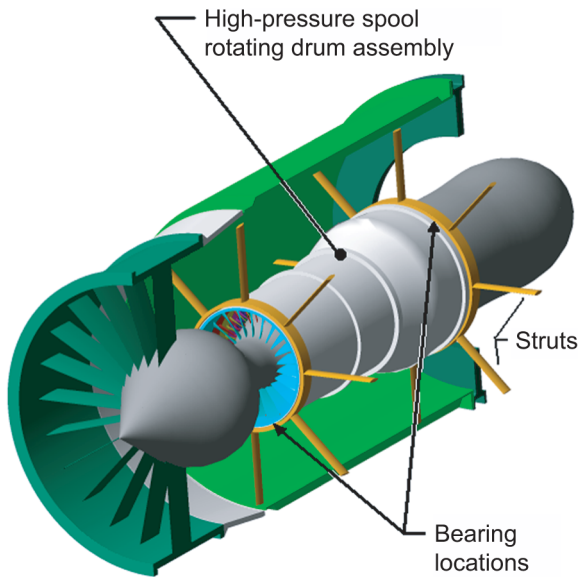
Figure 42.—Exoskeletal high-pressure spool assembly.
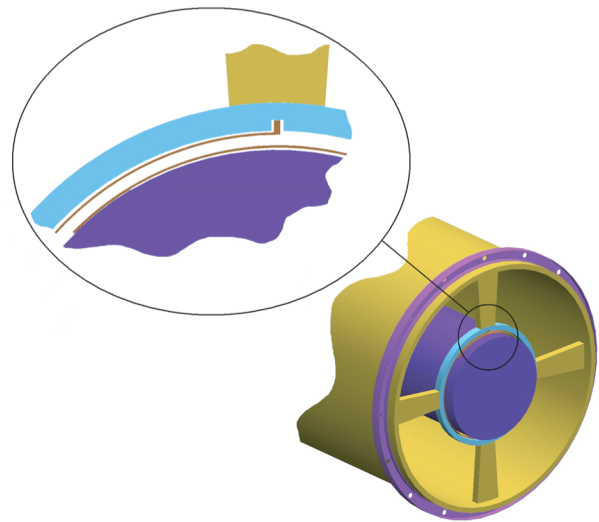
Figure 43.—Typical single-foil bearing.
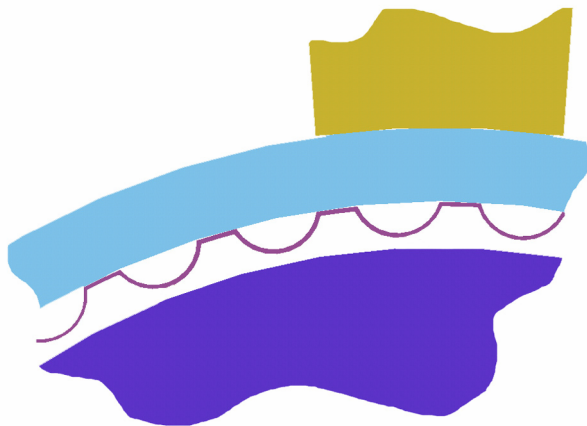
Figure 44.—Typical bumped-foil bearing.
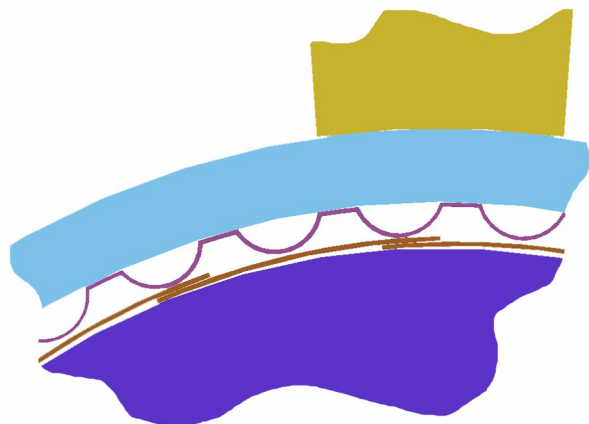
Figure 45.—Hybrid foil bearing.
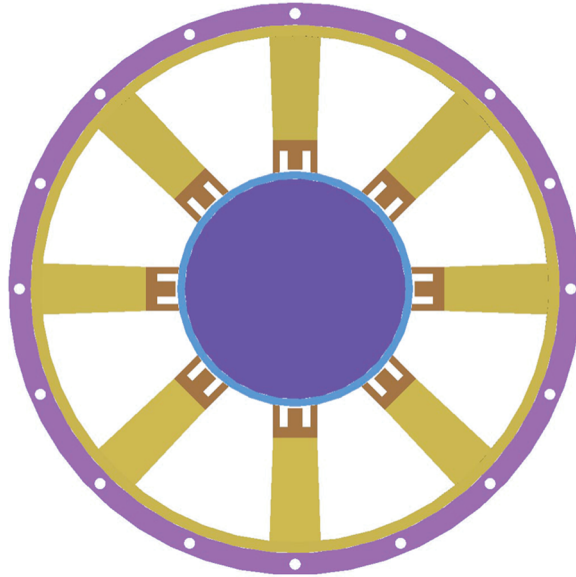
Figure 46.—Magnetic bearing.

Magnetic bearings.—In the case of a magnetic bearing system, there are some advances in this area of research and development (R&D). Most of this R&D, however, has been focused on small-diameter shafts that may be completely encased by a magnetic bearing housing. For the large-diameter shaft in this study, it was considered that a passive rotor may be applicable with a minimum of four electric magnetic poles at 90° apart, as shown in figure 46. The stiffness of the large-diameter system and radial growth after spinup are among the technical challenges to overcome. For example, an exoskeletal concept as studied would have a calculated radial growth of 0.040 in. at the bearing on the turbine end of the spool. Radial growth of this magnitude would result in stability problems; consequently, a magnet pole positioning system would be required to maintain the appropriate clearances for the operation of the magnetic bearing system. This positioning system would require high-speed sensing and positioning. The passive magnetic laminate and its mounting hardware will require high structural integrity to resist the extremely high inertial forces. This would most likely drive an increase in the weights; however, this is not considered for the present study in the total weight compilation. Although not inconsequential, the weight resulting from the magnetic bearing power consumption was not considered in this study.

Similar to the foil bearings, a backup bearing system is needed for off-nominal loading events. These events would include gust and hard-landing loads as well as loss-of-blade imbalance loads. The approximate sizing of the backup bearing system was done using a 5-g loading and a three-blade imbalance force of 76 000 lb. For this study, we assumed that this backup system would add 75 lb for the short-duration, off-nominal events considered. The above weight of 75 lb is only a place holder and should be considered as a low-fidelity number. This backup system would prevent excessive excursion from a centered position if temperatures were tolerable. Unfortunately, the high heat load prevents a system of this nature from functioning properly and without advances in lubrication and materials, would most certainly result in catastrophic bearing failure.

Bearing weights.—The support structure for the bearing system (discussed in the next section) requires nominally a 47-lb total structure weight for the rings and struts at the forward and aft bearing support locations. The computed weights for a magnetic and foil bearing system as applicable in an exoskeletal design are tabulated in table 20. These weights will be considered as minimum weights since the historical data needed for sizing large-diameter, noncontact bearings in a flight propulsion system are not available.

TABLE 20.—EXOSKELETAL ENGINE BEARING WEIGHT SUMMARY
[All weights are in pounds.]

Bearing concept alternatives			
Magnetic bearing system		Foil bearing system	
Bearing support structure	46.6	Bearing support structure	46.6
E-coils	96.8	Auxiliary power unit	84
Positioning motors	95	Compressor	42
Electrical controllers	30	Manifolding	24
Permanent magnets	54.3		
Backup bearing	75		
Total weight	397.7	Total weight	196.6

Summary.—The increase in diameter for a rotating drum versus the conventional shaft bearings creates bearing speeds well beyond the current operational capabilities for state-of-the-art lubricated bearing systems. This has prompted the consideration of other bearing schemes, such as a foil or magnetic systems. Both systems appear to meet the requirements of the exoskeletal application although neither technology is currently ready for operation at this size. Current developments in the foil bearing technologies indicate it may take 20 years to achieve foil bearings for this diameter. The magnetic bearings appear to be too heavy for this application and would also face a lengthy technology development program if selected. Regardless of these drawbacks, both bearing types were considered in the final comparison with the existing AE3007 high-pressure-spool weight comparison.

Bearing Housing Study

Description.—The bearing housing structure shown in figure 47 and modeled in figure 48 provides support for the exoskeletal rotor bearings located at each end of the rotor assembly. The fore and aft housings were designed as a ring structure attached to the engine nacelle frame through eight support vanes. The bearing rings and support vanes are made of 0.5-in.-thick titanium for strength and stiffness.
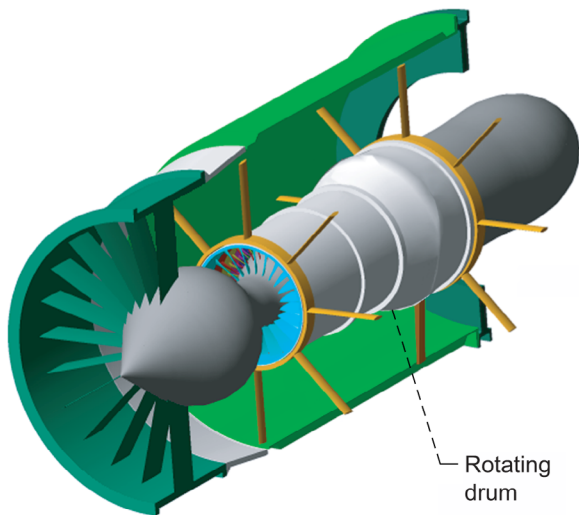
Figure 47.—Exoskeletal concept cutaway with stationary core at center.
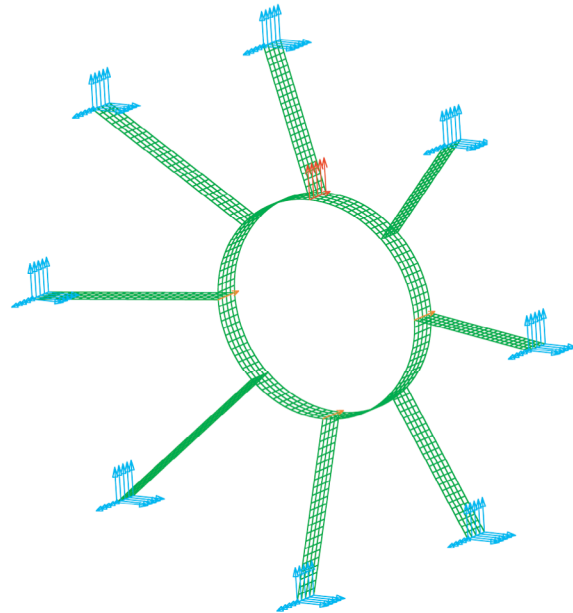
Figure 48.—Finite-element model of thrust bearing housing with applied loads. Material, titanium; vane thickness, 0.5 in.; bearing housing thickness, 0.5 in.; imbalance load, 7600 lb; thrust load, 2000 lb/bearing.
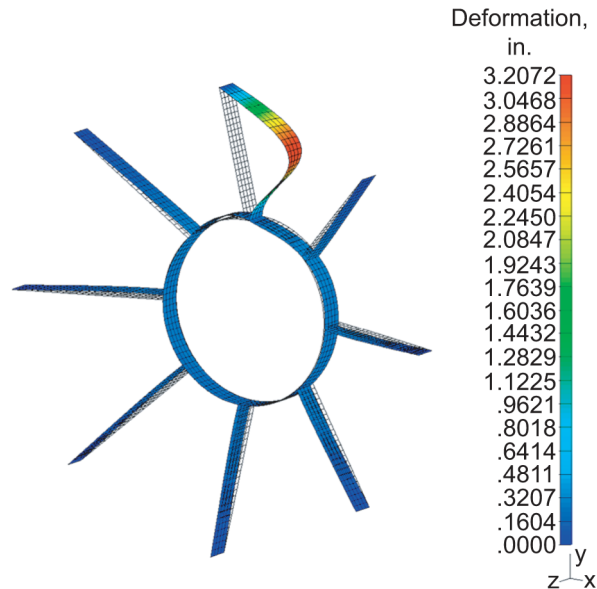
Figure 49.—Strut buckling due to imbalance load.
Buckling load factor, 7.9496.

Analysis.—Stress and stability analyses were performed to size the bearing housing structure and to estimate its weight. The design load condition assumes that three side-by-side compressor blades have been detached, which results in an imbalance load of 7600 lb at 16 400 rpm. A maximum 8000-lb engine thrust load and the 7600-lb imbalance load were applied simultaneously to the bearing housing FEM, and a static analysis solution was executed in MSC/NASTRAN. Results of the static analysis show a peak Von Mises stress of 34 klb/in.^{2} in the vanes and a maximum deformation of 0.0612 in. This stress result is well below the titanium compressive yield strength of 110 klb/in.^{2} Using the same model, a linear buckling analysis was also performed to check the stability of the bearing ring support struts. The results are shown in figure 49. In summary, the bearing support configuration would sustain the applied service loads with sufficient margin. The corresponding structural weight was calculated to be 46.6 lb for both the fore and aft bearing housings.

Findings, Observations, and Enabling Technology Identification

Findings

(1) The exoskeletal high-pressure spool with a foil bearing system provides no weight advantage over a conventional design. The exoskeletal high-pressure spool with a magnetic bearing system weighs significantly more than the conventional design. This weight takes into account the expected weight savings that could be realized if a conventional engine were to make use of ceramic materials and switch to integral bladed disks. In addition, the exoskeletal weights assume that the negative margins in the drum rotor and blades could be overcome without additional weight impact. A summary of these weights is given in table 21. These findings reveal that the conceptual exoskeletal rotor and stator can be lighter than their conventional counterparts, subject to the assumptions and conditions of this study. However, the integrated exoskeletal high-pressure spool system is as heavy as or is heavier than its conventional counterpart primarily because of the bearing system mass.

TABLE 21.—WEIGHT COMPARISON

[All weights are in pounds.]

Conventional		Exoskeletal with magnetic bearings		Exoskeletal with foil bearings	
Rotor		Rotor drum	142.6	Rotor drum	142.6
HPC	187.3				
HPT	79.7				
Total	267.0				
Stator		Stator	100.5	Stator	100.5
HPC	111.1				
HPT	54.1				
Total	165.2				
Bearings		Bearing system		Bearing system	
Shaft		Housings	46.6	Housings	46.6
Bearings		E-coils	96.8	Auxiliary power unit	84.0
Total	59.6	Position motors	95.0	Compressor	42.0
Weight savings		Controllers	30.0	Manifolds	24.0
Material change	−38.7	Permanent magnets	54.3		
Bladed disk design	−10.0	Backup bearings	75.0		
Total	−48.6	Total	397.7	Total	196.6
Total system weight	443.2	Total system weight	640.9	Total system weight	439.7

(2) A requirement for turbine blade cooling is indicated in the exoskeletal design of an AE3007-like high-pressure spool examined in this study. Differential temperatures at the blade-to-ring interface could introduce excessive blade stresses. Blade cooling is a conventional approach to avoiding such thermal-induced stresses, but the development of cooling strategies for ceramic blades (which today are used to *avoid* cooling) is beyond the scope of this study and is a significant technology challenge.

(3) Shell material choices are limited by high temperatures and the need for light weight (low rotational inertia). The rotating drum operational environment is very demanding such that stiff, strong, low-density materials are required to sustain the high inertial forces and, at the same time, high thermal loads in the vicinity of the combustor and turbine require materials that can survive in an elevated temperature environment. Unfortunately, the thermal-resistant materials are very dense, and the strong lightweight materials are not temperature resistant. Within the scope of this investigation, no solution was identified using currently available materials, which is an indication that high-temperature, lightweight shell structures appear to be a critical design and technology challenge should an exoskeletal engine development be undertaken.

(4) Compressor blade analysis revealed that the taller metallic compressor blades, if used, in the exoskeletal high-pressure spool would have been buckling critical. Negative margins were also obtained in shear for compressor blades. These findings are a basis for considering composite materials for taller blade rows in exoskeletal compressors.

Observations

(1) An inherent characteristic of the exoskeletal design approach is keeping rotational inertia low, which is opposed to providing a large central flow area for potential noise reduction or alternative cycle integration. The exoskeletal approach places blades and their supporting structure at the outer diameter of the system. Throttle response, maneuvering loads, and containment are among many factors that drive

rotating machinery masses down at larger diameters and/or reduce rotational speeds. Since reductions in rotational speed directly impact engine performance, exoskeletal engines are driven toward lower diameters (which restricts the core space available for noise reduction or other cycle implementation).

(2) The increased rotary inertia of an exoskeletal design will require higher power for starting and have a slower response to changes in throttle setting.

(3) The fabrication of a woven preform of exoskeletal bladed rings would be difficult because of the complexity of the yarn paths and the large ring diameters. The densification of complex structures with tight surface tolerances has not been demonstrated. CMC's are also difficult to densify without obstructing cooling passages. Machining the passages after densification would weaken the structure by cutting fibers. Inserting refractory metal rods in the cooling passages during densification could only be done if the passages were straight.

Enabling Technology Identification

(1) Large-diameter bearing capability for high-speed bearings, noncontact or contact types: Even under the best of assumptions, rotor and stator weight savings are offset by the weight of a noncontact bearing system such as foil bearings. The use of magnetic bearings may be less of a technology leap, but they increase the system weight beyond that of conventional engine systems.

(2) Manufacturing capability for a bladed-ring component: The capability of manufacturing CMC ring blades as an integrated component with precise geometry and uniform mechanical properties needs to be developed. Durability under life-cycle and environmental conditions (especially critical thermal conditions as noted in the Findings section) needs to be demonstrated before composite materials could be considered in a gas turbine engine.

Conclusions

1. The spool weight (neglecting bearings) of an exoskeletal engine may be equal to or less than the weight of the spool of a conventional engine. It was found that mounting blades inside a shell, rather than on a shaft, can result in rotating structure weights as low as or potentially lower than blades on shaft-mounted disks. This conclusion is based on an aggressive preliminary assessment of a potential exoskeletal design approach.

2. An advancement in bearing technology is required before a more precise assessment of exoskeletal engine feasibility can be undertaken. Current bearing technologies are inadequate for the high rotational speeds at large diameters required in exoskeletal systems. The present maturity of enabling bearing technologies is insufficient to provide a precise assessment of the system implications of their integration in an exoskeletal engine.

Recommendations

1. The next logical step in an examination of exoskeletal engine feasibility is to consider a "clean sheet" design approach to a specific exoskeletal design goal. The design of an exoskeletal system to its best advantage (especially involving changes to the engine cycle) was not attempted during this investigation. A clean sheet exoskeletal design, free of constraints driven by comparability to an existing engine, may discover alternatives that improve the weight and performance or lessen the technology challenges of the exoskeletal approach. Other applications of the exoskeletal concept have been suggested and may serve as compelling design goals. Noise reduction has been proposed through an inversion of the velocity profile at the convergence of "free flow" central core flow with the exhausts of

the spools. The open central core has also been proposed for the integration of a ramjet or other cycle. An extension of the exoskeletal approach appears in the concept of vaneless counterrotating gas turbines. A clean sheet exoskeletal implementation for a specific design goal that examines competitive weight characteristics is a logical next step in the assessment of exoskeletal viability.

2. Exoskeletal implementation has been shown to be reliant on advancements in bearing technology. Therefore, a critical path to exoskeletal engine consideration is through bearing technology advancement. It is recommended that consideration of exoskeletal requirements be added to goals for high-diameter-rotation-speed aerospace bearing technology programs.

Appendix A

Weight Analysis Turbine Engine (WATE) Output for AE3007

```
NEPP-WATE-98, March 1998
   50 PAX ENGINE - Current Technology Baseline (revised for '
 &D NMODES=1,DRAW=T,LONG=F,DOUTHD=T,NCODE=-1,AMAC=F,NCASE=1,BOAT=F,ICEC=0,
    TABLES=T,PINPUT=T,TLOAD=F,INST=0,MAPLOT=F,MAXNIT=100,ITERM=1,IWT=1, &END
 &D MODE=1,CALBLD=F,CBFLOW=0.020,ERCB=0.80,ICBCMP=5,
 KONFIG(1,1)=1,1,0,2,0,SPEC(1,1)=260.0,0,0,0,0.00,8600,1,1,0.,0,4.44,27.,
 KONFIG(1,2)=4,2,0,3,0,SPEC(1,2)=1.60,0,1,3401,1,3402,1,3403,1,0,
                                 0,.8750,1.62,0.9000,
 KONFIG(1,3)=7,3,0,4,20,SPEC(1,3)=5.3,0.00,0.015,
 KONFIG(1,4)=2,4,0,5,0,SPEC(1,4)=.010,
 KONFIG(1,5)=4,5,0,6,21,SPEC(1,5)=1.25,0.115,1,3707,1,3708,1,3709,1,0,
                                  .0,.8600,15.0,0.950,
 KONFIG(1,6)=2,6,0,7,0,SPEC(1,6)=.015,8*0,
 KONFIG(1,7)=2,7,0,8,0,SPEC(1,7)=.045,0.,0.,2760.,0.995,18400,5*0.,6,
 KONFIG(1,8)=5,8,21,9,0,SPEC(1,8)=3.45,0.977,1,3801,1,3802,1,1,
                                    .6850,1,.9100,7000.,1,1122,2,
 KONFIG(1,9)=2,9,0,10,0,SPEC(1,9)=0.005,6*0.,0.55,
 KONFIG(1,10)=5,10,0,15,0,SPEC(1,10)=2.10,0.,1,3803,1,3804,1,1,
                                     1.00,1,.920,5000.0,1,8888,4,
 KONFIG(1,14)=2,20,0,22,0,SPEC(1,14)=0,
 KONFIG(1,15)=2,15,0,16,0,SPEC(1,15)=0.01,
 KONFIG(1,11)=8,16,22,12,0,SPEC(1,11)=0,0,0.3,.95,1,
 KONFIG(1,12)=2,12,0,13,0,SPEC(1,12)=.0065,8*0.,

KONFIG(1,13)=9,13,0,14,0,SPEC(1,13)=0.0,7004,0.,0.,7003,0.,0.,0.,1.,3*0,0.5,11
'
 KONFIG(1,21)=11,5,8,23,0,SPEC(1,21)=18000.,8*1,
 KONFIG(1,22)=11,2,10,0,0,SPEC(1,22)=7000.,0.435,0.435,6*1,
 KONFIG(1,23)=10,0,0,0,0,SPEC(1,23)=-100.,

 /*            Design Point CNTLs... IF NEEDED          */
 KONFIG(1,31)=12,SPCNTL(1,31)=1,1,'STAP',1,5,35.5,0,
 KONFIG(1,32)=12,SPCNTL(1,32)=1,5,'DOUT',5,5,15.0,0,
 KONFIG(1,33)=12,SPCNTL(1,33)=13,2,'STAP',2,6,345.7,0,
 KONFIG(1,34)=12,SPCNTL(1,34)=4,7,'PERF',4,0,7580.,1,
 KONFIG(1,35)=12,SPCNTL(1,35)=4,7,'PERF',4,0,1955.,0,

 /*              Off-Design CNTLs                       */
 KONFIG(1,41)=12,0,0,0,0,SPCNTL(1,41)=1,1,'STAP',8,13,0,0,0,0,
 KONFIG(1,42)=12,0,0,0,0,SPCNTL(1,42)=1,2,'STAP',8,2,0,0,0,0,
 KONFIG(1,43)=12,0,0,0,0,SPCNTL(1,43)=1,5,'STAP',8,5,0,0,0,0,
 KONFIG(1,44)=12,0,0,0,0,SPCNTL(1,44)=1,8,'STAP',8,8,0,0,0,0,
 KONFIG(1,45)=12,0,0,0,0,SPCNTL(1,45)=1,10,'STAP',8,10,0,0,0,0,
 KONFIG(1,46)=12,0,0,0,0,SPCNTL(1,46)=2,11,'DOUT',8,11,0,0,0,0,
 KONFIG(1,50)=12,0,0,0,0,SPCNTL(1,50)=1,21,'DOUT',8,21,0,0,0,0,
 KONFIG(1,51)=12,0,0,0,0,SPCNTL(1,51)=1,22,'DOUT',8,22,0,0,0,0,

 /*            Part Power and Operational Controls      */
 KONFIG(1,55)=16,0,0,0,0,SPEC(1,55)=1,57,'DOUT',4,2,1.1,0,1,-1,0,1,9,
 KONFIG(1,56)=16,0,0,0,0,SPEC(1,56)=0,58,'DOUT',4,2,1.1,0,1,-1,0,1,9,
 KONFIG(1,57)=12,0,0,0,0,SPCNTL(1,57)=1,3,'DOUT',5,2,23.0,0,0,0,
 KONFIG(1,58)=12,0,0,0,0,SPCNTL(1,58)=1,3,'STAP',6,22,0.70,0,0,0,

 /*            control for marching via temp.           */
  KONFIG(1,60)=12,SPCNTL(1,60)=4,7,'PERF',4,0,7580,0,0,
 &END
```

```
 JFLOW =  (FLOCAL EXECUTION ORDER)
                    1     2     3     4     5     6     7     8     9    10    15    14    11
 12    13     0     0     0     0     0


                                                       1
                                                 <  INLT   1>
                                                       2
                                                 <  COMP   2>
                                                       3
                                                 <  SPLT   3>          <  SPLT   3>
                                                       4                     20
                                                 <  DUCT   4>          <  DUCT  14>
                                                       5                     22
                         <  COMP   5>           <  COMP   5>          <  MIXR  11>
                              21                      6
                         <  TURB   8>           <  DUCT   6>
                                                       7
                                                 <  BRNR   7>
                                                       8
                                                 <  TURB   8>
                                                       9
                                                 <  DUCT   9>
                                                      10
                                                 <  TURB  10>
                                                      15
                                                 <  DUCT  15>
                                                      16
                                                 <  MIXR  11>
                                                      12
                                                 <  DUCT  12>
                                                      13
                                                 <  NOZZ  13>
                                                      14


 0SHAFT (21) IS CONNECTED TO ( 5) AND ( 8) AND (23) AND
 0SHAFT (22) IS CONNECTED TO ( 2) AND (10) AND
 1
 0 THE FOLLOWING REPRESENTS THE CONFIGURATION FOR MODE=   1
    50 PAX ENGINE – Current Technology Baseline (revised for '
            CONFIGURATION DATA   22 STATIONS   60 COMPONENTS
```

COMPONENT NUMBER	NKIND	COMPONENT TYPE	UPSTREAM STATIONS		DOWNSTREAM STATIONS	
1	1	INLT	1	0	2	0
2	4	COMP	2	0	3	0
3	7	SPLT	3	0	4	20
4	2	DUCT	4	0	5	0
5	4	COMP	5	0	6	21
6	2	DUCT	6	0	7	0
7	2	BRNR	7	0	8	0
8	5	TURB	8	21	9	0
9	2	DUCT	9	0	10	0
10	5	TURB	10	0	15	0
11	8	MIXR	16	22	12	0
12	2	DUCT	12	0	13	0
13	9	NOZZ	13	0	14	0
14	2	DUCT	20	0	22	0

```
15        2       DUCT       15        0       16        0
21       11       SHFT        5        8       23        0
22       11       SHFT        2       10        0        0
23       10       LOAD        0        0        0        0
```

        VARIABLE CONTROL INFORMATION

     ACTIVE:
 CNTL 34: vary des. exit T or f/a   of BRNR   7
         so that net jet thrust   = 0.75800D+04

     INACTIVE:
 CNTL 31: vary weight-flow rate   of   1
         so that weight-flow rate   at station   5 = 0.35500D+02
 CNTL 32: vary "R" value   of   5
         so that % surge margin   of   5 = 0.15000D+02
 CNTL 33: vary design PR   of   2
         so that total pressure   at station   6 = 0.34570D+03
 CNTL 35: vary des. exit T or f/a   of BRNR   7
         so that net jet thrust   = 0.19550D+04
 CNTL 41: vary weight-flow rate   of   1
         so that flow-rate error   at station 13 = 0.00000D+00
 CNTL 42: vary "R" value   of   2
         so that flow-rate error   at station   2 = 0.00000D+00
 CNTL 43: vary "R" value   of   5
         so that flow-rate error   at station   5 = 0.00000D+00
 CNTL 44: vary PR used to read map of   8
         so that flow-rate error   at station   8 = 0.00000D+00
 CNTL 45: vary PR used to read map of   10
         so that flow-rate error   at station 10 = 0.00000D+00
 CNTL 46: vary inlet area JM2 flow of   11
         so that static press. error of   11 = 0.00000D+00
 CNTL 50: vary RPM or speed ratio   of   21
         so that (HP)net/(HP)total   of   21 = 0.00000D+00
 CNTL 51: vary RPM or speed ratio   of   22
         so that (HP)net/(HP)total   of   22 = 0.00000D+00
 CNTL 57: vary bypass flow ratio   of   3
         so that % surge margin   of   2 = 0.23000D+02
 CNTL 58: vary bypass flow ratio   of   3
         so that Mach number   at station 22 = 0.70000D+00
 CNTL 60: vary des. exit T or f/a   of BRNR   7
         so that net jet thrust   = 0.75800D+04

        CONDITIONAL CONTROL INFORMATION

     ACTIVE:
 VCNT 55: watch "R" value for maps   of   2;
         trigger value is 0.11000D+01 which turns on/off switch   of
 CNTL 57 to 0.10000D+01
 VCNT 56: watch "R" value for maps   of   2;
         trigger value is 0.11000D+01 which turns on/off switch   of
 CNTL 58 to 0.00000D+00

     INACTIVE:

 None!!!

1

    INPUT – Warning: the maximum component number used, 60, does not equal the
number of components configured in any one mode, 36!

    UPDATED INPUT DATA TO REFLECT CALCULATED INPUT
    COMPONENT
    NO.   TYPE   SPEC 1   SPEC 2   SPEC 3   SPEC 4   SPEC 5
    SPEC 6   SPEC 7   SPEC 8   SPEC 9
     1   INLT   260.0000000   0.000000000   14.69600000   0.000000000   0.000000000
    8600.000000   1.000000000   1.000000000   0.000000000
     2   COMP   1.600000000   0.000000000   3298.567025   3401.000000   0.871762004
    3402.000000   0.974387528   3403.000000   1.561712846
     3   SPLT   5.300000000   0.000000000   0.015000000   0.000000000   0.000000000
    0.000000000   0.000000000   0.000000000   0.000000000
     4   DUCT   0.010000000   0.000000000   0.000000000   0.000000000   0.000000000
    0.000000000   0.000000000   0.000000000   0.000000000
     5   COMP   1.250000000   0.115000000   17088.15477   3707.000000   29.85406452
    3708.000000   0.869525830   3709.000000   2.237728006
     6   DUCT   0.015000000   0.000000000   0.000000000   0.000000000   0.000000000
    0.000000000   0.000000000   0.000000000   0.000000000
     7   BRNR   0.045000000   0.000000000   0.000000000   2792.143036   0.995000000
    18400.00000   0.000000000   0.000000000   0.000000000
     8   TURB   3.450000000   0.977000000   1.108284344   3801.000000   0.196672238
    3802.000000   1.028548856   1.460070201   0.685000000
     9   DUCT   0.005000000   0.000000000   0.000000000   0.000000000   0.000000000
    0.000000000   0.000000000   0.550000000   0.000000000
    10   TURB   2.100000000   0.000000000   0.314600153   3803.000000   0.259514065
    3804.000000   1.009740547   2.554108500   1.000000000
    11   NOZZ   327.6979091   508.8929531   0.300000000   0.950000000   1.000000000
    0.000000000   0.000000000   0.000000000   0.000000000
    12   DUCT   0.006500000   0.000000000   0.000000000   0.000000000   0.000000000
    0.000000000   0.000000000   0.000000000   0.000000000
    13   NOZZ   696.0257350   7004.000000   0.000000000   0.000000000   7003.000000
    0.000000000   0.000000000   1.000000000   1.000000000
    14   DUCT   0.000000000   0.000000000   0.000000000   0.000000000   0.000000000
    0.000000000   0.000000000   0.000000000   0.000000000
    15   DUCT   0.010000000   0.000000000   0.000000000   0.000000000   0.000000000
    0.000000000   0.000000000   0.000000000   0.000000000
    21   SHFT   18000.00000   1.000000000   1.000000000   1.000000000   1.000000000
    1.000000000   1.000000000   1.000000000   1.000000000
    22   SHFT   7000.000000   0.435000000   0.435000000   1.000000000   1.000000000
    1.000000000   1.000000000   1.000000000   1.000000000
    23   LOAD   -100.0000000   0.000000000   0.000000000   0.000000000   0.000000000
    0.000000000   0.000000000   0.000000000   0.000000000

0MODE   1 NOW BEING USED
0CASE IDENTIFICATION   50 PAX ENGINE – Current Technology Baseline (revised
for '

                                          STATION PROPERTY OUTPUT DATA

        FLOW   WEIGHT   TOTAL   TOTAL   FUEL/AIR   CORRECTED
    MACH   STATIC   INTERFACE CORRECTED
       STATION   FLOW   PRESSURE   TEMPERATURE   RATIO   FLOW
    NUMBER   PRESSURE   FLOW ERROR
     NNEP-ARP?   STATP1   STATP2   STATP3   STATP4   STATP5
    STATP6   STATP7   STATP8
     1-1   257.4356705   14.69600000   545.6700000   0.000000000   264.0504947
    0.000000000   0.000000000   0.000000000

NASA/TM—2005-213369   54

```
  2-2        257.4388394   14.54904000    545.6700000   0.000000000   266.7176714
0.000000000   0.000000000  -0.000012309
  3-3        257.4388394   23.97330869    641.9425052   0.000000000   175.5684700
0.000000000   0.000000000   0.000000000
  4-4         41.68325273  23.97330869    641.9425052   0.000000000    28.42719819
0.000000000   0.000000000   0.000000000
  5-5         41.67950672  23.73357560    641.9425052   0.000000000    28.71434160
0.000000000   0.000000000   0.000089872
  6-6         36.05277331  353.4369834   1465.037705    0.000000000     2.519436716
0.000000000   0.000000000   0.000000000
  7-7         36.05277331  348.1354286   1465.037705    0.000000000     2.557803773
0.000000000   0.000000000   0.000000000
  8-8         36.84889128  332.4693343   2792.143036    0.022090407     3.779180147
0.000000000   0.000000000   0.82086D-05
  9-9         41.53179226   72.39087045  1942.626873    0.019550915    16.31713615
0.000000000   0.000000000   0.000000000
 10-10        41.53188612   72.02891609  1942.626873    0.019550915    16.39913181
0.000000000   0.000000000  -0.22600D-05
 12-12       257.2874728   21.04741771    775.7310774   0.003105043   219.6988497
0.519548746  17.52962411   0.000000000
 13-13       257.2470341   20.91060949    775.7310774   0.003105043   221.1362353
0.723876953  14.69600000   0.000312400
 14-14       257.2470341   20.91060949    775.7310774   0.003105043   221.1014786
0.721975555  14.69600000   0.000000000
 15-15        41.53188612  18.14278133   1426.019774    0.019550915    55.78185202
0.000000000   0.000000000   0.000000000
 16-16        41.53188612  17.96135352   1426.019774    0.019550915    56.34530507
0.282217026  17.03306232   0.000000000
 20-20       215.7555866   23.61370906    641.9425052   0.000000000   149.3820019
0.000000000   0.000000000   0.000000000
 21-21         4.793143273 353.4369834   1465.037705    0.000000000     0.000000000
0.000000000   0.000000000   0.000000000
 22-22       215.7555866   23.61370906    641.9425052   0.000000000   149.3820019
0.699577332  17.04007626   0.000000000
```

COMPONENT OUTPUT DATA

| COMPONENT NO. | TYPE | DATOUT1 | DATOUT2 | DATOUT3 | DATOUT4 | DATOUT5 |
DATOUT6	DATOUT7	DATOUT8	DATOUT9			
		Ram drag	V-fps	V-knots	T2/T1	P2/P1
Mach	(Eta)r	T2/518.67	Alt-ft			
1 INLT		0.000000000	0.000000000	0.000000000	1.000000000	1.000000000
0.000000000	0.990000000	1.052056221	0.000000000			
		HP in	RPM or ratio	Z-3Dmap	R-map	% Margin
Corr. Spd.	(Eta)poly.	(Eta)adia.	(PR)comp.			
2 COMP		-8427.558152	3073.102608	0.000000000	1.516729182	19.54189788
0.908306189	0.876769658	0.867798381	1.647758800			
		Bypass	(dP/P)main	(dP/P)2nd	Tot W main	React. W main
3 SPLT		5.176073663	0.000000000	0.015000000	257.4388394	0.000000000
0.000000000	0.000000000	0.000000000	0.000000000			
		(dP/P)mom.	dP/P	Des. M in		A-sq. in.
Mach in			T exit			
4 DUCT		0.000000000	0.010000000	0.000000000	0.000000000	0.000000000
0.000000000	0.000000000	0.000000000	641.9425052			
		HP in	RPM or ratio	Z-3Dmap	R-map	% Margin
Corr. Spd.	(Eta)poly.	(Eta)adia.	(PR)comp.			
5 COMP		-12123.73271	18006.80836	0.000000000	1.251725672	28.99598420
0.947194291	0.902213785	0.860591837	14.89185571			
		(dP/P)mom.	dP/P	Des. M in		A-sq. in.
Mach in			T exit			

```
   6   DUCT     0.000000000  0.015000000  0.000000000  0.000000000  0.000000000
0.000000000  0.000000000  0.000000000  1465.037705
              (dP/P)mom.    dP/P         Des. M in    Fuel/Wa      A-sq. in.
Fuel Flow    Mach In      (Eta)burn.    T burn.
   7   BRNR     0.000000000  0.045000000  0.000000000  0.022090407  0.000000000
2867.113603  0.000000000  0.995000000  2792.143036
              HP out       RPM or ratio Z-3Dmap      PR-Table     (Eta)poly.
Corr. Spd.   TRIT,deg R   (Eta)adia.    (PR)turb.
   8   TURB    12223.74322  18006.80836  1.000000000  3.460633063  0.894445188
7002.647694  2693.665432  0.909987829  4.592697011
              (dP/P)mom.    dP/P         Des. M in                 A-sq. in.
Mach in                   T exit
   9   DUCT     0.000000000  0.005000000  0.000000000  0.000000000  0.000000000
0.000000000  0.000000000  0.000000000  1942.626873
              HP out       RPM or ratio Z-3Dmap      PR-Table     (Eta)poly.
Corr. Spd.   TRIT,deg R   (Eta)adia.    (PR)turb.
  10   TURB     8428.951686  3073.102608  1.000000000  2.162877116  0.907538139
5047.414844  1942.626873  0.920815070  3.970114327
              Amain-sq in  A2nd-sq in   Mom. Coef.   Effectiv.    V-main
V-2nd        V-exit       (Del P)s      Aexit/Aent
  11   NOZZ     360.1563202  476.4345421  0.950000000  0.500000000  507.9996455
829.1265337  689.4721929  0.000411699  1.000000000
              (dP/P)mom.    dP/P         Des. M in                 A-sq. in.
Mach in                   T exit
  12   DUCT     0.000000000  0.006500000  0.000000000  0.000000000  0.000000000
0.000000000  0.000000000  0.000000000  775.7310774
              F gross      VJ act       Pt/Ps        Aex-sq in    Ath-sq in
(CD)flow     (CV)vel      FG Coeff.     (PR)nozz
  13   NOZZ    7467.934584  942.6401219  1.422877619  689.6592463  689.6592463
0.996935621  0.997373314  0.990853084  1.422877619
              (dP/P)mom.    dP/P         Des. M in                 A-sq. in.
Mach in                   T exit
  14   DUCT     0.000000000  0.000000000  0.000000000  0.000000000  0.000000000
0.000000000  0.000000000  0.000000000  641.9425052
              (dP/P)mom.    dP/P         Des. M in                 A-sq. in.
Mach in                   T exit
  15   DUCT     0.000000000  0.010000000  0.000000000  0.000000000  0.000000000
0.000000000  0.000000000  0.000000000  1426.019774
              Net HP       RPM or ratio RPM comp. 1  RPM comp. 2  RPM comp. 3
RPM comp. 4               HP net/HP tot
  21   SHFT     0.010503844  18006.80836  18006.80836  18006.80836  18006.80836
0.000000000  0.000000000  0.85930D-06  0.000000000
              Net HP       RPM or ratio RPM comp. 1  RPM comp. 2  RPM comp. 3
RPM comp. 4               HP net/HP tot
  22   SHFT     1.393533823  7064.603696  3073.102608  3073.102608  0.000000000
0.000000000  0.000000000  0.000165341  0.000000000
              Load HP      RPM or ratio
  23   LOAD    -100.0000000  18006.80836  0.000000000  0.000000000  0.000000000
0.000000000  0.000000000  0.000000000  0.000000000


                                              CONTROL INFORMATION
    ACTIVE CNTLs:     46    45    44    43    58    42    41    50    51
    ACTIVE VNTLs:     55    56



   MACH=  0.0000   ALTITUDE=       0.   RECOVERY= 0.9900


                                              4 ITERATIONS    14 PASSES


 AIRFLOW (LB/SEC)            257.44    GROSS THRUST               7467.93
 FUEL FLOW (LB/HR)          2867.11
```

```
 NET THRUST                        7467.93    TSFC                            0.3839
NET THRUST/AIRFLOW        29.0089
 INLET RAM/ADDED DRAG             0.00    TOTAL BRAKE SHAFT HP            1.40
BOATTAIL DRAG                     0.00
 INSTALLED THRUST              7467.93    INSTALLED TSFC                  0.3839
SPILLAGE + LIP DRAG              0.00
 TOTAL NACELLE DRAG              0.00    CET (T4)                       2792.1
RIT (T41)                      2693.7
 CORR AIRFLOW (LB/SEC)        266.72
 FNIN1                        7467.93    SFCIN1                          0.3839
 FNIN2                        7467.93    SFCIN2                          0.3839
 EI (G NOX/KG FUEL)            28.555
 MASS AVG. VJET                942.64
 PROPULSIVE EFFICIENCY     0.0000000
0 CUSTOMER BLEED WAS EXTRACTED FROM COMPRESSOR  5
 TOTAL TEMPERATURE = 1306.6705  TOTAL PRESSURE =  236.2536  WEIGHT FLOW =
0.8336  ENERGY RATIO =    0.8000
```

Appendix B

NASA Engine Performance Program (NEPP) Output

```
&D IWT=2, &END
0MODE    1 NOW BEING USED
 &W
    IPLT = T,
    ISII = F,
    ISIO = F,
    PLOT = T,
  SKIPIT = F,
  ILENG  =     1,     2,     3,     4,     5,     6,     7,     8,     9,    10,
           11,    12,13,
  ACCS   =      0.0950,
  DISKWC =          1.,
  DISKWI =          1.,
  DISKWT =          1.,

  IWMEC(1,  1) =            1,          12,           1,          10,         -12,
                           1,           0,           0,           0,           1,
                           0,
  IWMEC(1,  2) =          48,           3,           0,           1,           1,
                           0,           0,          -2,           0,           1,
                           0,           0,           0,           0,           0,
  IWMEC(1,  3) =           7,           0,
  IWMEC(1,  4) =           2,           2,           0,          -1,
  IWMEC(1,  5) =          47,           3,           0,           1,          14,
                          -3,           0,           0,          12,           0,
                           2,           0,           0,           0,           0,
  IWMEC(1,  6) =           2,           2,           0,
  IWMEC(1,  7) =          21,           1,           1,
  IWMEC(1,  8) =          51,           3,           0,           0,           2,
                           0,           5,           0,           0,           5,
                           0,           0,           1,           0,           1,
  IWMEC(1,  9) =           2,           2,           0,
  IWMEC(1, 10) =          52,           3,           0,           0,           3,
                           1,          -6,           0,           0,           2,
                           0,           0,           0,           0,           1,
  IWMEC(1, 11) =          82,           0,
  IWMEC(1, 12) =           2,           1,           0,
  IWMEC(1, 13) =           9,           1,           2,           0,           1,
                           1,           5,           0,           0,           0,
  IWMEC(1,14)  =           2,           3,           0,          -4,
  IWMEC(1,15)  =           2,           1,
  IWMEC(1, 21) =          11,           2,           8,           0,           0,
                           0,           5,           2,
  IWMEC(1, 22) =          11,           1,          10,           0,           0,
                           0,           2,           3,
  FRVAL(1,  1) =        0.11,          1.,         0.1,         1.0,           0,
                        0.10,         0.1,           0,           0,           0,
                         0.1,           0,           1,           2,           2,
                           0,           0,           0,
  FRVAL(1,   2) =       0.12,         1.0,         0.1,         1.4,           6,
                        0.12,         0.2,           0,           0,           0,
                          1.,           0,          -5,           0,           0,
                           1,        100.,         0.9,
```

```
FRVAL(1,   3) =      0.12,        1.0,        0.1,        0.8,          0,
                     0.12,        0.2,          0,          0,          0,
                     0.00,          1,         -2,          2,          3,
                        0,          0,          0,
FRVAL(1,   4) =      0.12,        1.0,        0.1,        1.8,          3,
                     0.12,        0.1,          0,          0,          0,
                       5.,          0,          0,          0,          0,
                        0,          0,          0,
FRVAL(1,   6) =      0.12,        1.0,        0.1,        1.2,          6,
                     0.12,        0.2,          0,          0,          0,
                     0.50,          0,          0,          5,          5,
                        0,          0,          0,
DESVAL(1, 1) =       .80,      1000.,         0.,         0.,          0,
                        1,          1,          1,          0,          0,
                      0.4,          0,      1650.,        70.,          0,
                      0.1,        0.1,       0.09,          0,          0,
                        8,
DESVAL(1, 2) =      .550,       .407,          0,          0,        1.8,
                        1,          0,       0.39,          0,          0,
                        0,          0,          0,          0,          0,
                       24,          0,        1.1,      0.024,       0.10,
                      2.8,        2.8,        1.4,          0,          0,
                        0,          0,          0,          0,          0,
                        0,          0,          0,          0,          0,
                       50,          0,          0,      0.135,        5.9,
                       1.,         1.,        2.5,        2.5,          0,
                        0,          1,          0,          0,          0,
                        0,          0,          0,          0,          0,
                       1.,        0.6,        1.5,        1.1,       0.05,
                        0,          0,          0,          0,          0,
DESVAL(83,2) =     1360.,
DESVAL(1, 3) =
DESVAL(1, 4) =      .500,          0,          0,          0,          0,
                      5.0,         -1,          0,          0,
DESVAL(1, 5) =      0.34,       0.31,          0,          0,        1.4,
                        1,        1.0,      0.455,          0,          0,
                        0,          0,          0,          0,          0,
                        0,          0,       0.84,      0.162,       0.08,
                      2.2,        0.8,      0.833,          0,          0,
                        0,          0,          0,          0,          0,
                        0,          0,          0,          0,          0,
                        0,          0,       0.75,      0.163,       0.18,
                      1.0,        1.0,        3.1,        1.2,          0,
                        0,          5,          0,          0,          0,
                        0,          0,          0,          0,          0,
                        0,          0,          0,          0,          0,
                        0,          0,          0,          0,          0,
                       36,          0,          0,        2.5,          0,
                        0,          0,          0,          0,          0,
                        0,          0,          0,          0,          0,
                        0,          0,      1000.,          0,          9,
DESVAL(1, 6) =       0.3,          0,          0,          0,          0,
                       4.,         -1,          0,          0,          0,
DESVAL(1, 7) =        50,      0.013,          0,          0,
                        0,          0,
DESVAL(16,7) =      0.29,       0.29,
DESVAL(1, 8) =      .100,       .300,       0.34,          0,          0,
                        1,          1,          0,          0,          0,
                        0,          0,          0,          0,          0,
                        0,       .281,       0.71,       0.70,        0.2,
                      1.2,        1.8,         1.,
```

```
DESVAL(36, 8)=          0,      0.28,      0.92,        0.38,        0.17,
DESVAL(76, 8)=       0.28,      0.32,   100000.,
DESVAL(1,  9)=        0.3,         0,         0,           0,           0,
                      0.8,        -1,         0,           0,
DESVAL(1, 10)=       .165,      .319,      .280,           0,           0,
                      1.3,        1.,         0,           0,           0,
                        0,         0,         0,           0,           0,
                        0,      .286,      1.22,        0.20,         0.2,
                      2.8,       3.7,        1.,
DESVAL(36,10)=          0,      0.28,      1.11,       0.057,        0.12,
DESVAL(76,10)=       0.28,      0.32,    100000,
DESVAL(1, 11)=       0.64,        12,       1.0,           0,           0,
                        0,         0,         0,           0,           0,
                        0,         0,         0,           0,           0,
                    0.156,       0.1,
DESVAL(1, 12)=       0.41,         0,         0,           0,           0,
                     0.25,        -1,         0,           0,
DESVAL(1, 13)=       0.18,     1000.,         0,         0.5,         8.3,
                        0,         0,         0,           0,           0,
                        1,         0,       0.8,           0,           0,
                    0.281,       0.1,        1.,          1.,           0,
DESVAL(26,13)=          0,       0.1,        1.,          1.,
DESVAL(1, 14) =      0.45,         0,         0,           0,           0,
                        0,        -1,         0,
DESVAL(7, 21)=      80000,       0.6,         5,           8,           0,
                        0,         0,         0,           0,        0.30,
DESVAL(21, 21)=     0.186,         3,       21.,         0.5,
DESVAL(26, 21)=     0.186,        -4,       60.,         0.5,
DESVAL(7, 22)=      80000,       0.6,         2,          10,           0,
                        0,         0,         0,           0,        0.30,
DESVAL(21, 22)=     0.186,         1,        5.,         0.5,
DESVAL(26, 22)=     0.186,         2,       6.5,         0.5,
DESVAL(31, 22)=     0.186,        -5,       70.,         0.5,
&END

  WEIGHT INPUT IS IN ENGLISH UNITS
  WEIGHT OUTPUT IS IN ENGLISH UNITS

  INPUT - Warning: the maximum component number used,  22, does not equal the
number of components configured in any one mode,  17!

 *************
 *           *
 *  FANH  2  *
 *           *
 *************2

 MAX CONDITIONS OCCUR AT
 ****************************************
       ALT         MN        VALUE
PTOT      0.      0.000       14.5 LB/SQIN
TTOT      0.      0.000      545.7 DEG R
CWIN  35000.      0.700      316.3 LB/SEC
 ****************************************
DUCT
 M NO   VEL   T TOT    P TOT    P STAT    AREA     GAM
0.550   612.   546.    2095.    1706.    6.8408   1.4001

 UTIPMAX STRESS     DEN   W/AREA    TR      H/T
 1519.9 71855.2    0.160   2.127   1.400   0.390
```

```
COMPRESSOR  2 MECHANICAL DESIGN

 LOADING   N STG   DIAM  U TIP C   RPM    C RPM   MAX RPM
   1.031    1.00   38.46  1360.0  8312.4  8104.1  9056.7


 STAGE    1
     WD      WB      WS    WSSF     WN      WC    WFCR   WTDRUM
    52.     52.     36.      6.      0.     43.     40.      9.
     CL   CL2   RHOD   RHOB  RHOS  RHOC RHOFCR    AR    ARS   NS    DFCR
   5.9  14.9  0.160  0.160 0.160 0.160  0.050   2.80   2.50   50   1.10
       PR DEL H  MACH   AREA  R HUB  R TIP  NB UTIPMAX    STR WEIGHT  TIN  TMAX
STAGE I
 1.6198 22.1 0.550  6.841   7.50  19.23  24 1519.9 71855.  238.  546.  546.
6724.

 COMPRESSOR COMPONENT WEIGHT SUMMARY
   WTDSK   WTBLD   WTDRM  WTST/IGV  WTSF   WTCAS   WTNAB   WTCR
   52.1    51.5     9.0     35.6     6.1    43.3     0.0    40.5

 FRAME COMPONENTS INFORMATION

 FRAME WT     LENGTH     GAP    #FRAMES   ARF    RHOF
   12.57       5.0       0.0       6     1.40   0.120
 CASE WT    HUB WT   UP SUPP   LW SUPP  RHOS   THSUP   WTTOWER   TS DIAM
   14.49     9.22     0.00      0.00   0.120   0.20    19.89      1.00

 FRAME WT  =   56.17




  N STG  WEIGHT  LENGTH  CENGRA   INERTIA LENGTH2
     1   294.37    5.92   15.9    6724.1   19.94

 DUCT
  M NO    VEL    T TOT    P TOT    P STAT    AREA    GAM
 0.407   495.    638.    3394.    3029.    5.7070   1.3981

   PR        AD EF        PO        TO        HP
  1.6200     0.8750     3394.0    637.7     8132.
   HI       HO      WI     CWI
 130.43   152.54   260.00  269.37

******************* TOTAL COMP WEIGHT IS   294.366

*************
*           *
*  DUCT  4  *
*           *
************2

MAX CONDITIONS OCCUR AT
**********************
      ALT        MN
PTOT      0.     0.000
TTOT      0.     0.000
**********************

 FRAME COMPONENTS INFORMATION

 FRAME WT     LENGTH     GAP    #FRAMES   ARF    RHOF
    2.40       1.7       0.2      45     1.00   0.110
```

```
CASE WT   HUB WT  UP SUPP  LW SUPP   RHOS  THSUP   WTTOWER   TS DIAM
  1.30     1.12    10.77     6.85   0.100   0.10     0.00      1.00


FRAME WT  =   22.43



DUCT ,   4
RH=   10.51 RT=   12.20 LENG=    8.46
AREA=   0.838 RHO=.168
   WTC(OUTER)   WTC(INNER)    WTT(REV)    WT(TOTAL)    TMIN
      5.4467      4.6912      0.0000      32.5692      0.0500




************
*          *
*  HPC  5  *
*          *
************2

MAX CONDITIONS OCCUR AT
****************************************
        ALT        MN        VALUE
PTOT     0.       0.000      23.7 LB/SQIN
TTOT     0.       0.000     641.9 DEG R
CWIN  35000.      0.700      31.4 LB/SEC
****************************************
DUCT
 M NO    VEL    T TOT    P TOT    P STAT    AREA     GAM
0.340   416.    638.     3360.    3102.    1.0638   1.3981

 UTIPMAX STRESS      DEN   W/AREA    TR      H/T
 1121.4 50562.4    0.300   1.211   0.833    0.455

 COMPRESSOR  5 MECHANICAL DESIGN

 LOADING   N STG    DIAM  U TIP C    RPM    C RPM   MAX RPM
  0.974    14.00   15.68  1000.0 16202.9 14613.0 16387.3

FRAME COMPONENTS INFORMATION

FRAME WT     LENGTH     GAP    #FRAMES   ARF     RHOF
 13.17        5.3       0.0      9      0.80     0.120
CASE WT   HUB WT  UP SUPP  LW SUPP   RHOS  THSUP   WTTOWER   TS DIAM
  6.32     2.87    13.36     3.97   0.120   0.20     0.00      1.00

FRAME WT  =   39.70




 STAGE    1
VARIABLE INLET GUIDE VANE PRESENT
  WIGV   RHOIGV   ARIGV   NBIGV
   8.     0.160    2.50     36

    WD     WB     WS    WSSF    WN     WC    WFCR   WTDRUM
    6.     4.     3.     2.     2.     8.     0.      1.
   CL   CL2  RHOD  RHOB  RHOS  RHOC RHOFCR    AR    ARS   NS    DFCR
 4.5   4.5  0.160 0.160 0.160 0.160 0.000   2.20  3.10   26   3.00
    PR DEL H  MACH   AREA R HUB  R TIP  NB UTIPMAX   STR WEIGHT  TIN   TMAX
STAGE I
```

```
 1.3363  14.7 0.340  1.064  3.57   7.84  21 1121.4 26967.   33.  638.   642.
107.


  STAGE     2
     WD      WB      WS     WSSF     WN      WC    WFCR   WTDRUM
     7.      2.      2.      1.      1.      6.      0.      1.
     CL    CL2   RHOD   RHOB   RHOS   RHOC  RHOFCR     AR     ARS   NS     DFCR
   3.4    3.4  0.160  0.160  0.160  0.160  0.000   2.09    2.95   35   3.00
     PR DEL H  MACH    AREA  R HUB  R TIP  NB UTIPMAX   STR WEIGHT  TIN    TMAX
STAGE I
 1.3043  14.7 0.338  0.838  4.80   7.84  28 1121.4 21341.   20.  699.   701.
127.


  STAGE     3
     WD      WB      WS     WSSF     WN      WC    WFCR   WTDRUM
     6.      1.      1.      1.      1.      5.      0.      1.
     CL    CL2   RHOD   RHOB   RHOS   RHOC  RHOFCR     AR     ARS   NS     DFCR
   2.7    2.7  0.160  0.160  0.160  0.160  0.000   1.98    2.81   44   3.00
     PR DEL H  MACH    AREA  R HUB  R TIP  NB UTIPMAX   STR WEIGHT  TIN    TMAX
STAGE I
 1.2779  14.7 0.336  0.674  5.53   7.84  35 1121.4 17202.   17.  759.   760.
137.


  STAGE     4
     WD      WB      WS     WSSF     WN      WC    WFCR   WTDRUM
     6.      1.      1.      1.      1.      4.      0.      1.
     CL    CL2   RHOD   RHOB   RHOS   RHOC  RHOFCR     AR     ARS   NS     DFCR
   2.3    2.3  0.160  0.160  0.160  0.160  0.000   1.88    2.66   53   3.00
     PR DEL H  MACH    AREA  R HUB  R TIP  NB UTIPMAX   STR WEIGHT  TIN    TMAX
STAGE I
 1.2558  14.7 0.334  0.552  6.02   7.84  42 1121.4 14095.   15.  820.   818.
142.


  STAGE     5
     WD      WB      WS     WSSF     WN      WC    WFCR   WTDRUM
     6.      1.      1.      1.      1.      3.      0.      1.
     CL    CL2   RHOD   RHOB   RHOS   RHOC  RHOFCR     AR     ARS   NS     DFCR
   1.9    1.9  0.160  0.160  0.160  0.160  0.000   1.77    2.52   62   3.00
     PR DEL H  MACH    AREA  R HUB  R TIP  NB UTIPMAX   STR WEIGHT  TIN    TMAX
STAGE I
 1.2372  14.7 0.331  0.458  6.36   7.84  49 1121.4 11716.   13.  880.   877.
146.


  STAGE     6
     WD      WB      WS     WSSF     WN      WC    WFCR   WTDRUM
     6.      0.      0.      1.      1.      3.      0.      1.
     CL    CL2   RHOD   RHOB   RHOS   RHOC  RHOFCR     AR     ARS   NS     DFCR
   1.7    1.7  0.160  0.160  0.160  0.160  0.000   1.66    2.37   71   3.00
     PR DEL H  MACH    AREA  R HUB  R TIP  NB UTIPMAX   STR WEIGHT  TIN    TMAX
STAGE I
 1.2210  14.7 0.329  0.386  6.62   7.84  56 1121.4 9859.   11.  940.   936.
146.


  STAGE     7
     WD      WB      WS     WSSF     WN      WC    WFCR   WTDRUM
     6.      0.      0.      1.      1.      3.      0.      1.
     CL    CL2   RHOD   RHOB   RHOS   RHOC  RHOFCR     AR     ARS   NS     DFCR
   1.5    1.5  0.160  0.160  0.160  0.160  0.000   1.55    2.22   80   3.00
     PR DEL H  MACH    AREA  R HUB  R TIP  NB UTIPMAX   STR WEIGHT  TIN    TMAX
STAGE I
```

```
 1.2071  14.7 0.327  0.328  6.82   7.84  62 1121.4  8387.   11.  999.  995.
146.


  STAGE    8
    WD      WB      WS     WSSF     WN      WC    WFCR   WTDRUM
    5.      0.      0.      0.      1.      2.      0.      1.
    CL   CL2  RHOD  RHOB  RHOS RHOC RHOFCR    AR    ARS   NS    DFCR
  1.4   1.4  0.160  0.160  0.160  0.160 0.000   1.45  2.08  88  3.00
     PR DEL H  MACH   AREA R HUB  R TIP  NB UTIPMAX   STR WEIGHT  TIN    TMAX
STAGE I
 1.1949  14.7 0.325  0.281  6.97   7.84  68 1121.4  7204.   10. 1058. 1053.
145.


  STAGE    9
    WD      WB      WS     WSSF     WN      WC    WFCR   WTDRUM
    5.      0.      0.      0.      0.      2.      0.      1.
    CL   CL2  RHOD  RHOB  RHOS RHOC RHOFCR    AR    ARS   NS    DFCR
  1.3   1.3  0.160  0.160  0.160  0.160 0.000   1.34  1.93  95  3.00
     PR DEL H  MACH   AREA R HUB  R TIP  NB UTIPMAX   STR WEIGHT  TIN    TMAX
STAGE I
 1.1841  14.7 0.323  0.244  7.09   7.84  74 1121.4  6239.    9. 1117. 1112.
144.


  STAGE    10
    WD      WB      WS     WSSF     WN      WC    WFCR   WTDRUM
    11.     0.      0.      0.      0.      4.      0.      1.
    CL   CL2  RHOD  RHOB  RHOS RHOC RHOFCR    AR    ARS   NS    DFCR
  1.2   1.2  0.300  0.300  0.160  0.300 0.000   1.23  1.78 101  3.00
     PR DEL H  MACH   AREA R HUB  R TIP  NB UTIPMAX   STR WEIGHT  TIN    TMAX
STAGE I
 1.1745  14.7 0.321  0.213  7.19   7.84  78 1121.4 10207.   17. 1175. 1171.
305.


  STAGE    11
    WD      WB      WS     WSSF     WN      WC    WFCR   WTDRUM
    11.     0.      0.      0.      0.      4.      0.      1.
    CL   CL2  RHOD  RHOB  RHOS RHOC RHOFCR    AR    ARS   NS    DFCR
  1.2   1.2  0.300  0.300  0.160  0.300 0.000   1.12  1.64 106  3.00
     PR DEL H  MACH   AREA R HUB  R TIP  NB UTIPMAX   STR WEIGHT  TIN    TMAX
STAGE I
 1.1659  14.7 0.319  0.187  7.28   7.84  82 1121.4  8967.   17. 1233. 1230.
306.


  STAGE    12
    WD      WB      WS     WSSF     WN      WC    WFCR   WTDRUM
    11.     0.      0.      0.      0.      4.      0.      1.
    CL   CL2  RHOD  RHOB  RHOS RHOC RHOFCR    AR    ARS   NS    DFCR
  1.1   1.1  0.300  0.300  0.160  0.300 0.000   1.02  1.49 110  3.00

 **** WARNING FOLLOWING STAGE DESIGN LIMIT EXCEEDED *****
 STAGE HUBTIP RATIO IS 0.94  DES LIMIT IS 0.94
 ** HUB TIP RATIO IS TOO HIGH REDUCE HUB TIP RATIO INPUT **
     PR DEL H  MACH   AREA R HUB  R TIP  NB UTIPMAX   STR WEIGHT  TIN    TMAX
STAGE I
 1.1582  14.7 0.316  0.165  7.34   7.84  84 1121.4  7926.   17. 1290. 1289.
309.


  STAGE    13
    WD      WB      WS     WSSF     WN      WC    WFCR   WTDRUM
    11.     0.      0.      0.      0.      4.      0.      1.
    CL   CL2  RHOD  RHOB  RHOS RHOC RHOFCR    AR    ARS   NS    DFCR
```

```
   1.1   1.1  0.300 0.300 0.160 0.300 0.000   0.91  1.35 112  3.00

 **** WARNING FOLLOWING STAGE DESIGN LIMIT EXCEEDED *****
 STAGE HUBTIP RATIO IS 0.94  DES LIMIT IS 0.94
 ** HUB TIP RATIO IS TOO HIGH REDUCE HUB TIP RATIO INPUT **
     PR DEL H  MACH   AREA R HUB  R TIP  NB UTIPMAX   STR WEIGHT  TIN   TMAX
STAGE I
 1.1512 14.7 0.314  0.147  7.40   7.84 85 1121.4 7044.  17. 1347. 1347.
315.

 STAGE   14
    WD     WB     WS    WSSF    WN     WC    WFCR   WTDRUM
    11.    0.     0.     0.     0.     4.     0.     1.
    CL    CL2   RHOD   RHOB   RHOS   RHOC RHOFCR    AR    ARS    NS    DFCR
  1.1   1.1  0.300 0.300 0.160 0.300 0.000   0.80  1.20 112  3.00

 **** WARNING FOLLOWING STAGE DESIGN LIMIT EXCEEDED *****
 STAGE HUBTIP RATIO IS 0.95  DES LIMIT IS 0.94
 ** HUB TIP RATIO IS TOO HIGH REDUCE HUB TIP RATIO INPUT **

 **** WARNING FOLLOWING STAGE DESIGN LIMIT EXCEEDED *****
 STAGE BLADE HEIGHT IS  0.39  DES LIMIT IS  0.40
 ** STAGE BLADE HEIGHT IS TOO SMALL CHANGE DES OPR OR REDUCE H/T INPUT **
     PR DEL H  MACH   AREA R HUB  R TIP  NB UTIPMAX   STR WEIGHT  TIN   TMAX
STAGE I
 1.1448 14.7 0.312  0.131  7.45   7.84 84 1121.4 6292.  17. 1403. 1406.
323.

 COMPRESSOR COMPONENT WEIGHT SUMMARY
   WTDSK   WTBLD   WTDRM  WTST/IGV  WTSF   WTCAS   WTNAB   WTCR
   109.2   10.4    10.9    17.5     9.4    55.7     9.5    0.0

  N STG  WEIGHT  LENGTH  CENGRA  INERTIA LENGTH2
    14   262.49   33.90   14.8   2797.8   33.90

 DUCT
  M NO   VEL    T TOT   P TOT    P STAT   AREA    GAM
 0.310  566.   1460.   50401.   47255.   0.1182  1.3526

   PR        AD EF       PO        TO        HP
  15.0000   0.8600    50400.9   1459.6    12028.
   HI       HO       WI     CWI
  152.54   358.53   41.27   28.82

 ****************** TOTAL COMP WEIGHT IS   262.489

 *************
 *           *
 *  DUCT  6  *
 *           *
 *************2

 MAX CONDITIONS OCCUR AT
 *********************
      ALT        MN
 PTOT     0.     0.000
 TTOT     0.     0.000
 *********************
 DUCT ,  6
 RH=    7.53 RT=    7.83 LENG=    1.21
 AREA=   0.102 RHO=.286
```

```
        WTC(OUTER)    WTC(INNER)    WTT(REV)     WT(TOTAL)     TMIN
          1.0137       0.9744       0.0000        1.9881       0.0593




     ************
     *          *
     *  PBUR  7 *
     *          *
     ************2

     MAX CONDITIONS OCCUR AT
     ****************************************
            ALT        MN       VALUE
     PTOT     0.      0.000      348.1 LB/SQIN
     TTOT     0.      0.000     1465.0 DEG R
     CWIN     0.      0.000        2.6 LB/SEC
     ****************************************
     BURNER NUMBER    7
       RIN    ROUT    LENGTH     MACH     WSPEC     TMIN
       5.772   9.197   7.800     0.027    2.282     0.080
       CAS WT   INC WT  LIN WT   NOZ WT    FRAME    WTOT
        10.5      6.6    16.2      4.1      76.8    129.8


      HPC STRUCTURAL CASE:  WEIGHT   LENGTH   DENSITY
                             15.6     12.1     0.160


     ************
     *          *
     *  HPT   8 *
     *          *
     ************2

     MAX CONDITIONS OCCUR AT
     ****************************************
            ALT        MN       VALUE
     PTOT      0.     0.000      332.5 LB/SQIN
     TTOT      0.     0.000     2792.1 DEG R
     CWOUT 39000.     0.800       16.4 LB/SEC
     ****************************************
     DUCT
      M NO    VEL   T TOT    P TOT    P STAT    AREA     GAM
     0.100   245.   2693.    47411.   47105.    0.4940   1.2957

      UTIPMAX STRESS      DEN   W/AREA    TR      H/T
     1353.5 23726.3   0.281   0.356    1.000   0.868

      TURBINE  8  MECHANICAL DESIGN
        H/T   N STG LOADING     AREA    GE LOADING
       0.868   2.000   0.340    0.494    0.843
         UT     RTIP    RHUB    DEL H     RPM    MAXRPM   TORQ
      1353.5    9.6     8.3     215.3  16202.9 16202.9  46992.

      STAGE    1
        WDISK   WISD    WID WBLADE  WVANE    WNB   WCASE     AR   ARS TLBLADE TLVANE
     RHOB RHOD  RHOS  RHOC  NS
        34.1    11.9    0.0    2.5    4.7    2.4   10.7   1.20  1.20  1.06   1.06
     0.281 0.320 0.280 0.280  52
        WSSFX   WTRS  WTSHRD   WDRUMX WTRSHD   WTDSB   WTACC
         2.7     1.1    2.3     6.2    0.0     0.0     11.7
```

```
    PR  DEL H  MACH   AREA  R HUB  R TIP  NB MAXUTIP   STR    WEIGHT    LENGTH
STAGE I
 2.0133 107.6 0.100  0.494   8.31   9.57  40 1353.5 23726.    90.24     2.83
1348.

   STAGE   2
   WDISK   WISD    WID  WBLADE   WVANE    WNB   WCASE    AR  ARS TLBLADE TLVANE
RHOB RHOD  RHOS  RHOC  NS
    22.4    7.8    0.0     1.5     2.8    1.5    6.8  1.80 1.80  0.67   0.67
0.281 0.320 0.280 0.280  82
   WSSFX   WTRS  WTSHRD  WDRUMX WTRSHD   WTDSB   WTACC
    1.7    0.7    1.5     3.9     0.0     0.0     7.4
    PR  DEL H  MACH   AREA  R HUB  R TIP  NB MAXUTIP   STR    WEIGHT    LENGTH
STAGE I
 2.2697 107.6 0.200  0.469   8.31   9.51  63 1345.1 22537.    57.99     1.57
876.

    TURBINE COMPONENT SUMMARY
   WTDSK   WTISD    WTID  WTDSB   WTBLD   WTRSH   WTDRM   WTRBS    WTST
WTSSH    WTSF   WTCAS   WTNAB    WTCC
    56.4   19.7     0.0     0.0     4.0     0.0    10.1     1.9     7.5
 3.8     4.3    17.5     3.9    19.1

 FRAME WT  =   44.91



  N STG  LENGTH  WEIGHT   CENGRA   INERTIA
    2     4.40   193.13      3.7     2224.

 DUCT
 M NO   VEL    T TOT    P TOT    P STAT    AREA     GAM
0.300   624.   1944.   10355.    9764.    0.6897   1.3166

   ***** AN**2 =   26.1 (BILLIONS IN2-RPM2) *****

  PR       TR     AD EF       PO        TO        TO.1
 4.5785   1.3739   0.9100   10355.2   1960.3    1943.5
 H IN    H OUT    AREA     FLOW       HP
 720.40  505.13    1.47    39.67    12081.

****************** TOTAL TURB WEIGHT IS    193.134


*************
*           *
*  DUCT  9  *
*           *
************2

MAX CONDITIONS OCCUR AT
**********************
     ALT        MN
PTOT     0.      0.000
TTOT     0.      0.000
**********************
DUCT , 9
RH=    8.25 RT=   10.00 LENG=    1.39
AREA=   0.694 RHO=.286
  WTC(OUTER)   WTC(INNER)    WTT(REV)    WT(TOTAL)    TMIN
```

```
     1.2524       1.0340       0.0000       2.2864       0.0500



  ************
  *          *
  *  LPT  10  *
  *          *
  ************2

  MAX CONDITIONS OCCUR AT
  ****************************************
         ALT       MN      VALUE
  PTOT      0.      0.000      72.0 LB/SQIN
  TTOT      0.      0.000    1943.6 DEG R
  CWOUT 35000.      0.700      63.6 LB/SEC
  ****************************************
  DUCT
   M NO   VEL   T TOT    P TOT    P STAT   AREA    GAM
  0.165   345.  1944.   10306.   10124.   1.2154  1.3166

   UTIPMAX STRESS     DEN  W/AREA   TR      H/T
    808.2 15638.4   0.286   0.821   1.000   0.742

   TURBINE 10  MECHANICAL DESIGN
     H/T   N STG LOADING     AREA    GE LOADING
    0.742  3.000   0.280    1.215    1.176
       UT    RTIP    RHUB    DEL H     RPM    MAXRPM  TORQ
    808.2   11.1     8.3    139.8   8312.4   8312.4  61667.

  STAGE    1
    WDISK   WISD    WID WBLADE   WVANE    WNB   WCASE     AR   ARS  TLBLADE TLVANE
  RHOB RHOD  RHOS  RHOC   NS
    20.2    7.1     0.0   11.2    14.4    2.1   11.2   2.80  2.80   1.02   1.02
  0.286 0.320 0.280 0.280   75
    WSSFX   WTRS  WTSHRD   WDRUMX WTRSHD   WTDSB   WTACC
     3.0    1.3    2.2     5.5     0.0     0.0     0.0
    PR  DEL H  MACH  AREA  R HUB  R TIP  NB MAXUTIP   STR    WEIGHT  LENGTH
  STAGE I
   1.4961  46.6 0.165  1.215  8.27  11.14  83   808.2  15638.   78.39    2.54
  1491.

  STAGE    2
    WDISK   WISD    WID WBLADE   WVANE    WNB   WCASE     AR   ARS  TLBLADE TLVANE
  RHOB RHOD  RHOS  RHOC   NS
    19.4    6.8     0.0   11.6    15.1    2.0   10.7   3.25  3.25   0.96   0.96
  0.286 0.320 0.280 0.280   82
    WSSFX   WTRS  WTSHRD   WDRUMX WTRSHD   WTDSB   WTACC
     2.9    1.2    2.1     5.2     0.0     0.0     0.0
    PR  DEL H  MACH  AREA  R HUB  R TIP  NB MAXUTIP   STR    WEIGHT  LENGTH
  STAGE I
   1.5564  46.6 0.216  1.339  8.27  11.39  90   826.3  17223.   77.09    2.38
  1499.

  STAGE    3
    WDISK   WISD    WID WBLADE   WVANE    WNB   WCASE     AR   ARS  TLBLADE TLVANE
  RHOB RHOD  RHOS  RHOC   NS
    20.0    7.0     0.0   15.0    19.2    2.1   11.6   3.70  3.70   0.99   0.99
  0.286 0.320 0.280 0.280   83
    WSSFX   WTRS  WTSHRD   WDRUMX WTRSHD   WTDSB   WTACC
     3.1    1.3    2.2     5.4     0.0     0.0     0.0
```

```
     PR  DEL H  MACH  AREA  R HUB  R TIP  NB MAXUTIP  STR   WEIGHT  LENGTH
STAGE I
 1.6348 46.6 0.268 1.621  8.27  11.95  92  866.6 20858.    86.89   2.23
1776.


    TURBINE COMPONENT SUMMARY
   WTDSK   WTISD   WTID   WTDSB   WTBLD   WTRSH   WTDRM   WTRBS    WTST
WTSSH    WTSF   WTCAS   WTNAB   WTCC
   59.6    20.9    0.0     0.0    37.9     0.0    16.1     3.9    48.7
6.5     9.0    33.6     6.2     0.0

FRAME COMPONENTS INFORMATION

FRAME WT     LENGTH     GAP    #FRAMES    ARF     RHOF
    4.93      3.8      1.9       6      1.20    0.120
  CASE WT   HUB WT  UP SUPP   LW SUPP   RHOS   THSUP   WTTOWER   TS DIAM
    7.48     4.80    0.00      9.28   0.120   0.20    0.00       1.00

 FRAME WT  =   26.49




 N STG  LENGTH  WEIGHT   CENGRA   INERTIA
    3   12.92  268.87     5.7      4766.

 DUCT
 M NO   VEL   T TOT   P TOT   P STAT   AREA    GAM
0.319   576.  1441.   2705.   2528.    2.1345  1.3401

   ***** AN**2 =  21.2 (BILLIONS IN2-RPM2) *****

  PR      TR     AD EF      PO       TO       TO.1
 3.8103  1.3491  0.9200   2704.9   1440.6   1440.6
 H IN   H OUT   AREA    FLOW      HP
 499.95 360.17   5.93   41.13    8133.

****************** TOTAL TURB WEIGHT IS   268.869


************
*          *
*  FMIX 11  *
*          *
************2

MAX CONDITIONS OCCUR AT
**********************
     ALT        MN
PTOT     0.     0.000
TTOT     0.     0.000
**********************
LENGTH= 14.77 WEIGHT =   46.81


************
*          *
*  DUCT 12  *
*          *
************2
```

```
MAX CONDITIONS OCCUR AT
*********************
        ALT      MN
PTOT    0.     0.000
TTOT    0.     0.000
*********************


*************
*           *
*  NOZ  13  *
*           *
************2

MAX CONDITIONS OCCUR AT
*********************
        ALT      MN
PTOT    0.     0.000
TTOT    0.     0.000
*********************
NOZZLE  13
 TOTAL NOZZLE COMPONENT WEIGHT =    67.49

NOZZ WEIGHT=    53.73 TOT LENGTH=   18.155 TR WT=    1.50
THROAT AREA=   689.66 EXIT AREA=   689.66
MIXER EJECTOR LENGTH =     0.00 TRANS DUCT LENGTH =     0.00

NOZZLE WEIGHT BREAKDOWN
OUTER WALL =           53.73  PLUG =            12.26  NOZZ DENS = .2810
INNER WALL =            0.00  MIXER-EJECTOR=    0.00  PLUG DENS = .2810
CONV INNER WALLS =      0.00  NOZ AC LIN =      0.00  CASE DENS = .2810
DIV INNER WALLS =       0.00  PLG AC LIN =      0.00  M/E  DENS = .2810
2-D SIDEWALLS =         0.00  AC SPLT PLATE =   0.00  ACOU DENS = .0900
VAR AREA C & A =        0.00
VAR AREA MISC =         0.00
2-D TRANS DUCT=         0.00



*************
*           *
*  DUCT 14  *
*           *
************2

MAX CONDITIONS OCCUR AT
*********************
        ALT      MN
PTOT    0.     0.000
TTOT    0.     0.000
*********************

FRAME COMPONENTS INFORMATION

FRAME WT    LENGTH     GAP    #FRAMES   ARF    RHOF
   3.20      3.7      18.3       3      1.80    0.120
CASE WT   HUB WT  UP SUPP  LW SUPP   RHOS   THSUP   WTTOWER   TS DIAM
  5.29     3.46    0.00    11.60    0.120   0.10    0.00      1.00

FRAME WT =  23.55


DUCT ,  14
```

```
RH=   12.52 RT=    19.12 LENG=    56.10
AREA=   4.557 RHO=.168
   WTC(OUTER)    WTC(INNER)     WTT(REV)     WT(TOTAL)      TMIN
      56.6164      37.0721       0.0000      117.2388       0.0500




************
*          *
*  DUCT 15  *
*          *
************2

MAX CONDITIONS OCCUR AT
**********************
       ALT        MN
PTOT      0.     0.000
TTOT      0.     0.000
**********************


************
*          *
*  SHAF 21  *
*          *
************2

MAX TORQUE CONDITION
**********************
 TORQUE
 0.7
**********************
SHAFT   21
   DO     DI    LENG     DN     WT
  2.24   2.07   13.41    0.92    6.6


BEARING  #   3     4
BEARING WT   3.8   4.8
TOTAL SHAFT WEIGHT =   15.22

TOTAL INERTIA OF THIS SPOOL IS     5022.

************
*          *
*  SHAF 22  *
*          *
************2

MAX TORQUE CONDITION
**********************
 TORQUE
 2.7
**********************
SHAFT   22
   DO     DI    LENG     DN     WT
  1.67   1.00   64.31    0.35   49.1


BEARING  #   1     2     5
BEARING WT   3.2   3.2   4.0
TOTAL SHAFT WEIGHT =   59.56
```

```
     TOTAL INERTIA OF THIS SPOOL IS     11490.

     *************
     *           *
     *  INLT  1  *
     *           *
     *************2

     MAX CONDITIONS OCCUR AT
     **********************
          ALT        MN
     PTOT     0.      0.000
     TTOT     0.      0.000
     **********************
     INLET    1

     MDA SUBSONIC LOW DRAG INLET

      INLET WEIGHT
      WTINLT =    0.00  DUCTWT =    0.00
      BDRWT  =    0.00  TDRWT  =    0.00
      ENG MT =   58.55  FIRE WL=    0.00
      FAN DIA=   38.46  LDUCT  =    0.00  LDUCTS =    0.00

      INLET LENGTH =   19.23


      NACELLE WEIGHT
      NAC WT          =  191.18
      INL CWL WT      =   49.10  INLET LEN    =   18.93
      FAN CWL WT      =    4.27  FAN BLD LEN  =    2.96
      FAN EXH CWL WT  =  126.02  FAN EXH LEN  =  106.00
      CORE CWL WT     =    0.00  CORE CWL LEN=    0.00  CWL AVG DIAM =   14.82
      ANTI-ICE WT     =    3.98
      ACOUSTIC WT     =    0.00
      BULKHEAD WT     =    7.81

      TOTAL INLET/NACELLE WEIGHT =   249.74


      *************
      *           *
      *  ACCS WT  *
      *           *
      *************2

       ACCS WT= 141.722
1
     COMP   WT   COMP  ACCU    UPSTREAM RADIUS        DOWNSTREAM RADIUS
      NO   EST   LEN   LEN   RI    RO    RI    RO    RI    RO    RI    RO
NSTAGE

       1  250.   19.2    0.   0.0   0.0   0.0   0.0   0.0   0.0   0.0   0.0
0
       2  294.    5.9    6.   7.5  19.2   0.0   0.0  10.4  19.2   0.0   0.0
1
       3    0.    0.0    6.  10.4  19.2   0.0   0.0  10.4  12.2  12.2  19.2
0
       4   33.    8.5   14.  10.5  12.2   0.0   0.0  10.5  12.2   0.0   0.0
0
```

```
  5  262.   33.9   48.   3.6   7.8  0.0   0.0   7.5   7.8  0.0   0.0
14
  6    2.    1.2   49.   7.5   7.8  0.0   0.0   7.5   7.8  0.0   0.0
0
  7  130.    7.8   57.   5.8   9.2  0.0   0.0   5.8   9.2  0.0   0.0
0
  8  193.    4.4   62.   8.3   9.6  0.0   0.0   8.3  10.0  0.0   0.0
2
  9    2.    1.4   63.   8.3  10.0  0.0   0.0   8.3  10.0  0.0   0.0
0
 10  269.   12.9   76.   8.3  11.1  0.0   0.0   8.3  12.9  0.0   0.0
3
 11   47.   14.8   91.   8.1  13.0 13.0  18.2   8.1  18.2  0.0   0.0
0
 12    0.    0.0   91.   8.1  18.2  0.0   0.0   8.1  18.2  0.0   0.0
0
 13   67.   18.2  109.   8.3  18.2  0.0   0.0   0.0  14.8  0.0   0.0
0
 14  117.   56.1   76.  12.5  19.1  0.0   0.0  12.5  19.1  0.0   0.0
0
 15    0.    0.0   76.   8.3  12.9  0.0   0.0   8.3  12.9  0.0   0.0
0
 21   15.   13.4    0.   3.6   7.8  8.3   9.6   0.0   0.0  0.0   0.0
0
 22   60.   64.3    0.   7.5  19.2  8.3  11.1   0.0   0.0  0.0   0.0
0
```

```
  BARE ENGINE WEIGHT        =    1491
  ACCESSORIES WEIGHT        =     141
  TOTAL ENGINE WEIGHT       =    1633
  INLET/NACELLE WEIGHT      =     249
  TOTAL ENGINE POD WEIGHT   =    1883

  ENGINE LENGTH             =   109.0
  TOTAL ENGINE POD LENGTH   =   128.2
  ENGINE MAX DIAMETER       =    38.5
  NACELLE MAX DIAMETER      =    45.8
  ENGINE POD C.G. LOCATION  =    33.4
```

ROTATING MACHINERY WEIGHT SUMMARY

COMP	NAME	TOT WT	ROTOR	STATOR	FRAME	LT	LTM
2	FANH	294.4	112.6	125.6	56.2	19.9	14.9
5	HPC	262.5	140.1	82.6	39.7	33.9	28.6
8	HPT	193.1	94.2	54.1	44.9	4.4	4.4
10	LPT	268.9	140.7	101.7	26.5	12.9	7.1

1

Appendix C

ANSYS Axisymmetric Model Input File for Exoskeletal Rotor

This appendix contains the input data for an ANSYS structural analysis of the exoskeletal rotor when it is spinning at the overspeed condition of 16 400 rpm. The centrifugal force from each row of blades is represented by discrete force applied to the rotor. This model was used to generate the analysis results discussed in the section Drum Rotor Investigation. The ANSYS computer program is a large-scale multipurpose finite-element program that may be used for solving several classes of engineering analyses. The program contains many special features, one of which allows the two-dimensional modeling of a solid of revolution or an axisymmetric body. The use of axisymmetry reduces the size of the model by simplifying the generation of the geometry, structural loads, and boundary conditions.

This input file contains preprocessing, solution, and postprocessing commands to create the model, perform the analysis, and plot the results. The general preprocessor (PREP7) section contains solid modeling and mesh generation commands and is also used to define all other analysis data (geometric properties (real constants), material properties, etc.). Parameters are used in the geometry definition to provide more flexibility for the analyst to change the design. Loads and constraints are defined in the solution section (SOLUTION) where the analysis is also executed. The analysis results are reviewed using the postprocessor (POST1), in which plots are created to display distorted geometries, stress contours, and margins of safety contours. All plots of the geometry, mesh, and results are stored in a graphics file (file.grph), which may be viewed with the ANSYS Display utility. Another analyst may re-create the model by inputting this listing in either an ANSYS interactive session or a batch job.

The following ANSYS FEA input listing was generated by Daniel N. Kosareo.

```
/BATCH
!
! ANSYS RELEASE= 7.0    UP20021010    01/08/03 Daniel N. Kosareo
!
/SHOW,file,grph
!
! DEFINE PARAMETERS
!
*ASK,DTHK,BLADE MOUNTING RING THICKNESS,0.375

*ASK,RTHK,ROTOR THICKNESS,0.125

*ASK,FHGT,FLANGE HEIGHT,0.5

!
! PREPROCESSING MODULE
!
/PREP7
/TITLE,Exoskeletal AE3007 Engine, Rotor Design, 16400 RPM
/WIN,1,-1,1,-.88,1
/VIEW,1,,,1
/VUP,1,X
!
! DEFINE ELEMENT TYPES (Plane Axisymmetric Elements)
```

```
!
ET,1,PLANE82,,,1
*REPEAT,21,1
!
! MATERIAL PROPERTIES FOR GRAPHITE-POLYIMIDE COMPOSITE Gr/P
!
MP,EX,1,24.0E+06
MP,NUXY,1,0.33
MP,DENS,1,(0.056/386.4)
MP,ALPX,1,20E-06
!
! MATERIAL PROPERTIES FOR TITANIUM Ti-6Al-4V
!
MP,EX,2,16.0E+06
MP,NUXY,2,0.31
MP,DENS,2,(0.160/386.4)
MP,ALPX,2,4.9E-06
!
! MATERIAL PROPERTIES FOR HASTALLOY X
!
MP,EX,3,29.8E+06
MP,NUXY,3,0.32
MP,DENS,3,(0.297/386.4)
MP,ALPX,3,7.5E-06
!
! MATERIAL PROPERTIES FOR SILICON-CARBIDE SiC/SiC
!
MP,EX,4,10.9E+06
MP,NUXY,4,0.07
MP,DENS,4,(0.08/386.4)
MP,ALPX,4,1.7E-06
!
! SOLID AXISYMMETRIC MODEL
!
K,1,7.84,0.00
K,2,7.84,2.25          ! Stage 1
K,4,7.84,3.59
KFILL,2,4
K,5,7.84,4.72          ! Stage 2
K,7,7.84,5.79
KFILL,5,7
K,8,7.84,7.24          ! Stage 3
K,10,7.84,8.15
KFILL,8,10
K,11,7.84,9.276        ! Stage 4
K,13,7.84,10.19
KFILL,11,13
K,14,7.84,11.314       ! Stage 5
K,16,7.84,12.01
KFILL,14,16
```

```
K,17,7.84,13.19          ! Stage 6
K,19,7.84,13.78
KFILL,17,19
K,20,7.84,14.585         ! Stage 7
K,22,7.84,15.23
KFILL,20,22
K,23,7.84,16.02          ! Stage 8
K,25,7.84,16.41
KFILL,23,25
K,26,7.84,17.37          ! Stage 9
K,28,7.84,17.80
KFILL,26,28
K,29,7.84,18.60          ! Stage 10
K,31,7.84,19.09
KFILL,29,31
K,32,7.84,19.86          ! Stage 11
K,34,7.84,20.32
KFILL,32,34
K,35,7.84,21.1           ! Stage 12
K,37,7.84,21.66
KFILL,35,37
K,38,7.84,22.38          ! Stage 13
K,40,7.84,22.74
KFILL,38,40
K,41,7.84,23.55          ! Stage 14
K,43,7.84,23.92
KFILL,41,43
K,44,7.84,24.68
K,45,7.84+0.5*(10.29-7.84)/(32.4-24.68),24.68+0.5
K,46,7.84+(32.4-24.68-0.5)*(10.29-7.84)/(32.4-24.68),32.4-0.5
K,47,10.29,32.4
K,48,10.29+0.5*(9.57-10.29)/(39.04-32.4),32.4+0.5
K,49,10.29+(39.04-32.4-0.5)*(9.57-10.29)/(39.04-32.4),39.04-0.5
K,50,9.57,39.04          ! HPT Stage 1
K,52,9.57,39.95
KFILL,50,52
K,53,9.51,41.4           ! HPT Stage 2
K,55,9.51,42.25
KFILL,53,55
K,56,9.51,42.25+0.5
L,1,2
*REPEAT,55,1,1
K,57,7.84+DTHK,0.00
K,58,7.84+DTHK,3.59
K,59,7.84+DTHK,5.79
K,60,7.84+DTHK,8.15
K,61,7.84+DTHK,10.19
K,62,7.84+DTHK,12/01
K,63,7.84+DTHK,13.78
K,64,7.84+DTHK,15.23
```

```
K,65,7.84+DTHK,16.41
K,66,7.84+DTHK,17.80
K,67,7.84+DTHK,19.09
K,68,7.84+DTHK,20.32
K,69,7.84+DTHK,21.66
K,70,7.84+DTHK,22.74
K,71,7.84+DTHK,23.92
KGEN,2,44,49,1,DTHK,,,
K,78,9.57+DTHK,39.04
K,79,9.57+DTHK,39.95
K,80,9.51+DTHK,42.25
K,81,9.51+DTHK,42.25+0.5
L,57,58
*REPEAT,24,1,1
L,1,57
*REPEAT,15,3,1
L,44,72
*REPEAT,7,1,1
L,52,79
L,55,80
L,56,81
KGEN,2,57,63,1,RTHK,,,
K,89,KX(64)+RTHK,15.23-0.5
K,90,KX(64)+RTHK,15.23
K,91,KX(64)+RTHK,15.23+0.5
KGEN,2,65,71,1,RTHK,,,
K,99,KX(71)+RTHK,24.68-0.5
KGEN,2,72,78,1,RTHK,,,
K,107,KX(78)+RTHK,39.04+0.5
KGEN,2,79,81,1,RTHK,,,
L,82,83
*REPEAT,28,1,1
L,57,82
*REPEAT,7,1,1
L,64,90
L,65,92
*REPEAT,7,1,1
L,72,100
*REPEAT,7,1,1
L,79,108
L,80,109
L,81,110
KGEN,2,89,91,1,FHGT,,,
KGEN,2,99,101,1,FHGT,,,
KMODIF,114,KX(116)
KMODIF,115,KX(116)
KGEN,2,105,107,1,FHGT,,,
KMODIF,118,KX(117)
KMODIF,119,KX(117)
L,111,112
```

```
L,112,113
L,89,111
*REPEAT,3,1,1
L,114,115
L,115,116
L,99,114
*REPEAT,3,1,1
L,117,118
L,118,119
L,105,117
*REPEAT,3,1,1
/PNUM,KP,1
KPLO
LPLO
/PNUM,KP,0
/NUM,-1
/DEVICE,VECT,ON
LPLO
/NUM,1
/DEVICE,VECT,OFF
/DEVICE,RAST,ON
LPLO
/COM
KSEL,S,KP,,1,4,1
KSEL,A,KP,,57,58
LSLK,S,1
AL,ALL                    ! Area 1
KSEL,S,KP,,4,7,1
KSEL,A,KP,,58,59
LSLK,S,1
AL,ALL                    ! Area 2
KSEL,S,KP,,7,10,1
KSEL,A,KP,,59,60
LSLK,S,1
AL,ALL                    ! Area 3
KSEL,S,KP,,10,13,1
KSEL,A,KP,,60,61
LSLK,S,1
AL,ALL                    ! Area 4
KSEL,S,KP,,13,16,1
KSEL,A,KP,,61,62
LSLK,S,1
AL,ALL                    ! Area 5
KSEL,S,KP,,16,19,1
KSEL,A,KP,,62,63
LSLK,S,1
AL,ALL                    ! Area 6
KSEL,S,KP,,19,22,1
KSEL,A,KP,,63,64
LSLK,S,1
```

```
AL,ALL                        ! Area 7
KSEL,S,KP,,22,25,1
KSEL,A,KP,,64,65
LSLK,S,1
AL,ALL                        ! Area 8
KSEL,S,KP,,25,28,1
KSEL,A,KP,,65,66
LSLK,S,1
AL,ALL                        ! Area 9
KSEL,S,KP,,28,31,1
KSEL,A,KP,,66,67
LSLK,S,1
AL,ALL                        ! Area 10
KSEL,S,KP,,31,34,1
KSEL,A,KP,,67,68
LSLK,S,1
AL,ALL                        ! Area 11
KSEL,S,KP,,34,37,1
KSEL,A,KP,,68,69
LSLK,S,1
AL,ALL                        ! Area 12
KSEL,S,KP,,37,40,1
KSEL,A,KP,,69,70
LSLK,S,1
AL,ALL                        ! Area 13
KSEL,S,KP,,40,43,1
KSEL,A,KP,,70,71
LSLK,S,1
AL,ALL                        ! Area 14
ALLSEL
A,43,44,72,71                 ! Area 15
*REPEAT,7,1,1,1,1             ! Areas 16-21
KSEL,S,KP,,50,52,1
KSEL,A,KP,,78,79
LSLK,S,1
AL,ALL                        ! Area 22
KSEL,S,KP,,52,55,1
KSEL,A,KP,,79,80,1
LSLK,S,1
AL,ALL                        ! Area 23
ALLSEL
A,55,56,81,80                 ! Area 24
A,57,58,83,82                 ! Area 25
*REPEAT,6,1,1,1,1             ! Areas 26-30
KSEL,S,KP,,88,90,1
KSEL,A,KP,,63,64
LSLK,S,1
AL,ALL                        ! Area 31
KSEL,S,KP,,90,92,1
KSEL,A,KP,,64,65
```

```
LSLK,S,1
AL,ALL                          ! Area 32
ALLSEL
A,65,66,93,92                   ! Area 33
*REPEAT,6,1,1,1,1               ! Areas 34-38
KSEL,S,KP,,98,100,1
KSEL,A,KP,,71,72
LSLK,S,1
AL,ALL                          ! Area 39
ALLSEL
A,72,73,101,100                 ! AREA 40
*REPEAT,6,1,1,1,1               ! Areas 41-45
KSEL,S,KP,,106,108
KSEL,A,KP,,78,79
LSLK,S,1
AL,ALL                          ! AREA 46
ALLSEL
A,79,80,109,108                 ! AREA 47
A,80,81,110,109                 ! AREA 48
A,89,90,112,111                 ! Area 49
A,90,91,113,112                 ! Area 50
A,99,100,115,114                ! Area 51
A,100,101,116,115               ! Area 52
A,105,106,118,117               ! Area 53
A,106,107,119,118               ! Area 54
ADEL,16,21,1,1
ASEL,S,AREA,,25,30,1
AADD,ALL                        ! AREA 16
ASEL,S,AREA,,31,49,18
AADD,ALL                        ! AREA 17
ASEL,S,AREA,,32,39,1
ASEL,A,AREA,,50,51,1
ASEL,A,AREA,,15,15,1
AADD,ALL                        ! AREA 18
ASEL,S,AREA,,40,45,1
ASEL,A,AREA,,52,53,1
AADD,ALL                        ! AREA 15
ASEL,S,AREA,,46,48,1
ASEL,A,AREA,,54,54,1
ASEL,A,AREA,,24,24,1
AADD,ALL                        ! AREA 19
ALLSEL
NUMCMP,AREA
/PNUM,AREA,1
APLO
/PNUM,AREA,0
/PNUM,KP,1
APLO
/PNUM,KP,0
/PNUM,AREA,1
```

```
APLO
APLO,1,14,1
APLO,15,19,1
APLO,20,21,1
/PNUM,AREA,0
*DO,ANUM,1,7,1
ASEL,S,AREA,,ANUM,ANUM,1
AATT,1,1,ANUM
*ENDDO
*DO,ANUM,8,14,1
ASEL,S,AREA,,ANUM,ANUM,1
AATT,2,1,ANUM
*ENDDO
ASEL,S,AREA,,15
AATT,3,1,15
ASEL,S,AREA,,16
AATT,1,1,16
ASEL,S,AREA,,17
AATT,2,1,17
ASEL,s,AREA,,18
AATT,2,1,18
ASEL,S,AREA,,19
AATT,3,1,19
ASEL,S,AREA,,20
AATT,4,1,20
ASEL,S,AREA,,21
AATT,4,1,21
ALLSEL
/pnum,mat,1
aplo
/pnum,mat,1
!
! AUTOMATED FINITE ELEMENT MESHING
!
esize,RTHK/2
MSHAPE,0,2D
MSHKEY,2
amesh,all
/pnum,type,1
eplo
/pnum,type,0
KSEL,S,KP,,1,57,56
KSEL,A,KP,,82,82,1
LSLK,S,1
NSLL,S,1
CP,1,UY,ALL
KSEL,S,KP,,56,81,81-56
KSEL,A,KP,,110,110,1
LSLK,S,1
NSLL,S,1
```

```
CP,2,UY,ALL
ALLSEL
FINI
!
! SOLUTION MODULE
!
/SOLU
ANTYPE,STATIC,NEW
OUTRES,ALL,ALL
TIME,1.0
!
! ROTATIONAL SPEED
!
ROTSPD=2*PI*16400/60
OMEGA,0,ROTSPD,0,0
!
! DISPLACEMENT CONSTRAINTS
!
DK,1,UY,0
! DK,82,UX,0
! DK,110,UX,0
!
! CENTRIFUGAL FORCES DUE TO WEIGHT OF BLADES AT EACH ROW
!
FK,3,FX,21*0.05825*7.84*ROTSPD*ROTSPD/386.4
FK,6,FX,28*0.02382*7.84*ROTSPD*ROTSPD/386.4
FK,9,FX,35*0.01176*7.84*ROTSPD*ROTSPD/386.4
FK,12,FX,42*0.0064084*7.84*ROTSPD*ROTSPD/386.4
FK,15,FX,49*0.0038977*7.84*ROTSPD*ROTSPD/386.4
FK,18,FX,56*0.0024879*7.84*ROTSPD*ROTSPD/386.4
FK,21,FX,62*0.0016691*7.84*ROTSPD*ROTSPD/386.4
FK,24,FX,68*0.0033844*7.84*ROTSPD*ROTSPD/386.4
FK,27,FX,74*0.0025427*7.84*ROTSPD*ROTSPD/386.4
FK,30,FX,78*0.0019597*7.84*ROTSPD*ROTSPD/386.4
FK,33,FX,82*0.0015143*7.84*ROTSPD*ROTSPD/386.4
FK,36,FX,84*0.0013144*7.84*ROTSPD*ROTSPD/386.4
FK,39,FX,85*0.0011129*7.84*ROTSPD*ROTSPD/386.4
FK,42,FX,84*0.0010030*7.84*ROTSPD*ROTSPD/386.4
/PBC,ALL,,1
APLO
/PBC,ALL,,0
SBCTRA
/PBC,ALL,,1
EPLO
/PBC,ALL,,0
LSWRITE,1
LSSOLVE,1
FINI
!
! POSTPROCESSING
```

```
!
/POST1
SET,1,1
/DSCALE,1,1.0
/ANNOT,ON
/TSPEC,15,.9,2,0.
/TLABEL,-.9,.94,Contour Plot of Radial Displacements (in)
PLNS,U,X
/ANNOT,DELE
/ANNOT,ON
/TSPEC,15,.9,2,0.
/TLABEL,-.9,.94,Contour Plot of Radial Stresses (Sx)
PLNS,S,X
/ANNOT,DELE
/ANNOT,ON
/TSPEC,15,.9,2,0.
/TLABEL,-.9,.94,Contour Plot of Axial Stresses (Sy)
PLNS,S,Y
/ANNOT,DELE
/ANNOT,ON
/TSPEC,15,.9,2,0.
/TLABEL,-.9,.94,Contour Plot of Tangential (Hoop) Stresses (Sz)
PLNS,S,Z
/ANNOT,DELE
/ANNOT,ON
/TSPEC,15,.9,2,0.
/TLABEL,-.9,.94,Contour Plot of 1st Principal Stress (S1)
PLNS,S,1
/ANNOT,DELE
/ANNOT,ON
/TSPEC,15,.9,2,0.
/TLABEL,-.9,.94,Contour Plot of 2nd Principal Stress (S2)
PLNS,S,2
/ANNOT,DELE
/ANNOT,ON
/TSPEC,15,.9,2,0.
/TLABEL,-.9,.94,Contour Plot of 3rd Principal Stress (S3)
PLNS,S,3
/ANNOT,DELE
/ANNOT,ON
/TSPEC,15,.9,2,0.
/TLABEL,-.9,.94,Contour Plot of Max. Equivalent Stress (Seqv)
PLNS,S,EQV
/ANNOT,DELE
FINI
/EXIT
```

Appendix D
Blade Profiles for Exoskeletal Rotor

This appendix contains the input data for the Pro/Engineer® models of the compressor and turbine rotor blades. The exoskeletal compressor rotor blade shapes are based on the NACA 65A010 compressor airfoil shape. The NACA 65A010 profile is a symmetric shape specifically developed for compressor applications. This profile is shown in figure 50 and is listed in table 22. This airfoil has a 10-percent-thickness-to-chord ratio.

TABLE 22.—NACA 65A010 COMPRESSOR AIRFOIL

[Leading-edge radius, 0.00636c; trailing-edge radius, 0.00023c.]

Length-to-chord ratio, x/c, percent	Thickness-to-chord ratio, y/c, percent	Length-to-chord ratio, x/c, percent	Thickness-to-chord ratio, y/c, percent
0	0.0	40	4.995
.5	.765	45	4.983
.75	.928	50	4.863
1.25	1.183	55	4.632
2.5	1.623	60	4.304
5	2.182	65	3.809
7.5	2.65	70	3.432
10	3.04	75	2.912
15	3.658	80	2.352
20	4.127	85	1.771
25	4.483	90	1.188
30	4.742	95	.604
35	4.912	100	0

A stagger angle θ is used for the base and the tip of the compressor blades, which gives the blade a twist along its length. The stagger angle is applied at the centroid of the airfoil, as shown in figure 51. In the high-pressure turbine, the airfoil camber line is curved, and the symmetric shape of the NACA 65A010 profile is distributed about the camber line. The curved camber line changes the fluid flow to the desired direction. In the case of the exoskeletal design, the curved camber line is a circular arc as shown in figure 52. The stagger angle θ of the curved airfoil is the average of the camber line inlet angle ϕ_i and exit angle ϕ_e. From basic trigonometry, the radius r of the camber line is given by the following equation:
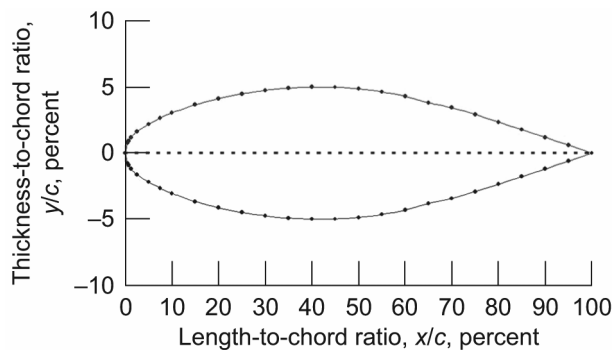
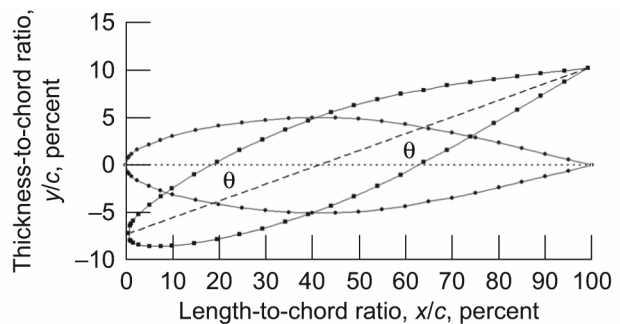Figure 50.—NACA 65A010 blade shape.
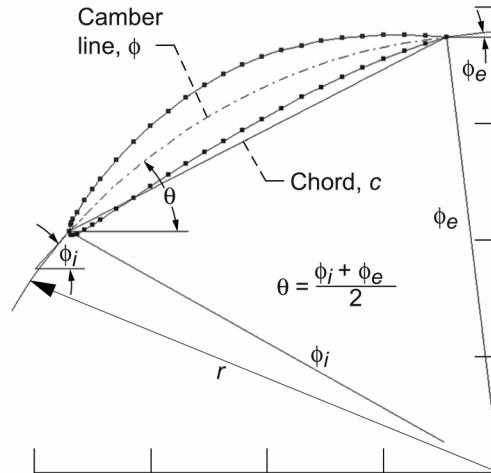

Figure 51.—Airfoil stagger angle for compressor blades.

Figure 52.—Circular arc camber line for
turbine blades.

$$r = \frac{c \sin \theta}{\cos \phi_e - \cos \phi_i} \tag{D1}$$

where c is the chord.

In the Pro/Engineer® model, each point of the NACA 65A010 profile has a local radius r_n and a local camber line angle ϕ_n, which are defined by the following set of equations:

$$\Delta \phi_n = 2\theta \left(\frac{x}{c} \right) \tag{D2a}$$

$$r_n = r + c \left(\frac{y}{c} \right) \tag{D2b}$$

$$\phi_n = 90 + \phi_i - \Delta \phi_n \tag{D2c}$$

The coordinates for each point on the profile are given by the following transformations:

$$x'_n = r_n \cos \phi_n + \frac{c}{2} \tag{D3}$$

$$y'_n = r_n \sin \phi_n - \frac{\frac{c}{2}}{\tan \theta} \tag{D4}$$

References

1. Mattingly, Jack D.: Elements of Gas Turbine Propulsion. McGraw-Hill, New York, NY, 1996.
2. Halliwell, Ian: Exoskeletal Engine Concept: Feasibility Studies for Medium and Small Thrust Engines. NASA/CR—2001-211322, 2002. http://gltrs.grc.nasa.gov/reports/2001/CR–2001–211322.pdf
3. Gunston, Bill, ed.: Jane's Aero-Engines. Issue 14, Jane's Information Group Limited, Coulsdon, Surrey, 2003.
4. Tong, Michael T., et al.: A Computer Code for Gas Turbine Engine Weight and Disk Life Estimation. ASME GT–2002–30500, 2002.
5. Onat, E.; and Klees, G.W.: A Method to Estimate Weight and Dimensions of Large and Small Gas Turbine Engines; Final Report. NASA CR–159481, 1979.
6. Pro/ENGINEER®, PTC Worldwide Headquarters, Needham, MA, 2001.
7. Maintaining U.S. Leadership in Aeronautics: Breakthrough Technologies to Meet Future Air and Space Transportation Needs and Goals. Contract No. NASW–4938, National Academy Press, Washington, DC, 1998.
8. Klann, John L.; and Snyder, Christopher A.: NEPP Programmers Manual (NASA Engine Performance Program). NASA TM–106575–VOL–1, 1994. Available from the NASA Center for Aerospace Information.
9. Converse, G.L.; and Giffin, R.G.: Extended Parametric Representation of Compressor Fans and Turbines. Volume 1: CMGEN User's Manual; Final Report. NASA CR–174645, 1984.
10. Converse, G.L.: Extended Parametric Representation of Compressor Fans and Turbines. Volume 2: Part User's Manual (Parametric Turbine); Final Report. NASA CR–174646, 1984.
11. Onat, E.; and Klees, G.W.: A Method to Estimate Weight and Dimensions of Large and Small Gas Turbine Engines; Final Report. NASA CR–159481, 1979.
12. Tong, Michael, et al.: A Computer Code for Gas Turbine Engine Weight and Disk Life Estimation. ASME GT–2002–30500, 2002.
13. Abumeri, Galib H.; Kuguoglu, Latife H.; and Chamis, Christos C.: Composite Fan Blade Design for Advanced Engine Concepts. NASA/TM—2004-212943, 2004.
14. Kuguoglu, Latife; Abumeri, Galib; and Chamis, Christos C.: Structural Evaluation of Exo-Skeletal Engine Fan Blades. AIAA 2003–1861, 2003.
15. MSC.Nastran 2001. MSC Software Corporation, Los Angeles, CA, 2001.
16. Metallic Materials and Elements for Aerospace Vehicle Structures. MIL–HDBK–5F, 1990.
17. HyperSizer™. Structural Sizing Software, Collier Research Corporation, Hampton, VA. http://www.collier-research.com/Products/products.htm Accessed Nov. 5, 2004.
18. MSC.Patran 2002 (r2). Release Guide, MSC Software Corporation, Santa Ana, CA, 2002.
19. ANSYS Verification Manual. Verification Test Case Descriptions, ©2002 SAS IP, Inc., 2002.
20. Shigley, Joseph Edward: Mechanical Engineering Design. Second ed., McGraw-Hill, New York, NY, 1972.
21. ANSYS Technical Overview (MBA–A15–9/97), ANSYS, Inc., ©1997.
22. Gunter, E.J.: Critical Speeds of a Flexible Rotor, Department of Mechanical Engineering, University of Virginia, Nov. 10, 1971.
23. Vance, John M.: Rotordynamics of Turbomachinery. Wiley, New York, NY, 1988.
24. Timoshenko, S.; Young, D.H.; and Weaver, W., Jr.: Vibration Problems in Engineering. Wiley, New York, NY, 1974.
25. Childs, Dara W.: Turbomachinery Rotordynamics: Phenomena, Modeling, and Analysis. Wiley, New York, NY, 1993.
26. Prohl, M.A.: A General Method for Calculating Critical Speeds of Flexible Rotors. J. Appl. Mech. Trans. ASME, vol. 12, no. 3, 1945, pp. A142–A148.

27. Myklestad, N.O.: A New Method of Calculating Natural Modes of Uncoupled Bending Vibration of Airplane Wings and Other Type of Beams. J. Aero. Sci., vol. 11, 1944, pp. 153−162.
28. Linn, F.C.; and Prohl, M.A.: The Effect of Flexibility of Support Upon the Critical Speeds of High-Speed Rotors. Trans. Soc. Naval Architects Mar. Eng., vol. 59, 1951, pp. 536−553.
29. Ehrich, Frederic F.: Handbook of Rotordynamics. McGraw-Hill, New York, NY, 1992.
30. DellaCorte, Chris; and Pinkus, Oscar: Tribological Limitations in Gas Turbine Engines: A Workshop to Identify the Challenges and Set Future Directions; Revised. NASA/TM—2000-210059/REV1, 2002. http://gltrs.grc.nasa.gov/reports/2002/TM−2000−210059−REV1.pdf
31. Sullivan, Roy: Thermal Analysis of a Carbon-Carbon Bearing Design for Exoskeletal Engine Bearings. NASA/TM—2001-210946, 2001. Available from the NASA Center for AeroSpace Information.
32. Dellacorte, Christopher; and Valco, Mark J.: Load Capacity Estimation of Foil Air Journal Bearings of Oil-Free Turbomachinery Applications. NASA/TM—2000-209782, 2000. http://gltrs.grc.nasa.gov/reports/2000/TM-2000-209782.pdf

REPORT DOCUMENTATION PAGE

1. AGENCY USE ONLY *(Leave blank)*	2. REPORT DATE	3. REPORT TYPE AND DATES COVERED
	August 2005	Technical Memorandum

4. TITLE AND SUBTITLE

Investigation of Exoskeletal Engine Propulsion System Concept

5. FUNDING NUMBERS

WBS–22–708–87–07

6. AUTHOR(S)

Joseph M. Roche, Donald T. Palac, James E. Hunter, David E. Myers, Christopher A. Snyder, Daniel N. Kosareo, David R. McCurdy, and Kevin T. Dougherty

7. PERFORMING ORGANIZATION NAME(S) AND ADDRESS(ES)

National Aeronautics and Space Administration
John H. Glenn Research Center at Lewis Field
Cleveland, Ohio 44135–3191

8. PERFORMING ORGANIZATION REPORT NUMBER

E–14837

9. SPONSORING/MONITORING AGENCY NAME(S) AND ADDRESS(ES)

National Aeronautics and Space Administration
Washington, DC 20546–0001

10. SPONSORING/MONITORING AGENCY REPORT NUMBER

NASA TM—2005-213369

11. SUPPLEMENTARY NOTES

Joseph M. Roche, Donald T. Palac, James E. Hunter, David E. Myers, and Christopher A. Snyder, NASA Glenn Research Center; Daniel N. Kosareo, ZIN Technologies, Inc., Brook Park, Ohio 44142; and David R. McCurdy and Kevin T. Dougherty, QSS Group, Inc., Cleveland, Ohio 44135. Responsible person, Kevin T. Dougherty, organization code PR, 216–433–3546.

12a. DISTRIBUTION/AVAILABILITY STATEMENT

Unclassified - Unlimited
Subject Category: 07   Distribution: Nonstandard

Available electronically at http://gltrs.grc.nasa.gov

This publication is available from the NASA Center for AeroSpace Information, 301–621–0390.

12b. DISTRIBUTION CODE

13. ABSTRACT *(Maximum 200 words)*

An innovative approach to gas turbine design involves mounting compressor and turbine blades to an outer rotating shell. Designated the exoskeletal engine, compression (preferable to tension for high-temperature ceramic materials, generally) becomes the dominant blade force. Exoskeletal engine feasibility lies in the structural and mechanical design (as opposed to cycle or aerothermodynamic design), so this study focused on the development and assessment of a structural-mechanical exoskeletal concept using the Rolls-Royce AE3007 regional airliner all-axial turbofan as a baseline. The effort was further limited to the definition of an exoskeletal high-pressure spool concept, where the major structural and thermal challenges are represented. The mass of the high-pressure spool was calculated and compared with the mass of AE3007 engine components. It was found that the exoskeletal engine rotating components can be significantly lighter than the rotating components of a conventional engine. However, bearing technology development is required, since the mass of existing bearing systems would exceed rotating machinery mass savings. It is recommended that once bearing technology is sufficiently advanced, a "clean sheet" preliminary design of an exoskeletal system be accomplished to better quantify the potential for the exoskeletal concept to deliver benefits in mass, structural efficiency, and cycle design flexibility.

14. SUBJECT TERMS

Propulsion system configurations; Turbofan engines; Jet engines; Turbine engines; Gas turbine engines

15. NUMBER OF PAGES

93

16. PRICE CODE

17. SECURITY CLASSIFICATION OF REPORT	18. SECURITY CLASSIFICATION OF THIS PAGE	19. SECURITY CLASSIFICATION OF ABSTRACT	20. LIMITATION OF ABSTRACT
Unclassified	Unclassified	Unclassified	